5-2013

NOVEL THERAPEUTIC TARGETS IDENTIFIED BY HIGH-THROUGHPUT TECHNOLOGIES FOR TRIPLE-NEGATIVE BREAST CANCER

Christine Shiang

NOVEL THERAPEUTIC TARGETS IDENTIFIED BY HIGH-THROUGHPUT TECHNOLOGIES FOR TRIPLE-NEGATIVE BREAST CANCER

by Christine Shiang, B.S.

APPROVED:

Lajos Pusztai, M.D., D.Phil., Supervisory Professor

Francisco Esteva, M.D., Ph.D., On-site Advisor

Michelle Barton, Ph.D.

Hui-Kuan Lin, Ph.D.

Jonathan Trent II, M.D., Ph.D.

APPROVED:

Michelle Barton, Ph.D., Michael Blackburn, Ph.D.

Deans, The University of Texas Health Science Center at Houston

Graduate School Biomedical Sciences

NOVEL THERAPEUTIC TARGETS IDENTIFIED BY HIGH-THROUGHPUT TECHNOLOGIES FOR TRIPLE-NEGATIVE BREAST CANCER

A

DISSERTATION

Presented to the Faculty of

The University of Texas

Health Science Center at Houston

and

The University of Texas

M. D. Anderson Cancer Center

Graduate School of Biomedical Sciences

in Partial Fulfillment

of the Requirements

for the Degree of

DOCTOR OF PHILOSOPHY

by

Christine Shiang, B.S.

Houston, Texas

May, 2013

Dedication

To my mother, Nina Su-Jen Kuo Shiang

To my sisters, Gloria, Elizabeth, and Nina

Acknowledgements

I am indebted to my mentors and plan to repay the scientific and personal lessons learned with my future contributions. Dr. Lajos Pusztai kindly provided his wisdom and experience. It is with his expert guidance, honest criticisms, and keen sense of prediction that I have begun the journey to thinking logically and creatively in the world of breast cancer genomics. Dr. Michelle Barton allowed me to experience how impactful a mentor could be; a few seconds under the warmth and exactness of her direction and a student's future is made ever brighter. Dr. Francisco Esteva exemplified how collaborations between the clinical and basic sciences results in thorough science. Dr. Hui-Kuan Lin provided deep insight into the powers of molecular biology and mouse models of human cancer. Dr. Jon Trent shined as a personal example of how a world-class education from The University of Texas Graduate School of Biomedical Sciences is the foundation for a physician scientist that considers the patient first.

I must give thanks to the extensive infrastructure – the dedicated staff, students, and faculty of The University of Texas Graduate School of Biomedical Sciences and M. D. Anderson Cancer Center. At every step of my education, they have inspired me in countless ways. They channeled my overreaching ideas into concrete action and paved the way to a focused future in cancer medicine. The hard-working members of the Breast Cancer Translational Laboratory taught me crucial lessons in technique and collegiality, and deserve more thanks than I can express. I must also thank the U. S. Department of Defense Breast Cancer Research Program for their funding support (USAMRMC support W81XWH-10-1-0001), in combination with support from Dr. Lajos Pusztai and the Breast Cancer Research Foundation.

To my family, I share only a few words because the forces behind them cannot be expressed adequately. To my mother and father, thank you for your sacrifices in bringing us to this country. To my sisters, thank you for all the lessons and your love. To my beautiful nephew and nieces, thank you for your laughter and joy. To Tim, you are my rock.

NOVEL THERAPEUTIC TARGETS IDENTIFIED BY HIGH-THROUGHPUT TECHNOLOGIES FOR TRIPLE-NEGATIVE BREAST CANCER

Publication No. _____

Christine Shiang, B.S.

Supervisory Professor: Lajos Pusztai, M.D., D.Phil.

Triple-negative breast cancers (TNBC) are characterized by the lack of or reduced expression of the estrogen and progesterone receptors, and normal expression of the human epidermal growth factor receptor 2. The lack of a well-characterized target for treatment leaves only systemic chemotherapy as the mainstay of treatment. Approximately 60-70% of patients are chemosensitive, while the remaining majority does not respond. Targeted therapies that take advantage of the unique molecular perturbations found in triple-negative breast cancer are needed. The genes that are frequently amplified or overexpressed represent potential therapeutic targets for triple-negative breast cancer. The purpose of this study was to identify and validate novel therapeutic targets for triple-negative breast cancers.

681 genes showed consistent and highly significant overexpression in TNBC compared to receptor-positive cancers in 2 data sets. For two genes, 3 of the 4 siRNAs showed preferential growth inhibition in TNBC cells. These two genes were the low density lipoprotein receptor-related protein 8 (LRP8) and very low-density lipoprotein receptor (VLDLR). Exposure to their cognate ligands, reelin and apolipoprotein E isoform 4 (ApoE4), stimulated the growth of TNBC cells in vitro. Suppression of the

expression of either LRP8 or VLDLR or exposure to RAP (an inhibitor of ligand binding to LRP8 and VLDLR) abolished this ligand-induced proliferation. High-throughput protein and metabolic arrays revealed that ApoE4 stimulation rescued TNBC cells from serum-starvation induced up-regulation of genes involved in lipid biosynthesis, increased protein expression of oncogenes involved in the MAPK/ERK and DNA repair pathways, and reduced the serum-starvation induction of biochemicals involved in oxidative stress response and glycolytic metabolism. shLRP8 MDA-MB-231 xenografts had reduced tumor volume, in comparison to parental and shCON xenografts. These results indicate that LRP8-APOE signaling confers survival advantages to TNBC tumors under reduced nutrient conditions and during cellular environmental stress.

We revealed that the LRP8-APOE receptor-ligand system is overexpressed in human TNBC. We also demonstrated that this receptor system mediates a strong growth promoting and survival function in TNBC cells in vitro and helps to sustain the growth of MDA-MD-231 xenografts. We propose that inhibitors of LRP8-APOE signaling may be clinically useful therapeutic agents for triple-negative breast cancer.

Table of Contents

List of Figures

List of Tables

Chapter 1 – Introduction

1.1. Triple-negative breast cancer

Approximately 20% of all breast cancers are referred to as triple-negative breast cancers, which lack the immunohistochemical expression of the estrogen and progesterone receptors and of the human epidermal growth factor receptor 2, HER2 (1). Currently, effective treatment options are limited to chemotherapy, but the majority of patients who fail to achieve pathologic complete response after chemotherapy has unfavorable prognosis (2, 3). Therapeutics that target the unique molecular features of TNBC are needed.

1.2. Common molecular alterations

Triple-negative breast cancer (TNBC) is characterized by the lack of or reduced expression of the estrogen and progesterone receptor (ER and PR), and normal expression of the human epidermal growth factor receptor 2 (HER2) (2, 3). This convenient naming system is based on routing immunohistochemistry performed in the clinic. It is also referred to as the basal-like breast cancers due to the expression of basal epithelial cell type markers and is one of the five intrinsic breast cancer subtypes distinguished on the basis of their gene expression patterns (2, 3). However, the overlap between the two different identification systems is approximately 80%, with discordance in the expression of basal markers, immune response markers, and types of p53 mutation (4-8). 15-40% of TNBC tumors have *BRCA*-related epigenetic down-regulation and increased expression of the inhibitors of *BRCA1* function (9). This indicates that the label "triple-negative breast cancer" describes a more heterogeneous subtype than other breast cancer subtypes (10, 11).

Triple-negative breast cancers are differentiated from receptor-positive breast cancers by large-scale DNA copy number changes and gene expression differences (5, 12). Key mediators of immunological response, proliferation, and neuronal signaling, such as MYC, LYN, EGFR, and CEBPB, are either amplified or overexpressed in TNBC in comparison to other breast cancer subtypes (13). These differences reflect the unique molecular landscape of triple-negative breast cancers and represents potential therapeutic targets that require experimental validation.

Human gene expression profiling provides the opportunity to start the target identification process in human triple-negative breast cancers (4, 5). Consistently observed genomic abnormalities have specific roles in the proliferation of breast tumors, such as dysregulation of the estrogen receptor (ER) in ER+ disease and overexpression of the human epidermal growth factor receptor-2 (HER2) in HER2+ disease (5). Results from high-throughput microarray analyses have revealed large-scale gene expression and DNA copy number pattern differences between these clinical subsets of breast cancers (5-8). The distinct genomic differences have important clinical implications for patient outcome. These molecular differences may be the source of potential novel therapeutic targets for unsuccessfully targeted subsets, such as triple-negative breast cancer (7, 9, 13). Experimental and empirical validation of the various potential therapeutic targets identified in human genomic data is central to future treatment success in the clinic.

1.3. Clinicopathologic features of patient population

There are aggressive clinical features that typify patients with triple-negative breast disease. Younger age of disease onset and women of African or Hispanic descent

have been associated with higher rates of triple-negative disease. An increased proportion of TNBC patients have higher rates of CNS, visceral, and bony metastases and overall poor outcome despite therapeutic treatment (2). This metastatic phenotype of TNBC is due in part to the high nuclear grade of TNBC tumors and results in shorter time to disease recurrence and shorter median survival time in of advanced metastatic TNBC (1, 2).

The TNBC paradox details that there is a high proportion of responsive patients that exhibit pathologic complete response to neoadjuvant chemotherapy, while the survival (both disease-free and overall) of the entire basal-like group was significantly worse in comparison to the luminal or ER-associated subtypes (1, 2). However, this worse overall survival is comprised of patients with residual cancer (1, 2).

1.4. Existing chemotherapeutic treatment options and targeted therapies

Currently, treatment options are limited to conventional chemotherapy with limited long-term success (1, 2). Two-thirds of patients are chemosensitive, while the remaining portion of patients does not respond to chemotherapy. TNBC patients have a better response to chemotherapy in the neoadjuvant setting, in comparison to non-TNBC patients (1, 2). TNBC patients that are initially non-responsive have higher relapse risk and worse overall survival at 68% than responders who exhibit pathologic complete response at 94% overall survival (14). Non-TNBC or receptor-positive breast cancers with residual disease have the benefit of selective estrogen receptor modulators and trastuzumab (14).

In light of the heterogeneous nature of TNBC and lack of targeted therapy options, several classes of targeted therapeutics have been tested to provide non-responsive patients with a therapeutic alternative. Epidermal growth factor receptor (EGFR) has been identified as a frequently overexpressed marker in triple-negative breast cancer (15). anti-EGFR agents such as the monoclonal antibody cetuximab have resulted in a minimal efficacy in retrospective and prospective studies (16). BALI-1, the largest EGFR clinical trial to date that is testing the combination of cetuximab and cisplatin, did not result in improved overall recurrence or overall survival rates (16). The combination of cetuximab to carboplatin and irinotecan did not improve progression-free or overall survival. The combination of carboplatin and cetuximab increased extended progression-free survival from 2 to 8 months, but the overall progression-free and overall survival data is still pending (16).

Tyrosine-kinase inhibitors such as erlotinib and lapatinib have been tested with inconsistent results (17). Erlotinib with docetaxel and carboplatin neoadjuvant treatment resulted in a 40% pathologic complete response in TNBC patients (17). However, the combination of lapatinib with paclitaxel did not result in antitumor activity in metastatic TNBC patients (17).

Laboratory studies suggested that upregulated mTOR levels result in increased sensitivity to mTOR inhibitors and initial clinical results yielded promising levels of activity (18). Inhibitors of the mammalian target of rapamycin (mTOR) such as everolimus have been tested with standard chemotherapy in TNBC patients (randomized Phase II) and did not significantly improve pathologic complete response (18, 19).

Angiogenesis inhibitors have been tested in the clinic with modest overall results. The Avastin and Docetaxel (AVADO) trial reduced risk of progression by 47%, while the combination of bevacizumab and chemotherapy in the Regimens in Bevacizumab for Breast Oncology (RiBBOn)-1 resulted in no benefit for TNBC patients (20, 21). The long-term disease-free and overall survival data of the National Surgical Adjuvant Breast and Bowel Project 40 (NSABP)-B40 and GeparQuinto trials combining bevacizumab and anthracycline-taxane are still pending, but preliminary results indicate significantly increased pCR in TNBC patients and no improvement in pCR rates respectively in the trials (20, 21).

Poly (ADP-ribose) polymerase 1/2-inhibitors such as veliparib and olaparib have demonstrated activity in *BRCA* mutated breast cancer (34). However, the activity of PARP inhibitors has not been demonstrated in TNBC tumors without *BRCA* mutation (22). Further, dosing of paclitaxel and olaparib have been complicated by side effects (22).

1.5. Central hypothesis and specific aims

Central hypothesis. There are frequently amplified or overexpressed genes in triple-negative breast cancer, which represent novel therapeutic targets. The goals of this study were to (i) identify candidate target genes from human genomic data, (ii) assess the effect on cancer cell proliferation in a custom siRNA screen in 18 breast cancer cell lines, and (iii) to validate the top tier siRNA hits as potential TNBC target genes through functional and mechanistic analyses (Figure 1). The low density lipoprotein receptor-related protein 8 (LRP8) and very low density lipoprotein receptor (VLDLR) are

membrane receptor proteins that have well-characterized roles in cholesterol trafficking and lipid metabolism, as well as neuronal signaling during development and after traumatic brain injury (23, 24). In this current study, these 2 receptors were characterized for their functional roles in the growth of TNBC cells, in response to their cognate ligands, reelin and apolipoprotein E. This study examines the functional role of the ApoE – LRP8/VLDLR signaling axis in TNBC as mediators of lipid metabolism that are important in the growth and survival of triple-negative breast cancer.

Specific aim 1. To identify amplified or overexpressed genes in triple-negative breast cancer as candidate target genes. The hypothesis that there are frequently amplified or overexpressed genes in triple-negative breast cancer was tested using bioinformatics analyses of 2 independent datasets of gene expression profiling on human breast cancers and matching CGH results on a subset of those tumors.

Specific aim 2. To test how the proliferation of an 18 breast cancer cell line panel was affected after siRNA depletion of the previously identified candidate targets. The hypothesis that growth inhibition would be preferential to TNBC cell lines (n=10) vs. non-TNBC cell lines (n=8) was tested using 4 unique siRNAs against each candidate target.

Specific aim 3. To identify signaling pathways and experimentally validate the functional importance of the potential target genes in triple-negative breast cancer *in vitro* and *in vivo*. The hypothesis that TNBC has a unique molecular biology and pathway signaling was tested in ligand stimulation assays, after which transcriptional profiling and metabolomics arrays were performed to identify global gene expression and metabolic patterns that drive TNBC tumor biology.

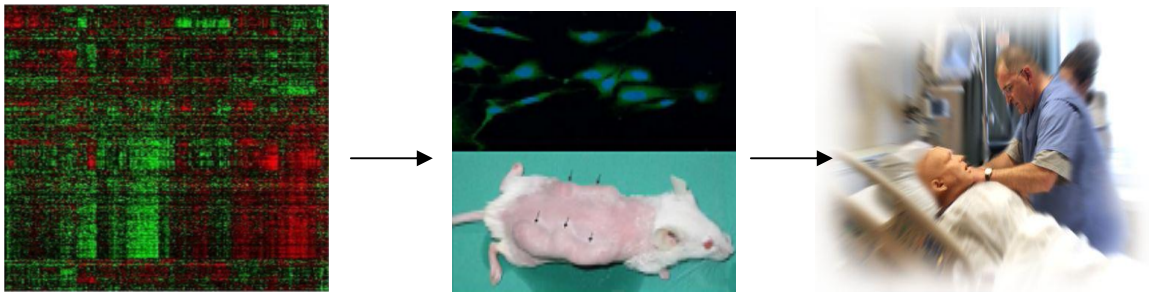

Figure 1. Target identification and validation strategy for the treatment of triple-negative breast cancer. The research strategy is to start the target discovery process by molecularly interrogating human breast tumors, identify and validate target genes using experimental models of breast cancer, and bring back specific therapeutic agents for a molecularly defined patient population. The research strategy entails a complementary strategy to traditional laboratory testing and starts the discovery process in human cancer tissues, identify novel therapeutic targets through bioinformatics analysis of human breast cancer genome expression data, and assess the functional importance of these novel genes the laboratory. Some of the functionally important targets that may be identified can be inhibited with existing drugs and new therapeutic agents will need to be developed for others.

1.6. High-throughput discovery of candidate targets for TNBC

Initial discovery of the candidate targets for TNBC were performed through bioinformatics analyses of 2 publicly available gene expression profiling datasets of human breast cancers (25, 26). After using an initial discovery dataset that was verified by the second validation dataset, 681 genes were identified as being significantly and highly overexpressed in TNBC vs. non-TNBC patients. These 681 candidate genes for TNBC therapy were submitted to a custom siRNA screen, in which 18 breast cancer cell lines were treated with 4 unique siRNAs against each gene to determine the growth inhibitory effect mediated by siRNA depletion of each candidate gene. A list of siRNAs that resulted in preferential growth inhibition of the TNBC cell line group (n=10) was compared to that of the non-TNBC cell line group (n=8). The top tier hits were binned according to number of siRNAs that resulted in growth inhibition of the candidate gene, with 3 of 4 siRNAs resulting in preferential TNBC growth inhibition being assigned as the most consistently reproducible inhibitory effect on growth (Dharmacon rational siRNA design for RNA interference). The two genes that occupied this top tier assignment were the low density lipoprotein receptor-related protein 8 (LRP8) and very low-density lipoprotein receptor (VLDLR).

1.7. LRP8-APOE receptor-ligand system

The low density lipoprotein receptor-related protein 8 (LRP8) and very low-density lipoprotein receptor (VLDLR) function together and separately and are members of the low density lipoprotein (LDL) receptor family which has a historically prominent role in the homeostatic management of lipid and cholesterol trafficking in the central

nervous system and the peripheral circulation of the human body (23, 24, 27). Dysfunction of the receptor family members has been implicated in the imbalance between extracellular and intracellular pools of cholesterol in the context of familial hypercholesterolemia and atherosclerotic disease (27). The structural motifs that are common to LDL receptor family members are (i) type A binding repeats of ~40 amino acids with 6 cysteine pairs which is the ligand-binding domain, (ii) type B repeats with 6 pairs of cysteines, (iii) 50 amino acids with consensus peptide YWTD, (iv) a serine-threonin rich region named the O-linked sugar domain, (v) a 20 amino acid transmembrane region, and (vi) a cytoplasmic region with a receptor internalization signal (27).

The ligand binding region regulates binding interactions between reelin and APOE (2 well-characterized ligands) to LDL receptor family members (23, 27). The seven type A LDL repeats (LA indicating LDL receptor type A) mediates folding through the paired cysteines that form cysteine bridges and enable negatively charged acidic Asp and Glu residues to interact with positively charged residues on reelin and APOE (23, 27). This process is concentrated in LA repeats 2-7 of the receptor (27).

LRP8, otherwise known as the apolipoprotein E receptor 2 (ApoER2), may have 3, 4, 5, 7, or 8 type A binding repeats in its ligand binding depending on the species and tissue of origin (27). LRP8 is prone to distinct products due to differential transcriptional splicing (27). In humans, LRP8 has a more restricted expression profile and is found in the brain, testis, and placenta. VLDLR contains an eighth type A repeat and is expressed in the brain and throughout many tissue types in the periphery (23).

1.8. Role of LRP8 and APOE in traumatic brain injury, Alzheimer's disease and hyperlipidemia

The interaction of LRP8 and VLDLR is well-documented after traumatic brain injury whereby they interact after binding reelin (28). Disabled-1, an intracellular adaptor protein, is phosphorylated after binding to the NPxY motifs of the receptors (29). The phosphorylation starts a kinase cascade the regulates motility and regeneration of injured neuronal cells (29). More recently, the ApoE4 allelle has been associated with earlier age of onset for Alzheimer's disease (30). Studies suggest that binding of the ApoE4 isoform results in impaired synaptic plasticity by reducing ApoER2 expression and Reelin responsivity (30).

Alternatively, the two receptors also coordinate the uptake of extracellular cholesterol through APOE cholesterol-bound moieties that allows cholesterol to be metabolized for energy (27). The genotype-specific properties of ApoE4 are also seen here; people with one copy of the *APOE* ε4 allele have an increased risk of hypercholesterolemia and atherosclerosis, while the *APOE* ε2 allele increases the risk of hyperlipoproteinemia type III (30). This is related to the differential binding affinities of the protein isoforms of the alleles, whereby APOE4 has an increased binding affinity due to more positively charged residues which are available to LRP8 and VLDLR as a result of a single nucleotide polymorphism (Cys to Arg 130) (30). In contrast, APOE2 protein isoform has reduced binding affinity to its receptors (Arg to Cys 176) (30).

1.9. LRP8 and APOE in cancer

Ectopic expression of LRP8 in malignant lung carcinoma has been linked to aberrations on the 1p chromosomal arm (31). There is early evidence that ApoE inhibits invasion in melanoma cell lines by binding LRP1 and LRP8 on adjacent endothelial cells, which is regulated by a three membered miRNA group (32). This study describe that APOE, irrespective of isoform type, mediates metastasis and that increasing APOE expression can act as an antiangiogenic or antimetastatic treatment route. In neuroblastoma cell lines, Reelin acts as a chemoattractant and promotes dissemination of tumor cells (33). Alternatively, other studies have reported that VLDLR downregulation inhibits cell motility in mouse embryonic fibroblasts and the MCF-7 (ER+) breast cancer cell line (34). ApoE knockout mice, ApoE(-/-), have increased circulating cholesterol and therefore higher triglyceride levels (35). These mice also had increased tumor growth and lung metastases after injection of metastatic mammary cancer cells (35).

A case-control study of gastric cancer cases revealed that having one copy of the *APOE ε2* allele was associated with a 60% decreased incidence of gastric cancer (36). An eight biomarker model for the detection of bladder cancer contains APOE as a highly accurate marker for the diagnosis of bladder cancer. A meta-analysis of 3,835 subjects revealed that the *APOE ε4* allele is associated with breast cancer from studies out of Asia, however the *ε2* allele was not associated with breast cancer (37). There were no associations found in Caucasians (37). ApoE3 protein isoform has also been found in the tumor endothelial vasculature of prostate cancer patient samples and required for proliferation of ovarian cancer cells (38, 39). Conversely, one analysis of the Copenhagen

City Heart Study suggests that low LDL levels are associated with cancer risk, but that APOE polymorphisms are not associated with increased cancer risk (40).

In 2010, Porrata-Doria et al. reported that the E4/E4 genotype was significantly associated with younger onset breast cancer (21-50 years) in a cohort of Puerto Rican women (41). These studies suggest that LRP8/VLDLR and APOE/reelin may have a role in breast cancer that is not yet understood.

1.10. Rationale for pursuing LRP8 and APOE as potential targets for TNBC

In summary, there were 3 major reasons for pursing LRP8 and VLDLR as potential therapeutic targets for TNBC. The receptors and ligands are either co-expressed or highly overexpressed in human TNBC. The ligands are also found in the breast tumor microenvironment and have pathologic roles in hypercholesterolemia and Alzheimer's disease. Single nucleotide polymorphisms are responsible for three major isoforms of apolipoprotein E and there is some early indication that ApoE4 carrier status is more prevalent in early onset breast cancer. In addition, LRP8 and VLDLR were found to be important in the growth and viability of triple-negative breast cancer cell lines, as the 2 top tier hits from the siRNA screen.

Chapter 2 – Materials and Methods

2.1. Gene expression profiling

To determine global gene expression changes after ApoE4 stimulation, breast cancer cell lines were treated with 600 nM of ApoE4. BT-549 and MDA-MB-436 TNBC cell lines were treated with 600 nM of ApoE4 using three technical replicates. Total RNA was isolated at baseline (0 hours) and at 8 and 48 hours after stimulation from control and ApoE4 treated cells, using the animal cell pin protocol from RNeasy Mini kit (Qiagen). In brief, breast cancer cells were trysinized and pelleted by centrifugation. Cells were lysed and the lysate homogenized using three 30 second pulses in a Sonics Vibra-Cell sonicator. Total RNA was then bound to a microcentrifuge RNeasy spin column and purified, eluted using RNase-free water, quantified using A260 in a NanoDrop ND1000 spectrophotometer, and stored at -20^0C. Gene expression profiling was performed on the Affymetrix HG-U133A array, as previously described (3, 12). Unequal variance t-test was used to identify differentially expressed genes and FDR was calculated as described below.

2.2. Data analysis of gene expression profiles

We used two independent data sets to define genes which are overexpressed in ER- and HER2-negative cancers. The first data set included Affymetrix U133A gene expression data from 294 fine-needle aspiration samples of stage I-III breast cancers obtained at MDACC, GSE16716 (n=294, 73 TNBC and 221 non-TNBC cases). This data was the discovery set to define candidate TNBC-genes. RNA extraction, hybridization, data normalization methods and results from these experiments have been published previously (5, 12). The second dataset was comprised of gene expression profiles

obtained from frozen tissues of surgically resected breast cancer specimens from 286 lymph node-negative patients including 56 TNBC and 230 receptor-positive cases, GSE2034 (26). This data set was used as a validation set to confirm overexpression of the 1871 genes. We used unequal variance t-test to compare each probe set between TNBC and non-TNBC cases. To account for multiple comparisons, we performed beta uniform mixture analysis (BUM) of the p values. This showed a non-uniform distribution and was used to calculate false discovery rates (FDR) for particular p-values. Unequal variance t-test was used to identify differentially expressed genes and false discovery rates (FDR) were calculated using the method by Pounds et al. (42, 43).

In further analysis, we used 2 additional human data sets from the TRANSBIG (GSE7390), and Mainz (GSE11121) studies (44, 45). Cell line data sets (51 cell line with ArrayExpress accession number E-TABM-157 and 19 cell line data set from M.D. Anderson Cancer Center) were also used to determine co-expression of the ApoE – LRP8 signaling members (46). All gene expression data was generated with Affymetrix gene chips, normalized with Affymetrix MAS5.0 algorithm, mean centered to 600, and log 2 transformed before further analysis. ER and HER2 status were identified using ESR1 mRNA expression (probe set 205225_at) and HER-2 mRNA expression (probe set 16836_s_at), as previously published (47). When one gene had two or more probe sets, we retained the probe set with the highest average expression value. We performed the class comparison with T-test between ER-positive/HER2-normal and ER-negative/HER2-normal breast cancer in LRP8 and VLDLR genes. To adjust for the multiple comparisons we calculated False Discovery Rates (FDR) using BRB Array tools. The FDR was calculated with the Significance Analysis of Microarrays (SAM) tool

as the median number of false positive genes from permutation testing divided by the number of nominally significant genes defined from the unperturbed data (44). Statistical analyses were performed using the BRB-ArrayTools v 3.8.1 (http://linus.nci.nih.gov/BRB-ArrayTools.html) and the R software v 2.7.2 (http://www.r-project.org). All statistical tests were two-sided.

2.3. siRNA screen

siRNA screening for each gene was performed in 18 different breast cancer cell lines (46). Each of these cell lines were purchased from the ATCC and have been previously fully characterized in our laboratory with gene expression profiling and CGH analysis. The cell lines included 10 TNBC and 8 receptor-positive cell lines or non-TNBC. All cell lines were tested for Mycoplasma contamination using MycoAlert Test kit (Lonza, Inc.) and growth curves under standard culture conditions were established.

The methods for the siRNA screen were optimized in the following manner. 3 different negative controls were used, (i) cells grown in regular OptiMEM media (Invitrogen, Inc.), (ii) cells transfected with control siRNA, and (iii) cells grown in transfection reagents alone. For siRNA controls, Dharmacon siGENOME-1,-2,-3,-4 and Dharmacon ON-TARGETplus siRNA oligonucleotides were tested. PLK1 (polo-like kinase 1), KIFF11 (kinesine family member 11), COPB2 (coatomer protein beta2) genes and siCONTROL TOX were used as positive controls for gene knockdown and to assess transfection efficiency. 96 hours after transfection, viability was determined using Promega's Cell Titer Blue cell viability assay (Madison, WI). Colorimetric measurements were performed using a Beckman Coulter Biomek 3000 reader. The optimal transfection

conditions were determined for each cell line and included the following considerations, (i) best positive and negative siRNA controls as quantified by Z-factor ~1.0 (Z=1-(3 x SSD/R) where SSD = sum of standard deivations and R = dynamic range), (ii) the most efficient transfection reagent with no viability change in the transfection reagent only cells.

After finding the optimal growth and transfection conditions, the full siRNA screen was performed for 674 target genes, each targeted with 4 independent siRNA oligonucleotides purchased from Dharmacon, Inc. The original 681 was reduced to 674 due to the availability of siRNA oligonucleotides. 384-well plates were seeded with target siRNAs and the cell line-specific negative and positive control siRNAs with a final concentration of 40 nM in 50μl total volume per well in 3 parallel technical replicates. Each cell line was added and the plates were incubated at 37^{o}C for 96 hours. The cell seeding density that yielded 70-90% confluence in the control wells at 96 hours was used for each cell line. Each cell line screen was performed in 3 technical replicates. For every 10 test plates, a control plate with negative and positive siRNA controls and cells in OptiMEM alone was tested. A control plate, including only replicates of positive and negative siRNA controls and cells grown in OptiMEM media alone, was inserted every 10 test plates to assess stability of the assay read out. Cell viability was calculated as follows; median value of absorbance in wells containing media alone was subtracted from absorbance readings of all other wells, individual readings of each test wells was divided by the median value of absorbance corresponding to negative siRNA control wells in the same plate and the fraction was multiplied by 100 to derive percent viability. Average percent viability across the 3 replicate plates was reported for each siRNA

oligonucleotide. Unequal variance t-test was used to assess significant decrease in viability compared to control wells. siRNA oligonucleotides for all other experiments were from Dharmacon, Inc.

2.4. Bioinformatic analysis to determine top tier hits from siRNA screen

The siRNA screen data was regionally normalized to account for differences in the dynamic range for the viability results of each cell line. Each cell line was treated with 2696 unique siRNAs using three technical replicates per siRNA. Each cell line was tested on 9 different test plates with each plate containing 16 negative controls and 8 positive controls.

To identify siRNAs that significantly inhibited growth in each cell line, all negative control values were pooled for each test plate, the three siRNA technical replicates were pooled for each plate, and a one-sided t-test was performed between the three siRNA replicates and the pooled negative control values. Beta-uniform mixture (BUM) was used to model the p-values of these t-tests and determine threshold cutoff values for specific false discovery rates (FDR) (19).

To construct a heatmap and siRNA data matrix, the following procedure was performed. Shifting of the baseline absorbance status of each plate was accounted for by subtracting the values from each well of the regionally normalized data. Therefore, the more negative values were identified as evidence of greater growth inhibitory effect and more positive values as lower growth inhibitory effect, with the negative controls centered at 0 growth inhibitory effect.

To identify genes that show significantly differential cell growth inhibition in the

group of TNBC cell lines compared to the rest, for each siRNA, we pooled the viability values of each siRNA from all 10 TNBC cell lines * 3 replicates. We also pooled the viability values of this siRNA from all 8 non-TNBC cell lines * 3 replicates. Two-sided t-test was used to compare each siRNA in TNBC cell line group to the non-TNBC cell line group. BUM and FDR calculations were also performed. The following parameters were looked at to compare the inhibitory effect, (i) the magnitude of difference in mean inhibition between TNBC cell line group and non-TNBC cell line group and (ii) comparison of the number of siRNAs inhibiting the same gene between TNBC cell line group and non-TNBC cell line group.

To remove inconsistent results, the 61 siRNAs that occurred in the inhibiting TNBC group more and inhibiting non-TNBC group were removed from consideration.

2.5. Cell culture conditions

Breast cancer cell lines were obtained from the American Type Culture Collection (ATCC). The cell lines were cultured in accordance to their recommendations. In accordance to ATCC cell line verification recommendations, microscopic examination to verify morphology, doubling rate analyses, mycoplasma testing, and short tandem repeat (STP) fingerprinting was performed.

2.6. Plasmid rescue experiments

To test the specificity of siRNA results, two distinct silent mutations were introduced to the siRNA binding regions of an exogenous plasmid of LRP8 (human LRP8 pCMV6-AC-GFP) or VLDLR (human VLDLR pCMV6-AC-GFP) to create rescue

plasmids of each receptor protein using Agilent Technologies' QuikChange II XL Site-Directed Mutagenesis Kit. In brief, mutant strand synthesis was performed by denaturing the plasmid DNA templates, annealing mutagenic primers (Sigma-Aldrich, St. Louis, MO) with the desired rescue mutation, and primer extension with *PfuUltra* DNA polymerase. Restriction enzyme digestion with *Dpn* I of the parental strand was performed followed by transformation into XL10-Gold ultracompetent cells for propagation of the rescue plasmid. The Qiagen Plasmid Maxi kit was used to purify rescue plasmids. Breast cancer cell lines expressing either LRP8 or VLDLR were treated with siLRP8 or siVLDLR alone or in combination with the siRNA resistant rescue plasmid. In combination, the cells were treated with the rescue plasmid for 48 hours followed by treatment with the respective siRNA for another 48 and 72 hours. Cell viability was assessed at 48 and 72 hours after siRNA transfection using the CellTiter 96_ AQueous One Solution Cell Proliferation Assay (Promega).

2.7. Ligand stimulation studies

Reelin and apolipoprotein E (ApoE) isoforms 2, 3, and 4 were obtained from R&D Systems and MBL International. Both ligands were dissolved in deionized and distilled water. Therefore, TNBC cells were serum-starved overnight and grown in serum-free media to study the effects of ApoE. In these experiments, controls cells were grown in serum-free medium alone. Breast cancer cell lines were treated with 0.030 nM, 0.060 nM, or 0.120 nM reelin and 150 nM, 300 nM, 600 nM, or 1200 nM of the ApoE isoforms for 72 hours. ApoE is found in fetal bovine serum that supplements media. Low density lipoprotein receptor-related protein associated protein 1 (LRPAP1 or RAP1, Enzo

Life Sciences), an endogenous inhibitor of LRP8 ligand binding, was added at 200 nM in combination with the ApoE isoforms. The CellTiter 96_ AQueous One Solution Cell Proliferation Assay (Promega) was used to determine cell proliferation at 24, 48, and 72 hours. Independent experiments were performed three times for each cell line.

2.8. BrdU incorporation and apoptosis assays

Cells were treated with 25 nM siLRP8 or siVLDLR and exposed to 600 or 1200 nM ApoE4. Bromodeoxyuridine incorporation was measured at 48 and 72 hours using the BrdU Cell Proliferation ELISA assay (Roche Applied Science, Indianapolis, IN). Caspase-3/7 activity was assayed at 48 and 72 hours after treatment using the Apo-ONE Homogeneous Caspase-3/7 Assay (Promega, Madison, WI). Independent experiments were performed three times for each cell line.

2.9. LRP8-ApoE4 solid phase ELISA assay

Recombinant human LRP8-Histidine tagged (R&D Systems, catalog number 3520-AR) was bound overnight at 4^0C to nickel coated 96 well black plates (ThermoFisher Scientific, catalog number 15342) at a final concentration of 10^5 pM in PBS on a lateral rocker. In this assay, we tested the effects of RAP and 3 distinct commercially available anti-LRP8 antibodies, including LRP8 mouse monoclonal antibody targeting amino acids 83-171 (Novus, catalog number H00007804-M01), ApoER2/LRP8 polyclonal antibody targeting the C-terminus (Novus, catalog number NBP1-96573), and mouse IgG as an isotype control (Abcam, catalog number ab37355). RAP was tested at concentrations ranging from 0.01 to 1000 nM and the antibodies were

used at final concentrations of 0.01 to 1000 ug/mL. Each antibody was co-incubated with 600 nM ApoE4 (R&D Systems) for 4 hours at room temperature with the LRP8-coated wells. ApoE4-HRP (ApoE4 conjugated to horseradish peroxidase, Novus, catalog number NBP1-49529H, 1:2000) was incubated for 1 hour at room temperature. The wells were washed twice with 0.01% PBS with Tween-20 (0.01% PBST). Ligand binding was quantified using Thermo Scientific QuantaBlu Fluorogenic Peroxidase Substrate Kits (catalog number 15162) at excitation 315-340 nm and emission 370-470 nm.

2.10. mRNA quantitation and qRT-PCR

Total mRNA was obtained after siLRP8 and siVLDLR transfection experiments with the Qiagen RNeasy kit. Total RNA was reverse transcribed into cDNA and quantitative real-time PCR was performed to determine the level of LRP8 and VLDLR mRNA knockdown using primers Hs01045922_m1 for VLDLR and Hs00171168_m1 for LRP8 (Applied Biosystems).

2.11. Protein quantitation and Western immunoblotting

To determine the level of LRP8 and VLDLR protein, total cell lysates were collected in RIPA lysis buffer (50 mM Tris HCl pH 8, 150 mM NaCl, 1% NP-40, 0.5% sodium deoxycholate, 0.1% SDS, protease inhibitor cocktail from Calbiochem catalog number 539131) and protein was quantified using the BCA Protein Assay (ThermoFisher Scientific, Pittsburgh, PA). Western immunoblotting for LRP8 and VLDLR was performed using antibodies against LRP8 (H00007804-M01 from Novus, 1:500) and VLDLR (NB110-68193 from Novus, 1:1000). The following antibodies and

concentrations were used for reverse phase protein array protein validation: pS473 AKT (Cell Signaling, catalog number 9271, 1:1000), AKT (Cell Signaling, catalog number 9271, 1:1000), pS139 Histone H2AX (Cell Signaling, catalog number 9718, 1:1000), Histone H2AX (Cell Signaling, catalog number 2595, 1:1000), pT202 / pY204 ERK1/2 (Cell Signaling, catalog number 92101L, 1:1000), ERK1/2 (Cell Signaling, catalog number 9102, 1:1000), pT180 / p182 p38 (Cell Signaling, catalog number 9211, 1:1000), p38 (Cell Signaling, catalog number 9212, 1:1000), COX2 (Epitomics, catalog number 2169-1, 1:500), Rab25 (Cell Signaling, catalog number 4314, 1:1000), Snail (Cell Signaling, catalog number 3895, 1:5000), β-actin (Santa Cruz, catalog number sc-1615, 1:1000).

2.12. Reverse phase protein array

To assess the effects of ApoE4 stimulation on oncogenic protein expression and determine the phosphorylation status of important regulatory proteins, BT-549 and MDA-MB-436 TNBC cell lines were treated with 600 nM of ApoE4 using three technical replicates and reverse phase protein array was performed. Total cell lysates were isolated at baseline (0 hours) and at 8 and 48 hours after stimulation from control and ApoE4 treated cells. In brief, breast cancer cells were trysinized and pelleted by centrifugation. Cells were lysed using RIPA lysis buffer. Total protein of the cleared total cell lysate was quantified using the BCA Protein Assay. Reverse phase protein array was performed as previously described, using 230 antibodies against 201 proteins (48). In brief, cellular proteins were denatured with 1% SDS and beta-mercaptoethanol. Serial dilution series was prepared in 1% SDS lysis buffer and arrayed onto nitrocellulose-

coated slides, along with corresponding positive and negative controls. Primary antibodies and biotin-conjugated secondary antibodies were used to probe each array. For each antibody, the correlation between RPPA signal and Western immunoblotting was >0.7. For data analyses, signal intensities were modeled using Supercurve Fitting, log-2 transformed, and median centered. Unequal variance t-test was used to identify differentially expressed proteins and FDR was calculated as described above.

2.13. Metabolomic profiling

For metabolomic analysis, BT-549 cells were cultured using seven different treatment conditions and five technical replicates for each condition. The treatment groups are as follows: (i) regular media (T=0 hrs), (ii) regular media (T=48 hours), (iii) serum-free media (T=48 hrs), (iv) serum-free media with 600 nM ApoE4 (T=48 hours), (v) serum-free media with siCON (T=48 hours), (vi) serum-free media with siLRP8 (T=48 hours), and (vii) serum-free media with siLRP8/600 nM ApoE4 (T=48 hours). After 48 hours, cells were harvested with trypsinization, washed twice with PBS, and were stored in liquid nitrogen until shipment to Metabolon, Inc. (Durham, NC) for metabolic profiling. Metabolomic profiling was performed using gas chromatography/mass spectrometry (GC/MS) and liquid chromatography/tandem mass spectrometry (LC/MSMS) methods as described previously (49, 50).

2.14. shLRP8 MDA-MB-231 stable knockdown cell line

Mission shRNA lentiviral transduction particles against LRP8 were used to generate stable knockdown of LRP8 in MDA-MB-231 (Sigma-Aldrich, St. Louis, MO). 5 shRNA clones (TRCN0000055498, TRCN0000055499, TRCN0000055500, TRCN0000055501, TRCN0000055502) were tested to generate the stable knockdown cell line. Clones from TRCN0000055498 and TRCN0000055499 batches resulted in the most efficient and sustainable LRP8 protein knockdown. Optimal MOI and puromycin responses were tested for MDA-MB-231 and optimal conditions were maintained. In brief, target cells were transduced with each shLRP8 clone at an MOI of 20 and polybrene (Sigma-Aldrich, St. Louis, MO) at final concentration of 8 μg/mL. 48 hours after transduction, target cells were selected for with 4 μg/mL puromycin (Sigma-Aldrich, St. Louis, MO) in DMEM-F12 media (Invitrogen, Grand Island, NY). After initial selection, the stable knockdown cell lines were maintained in DMEM-F12 media with 2 μg/mL puromycin. Stable knockdown clones were selected using GFP expression and level of LRP8 knockdown assessed with Western immunoblotting.

2.15. shLRP8 MDA-MB-231 mouse xenograft studies

Female athymic Nude-Foxn1 nude mice (Nu/Nu) were purchased from Harlan (Indianapolis, Indiana USA). The mice were housed in laminar flow cabinets under specific pathogen-free conditions and used when they were 8 weeks old. The animals were maintained in facilities approved by the American Association for Accreditation of Laboratory Animal Care in accordance with the current regulations and standards of the U.S. Department of Agriculture, Department of Health and Human Services, and

National Institutes of Health. For all in vivo experiments, MDA-MB-231 tumor cells stably transfected with shRNA against LRP8 in the exponential proliferation phase were harvested after brief exposure to a 0.25% trypsin/0.02% EDTA solution. The cell suspension was pipetted to obtain single-cell suspensions. The cells were washed, resuspended in PBS, and diluted to the desired cell number. Cell viability was determined using trypan blue exclusion on an automated ViCELL cell counter. Single-cell suspensions of >95% viability were used. In brief, 2 x 10^6 tumor cells in 0.1 mL of RPMI-1640 serum free medium with 50% Matrigel (BD Matrigel, BD Biosciences, San Jose, CA, USA) were injected subcutaneously at the 4th pair mammary gland on each side. Tumor growth was monitored by palpation and the onset of tumors was noted. Tumor size was measured with digital calipers and tumor volume was calculated assuming an ellipsoid shape with the following equation: Tumor volume (mm3) = (Length x Width^2) x $\pi/6$. The animals were killed 10 weeks after tumor cell inoculation. Afterwards, subcutaneous tumors were harvested and weighed. Individual tumors were split for fixation in 4% paraformaldehyde for histology and immunostaining and flash frozen in liquid nitrogen for RNA and protein collection. Organs were fixed in Bouin's solution for 24 hours to differentiate neoplastic lesions from organ parenchyma. Metastases were counted with the aid of a dissecting microscope, and confirmed by routine histology. Representative data were obtained from five mice per experimental group.

2.16. Immunohistochemistry

59 ER-negative and ER-positive patient tumor samples were identified for testing. In brief, patient data was extracted for all cases, tissue slides were collated, and immunohistochemical testing through The University of Texas M.D. Anderson Cancer Center Histology Core Laboratory was ordered. The following was the general staining protocol performed by the Histology Core. Slides were hydrated with deionized and distilled water. Antigen retrieval was performed with citrate buffer. The slides was cooled in buffer for 15 minutes and transferred to tris buffered saline (TBS). Slides were blocked 15 minutes with 3% hydrogen peroxide and rinsed twice with TBS for 5 minutes each rinse. Slides were blocked with avidin for 10 minutes and rinsed twice in TBS for five minutes each. Slides were blocked with biotin for 10 minutes and rinsed twice in TBS for five minutes each. All slides were blocked for 15 minutes with whole serum from the animal species corresponding to the secondary antibody (i.e., if the secondary was anti-mouse biotinylated then the blocking serum was whole mouse IgG). After blocking, the serum was drained off each slide. LRP8 (Abnova PAB4740 – rabbit polyclonal antibody) was diluted at 1:50 and VLDLR (Abcam ab 62543 – mouse monoclonal antibody) was diluted at 1:50 with TBS buffer for an hour.

The association between clinicopathologic variables (age, ER status, HER2 status, stage, nuclear grade, and Ki67) and LRP8 protein expression was tested. P-values were based on Fisher's exact test with $N \leq 5$ (two-sided, 95% confidence interval, $\alpha<0.05$). LRP8 protein expression was divided into discrete variables: (i) LRP8 strong expression, LRP8 moderate expression, LRP8 weak expression, or (ii) LRP8 positive, LRP8 negative.

2.17. APOE genotyping of breast cancer patient samples

To compare the rate of apolipoprotein E4 (ApoE4) carrier genotype between women with ER-negative / ER-positive breast cancer who are <50 years and those who are >70 years of age, ApoE genotyping was performed (M. D. Anderson Cancer Center Institutional Review Board protocol LAB11-0009). DNA from 50 ER-negative and 50 ER-positive patients were collected under M. D. Anderson Cancer Center protocol LAB03-0479 and used for ApoE genotyping. DNA from late onset breast cancer patients (>70 years of age) was collected under M. D. Anderson Cancer Center protocol 2005-0388 and LAB90-049 and obtained from the M. D. Anderson Cancer Center Breast Serum Bank. DNA was quantified using NanoDrop 2000 spectrophotometer and stored at -80C until shipment to Kimball Genetics for APOE genotyping through restriction fragment length polymorphism analysis. In brief, PCR amplification using primers surrounding the APOE gene was performed and followed by restriction digestion cleavage of amplified products. Polyacrylamide gels were used to resolve the fragments and APOE genotype was determined by band migration patterns.

Chapter 3 – Results

3.1. Identification of 681 overexpressed genes in human triple-negative breast cancer

In the discovery dataset (n=294), 3,473, 5,413, and 8,418 probe sets were differentially expressed in TNBC (n=73) compared to non-TNBC (n=221) at an FDR of <0.00001, <0.0001, and <0.001 respectively. Among these probe sets, 1,871, 3,380, and 5,748 were then overexpressed in TNBC at an FDR of <0.00001, <0.0001, and <0.001 respectively. Our focus was on the 1871 genes that are overexpressed at an FDR level of <0.00001. Sixty-two percent of these genes (n=1162) were also overexpressed in TNBC cases (n=56) vs. non-TNBC (n=230) in the second independent validation dataset (n=286, individual p-values <0.05). We introduced another filter to reduce the number of genes and increase our confidence in these genes by removing all genes with <2.0 fold overexpression and with p-values >0.0001 observed in the validation dataset. This resulted in 681 genes with at least two-fold overexpression in TNBC with p<0.0001 in two independent data sets. The 681 candidate genes belonged to six distinct functional categories (Figure 2).

To increase confidence in these results, we examined what proportion of the 681 TNBC genes are located in DNA segments that are amplified in TNBC. We used data from a subset of 103 cases, including 35 TNBC, from the MDACC discovery set that also had matching CGH results from Agilent Human 4x44K CGH arrays. The ADM-2 algorithm of CGH Analytics v3.4.40 software was used to identify DNA copy number anomalies, low level copy number gain was defined as a log2 ratio >0.25. Seventy-three TNBC genes (11%) were mapped to DNA segments that showed at least low level copy number gain in ≥10% of TNBC cases.

2 independent gene expression datasets of human breast cancer	Number of overexpressed genes in TNBC >2-fold overexpression p<0.0001 FDR 0.00001
TNBC vs. non-TNBC	681 Involved in CELL CYCLE IMMUNE METABOLISM MITOGENS NEURONAL TRANSCRIPTION

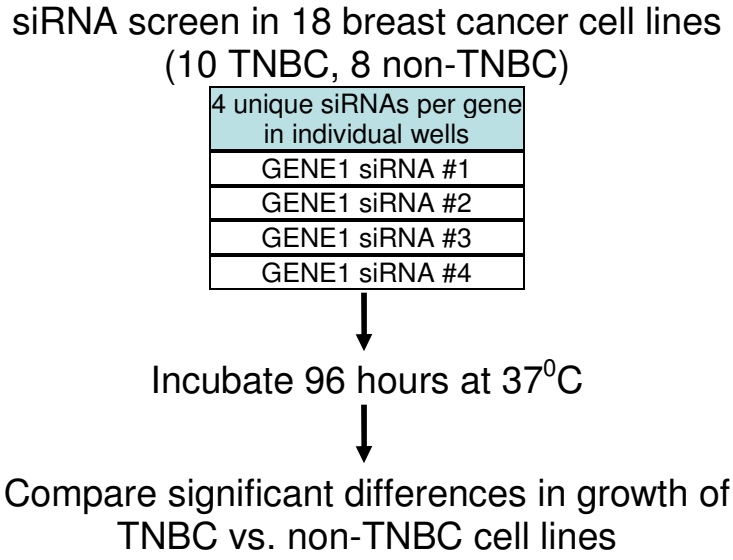

Figure 2. Functional categorization and growth inhibition testing of the 681 candidate genes identified through analyses of gene expression profiles. Using Ingenuity Pathway Analysis, the 681 candidate genes belonged to 6 distinct functional families. The inhibition of each gene in a growth assay was tested in a custom siRNA screen of 18 breast cancer cell lines. 4 distinct siRNA oligonucleotides against each gene were tested in each cell line and the growth inhibitory effect was compared between TNBC and non-TNBC cell lines.

3.2. Identification of critical growth genes that sustain the viability of triple-negative breast cancer cell lines

Each cell line was treated with 4 unique siRNAs against each candidate target in 384-well plate format. The list of candidate targets was reduced from 681 to 674 due to the availability of complete sets of 4 siRNAs for each submitted. Optimized negative and positive controls were also included on each plate. The data values were regionally normalized to account for multiple standard deviations from the mean. Bioinformatic analysis of the results to identify the siRNAs that significantly inhibited cell growth in a given cell line was performed by (i) one-sided t-test between the three replicates of each siRNA and pooled negative control values and (ii) Beta-uniform mixture (BUM) to construct a distribution model of the p-values from the t-tests and establish a threshold cutoff value for multiple false discovery rates (FDR) of varying stringency levels.

To identify the siRNAs that significantly inhibited cell growth differently between the TNBC vs. non-TNBC cell lines, pooled viability values for the three replicates for each siRNA from all 10 TNBC cells lines was compared by two-sided t-test to the pooled viability values for the three replicates for each siRNA from the 8 non-TNBC cells lines. The receptor status according to gene expression distribution is displayed in Appendix A1. BUM modeling was performed to establish p-value cutoffs and FDR levels. A list of siRNAs that inhibited growth preferentially in the TNBC cell line group was generated (Appendix Table A2). A separate list of siRNAs that preferentially inhibited growth in the non-TNBC group was also generated (Appendix Table A3).

3.3. Two high confidence hits, LRP8 and VLDLR, from the siRNA screen

The number of siRNAs that inhibited growth preferentially out of the set of 4 for each gene was compiled from the above comparisons to determine the top tier siRNA hits that generated the most reproducible growth inhibition for any one gene. Screen hits were categorized by the number of siRNA oligonucleotides which preferentially inhibited TNBC cell lines (n=10) compared to non-TNBC cell lines (n=8). There were 27 genes which were preferentially inhibited by 2 or more siRNA oligonucleotides in the TNBC group. There were 2 genes (LRP8 and VLDLR) which were preferentially inhibited by 3 of 4 siRNA oligonucleotides in TNBC cell lines and were the highest confidence hits of the siRNA screen. They are the low density lipoprotein receptor-related protein 8 (LRP8) and the very low density lipoprotein receptor (VLDLR). There were no genes that were preferentially inhibited by 4 out of 4 siRNAs in either the TNBC or non-TNBC cell line groups.

The hits belonged to a variety of functional groups involved in cancer cell proliferation and cell cycle regulation. There were also several genes which belonged to functional groups that have not been characterized in the context of cancer, including several neural signaling components and mediators of metabolism. Initial assessments of overall druggability of each candidate targets were performed on the basis of their roles in other cancer types, their presence in a successfully targeted gene family, and availability of methods and reagents for experimental investigation.

3.4. LRP8 and VLDLR, and their ligands, are co-expressed or overexpressed in human triple-negative breast cancers

To investigate the potential role of LRP8 and VLDLR pathway members in human TNBC, re-analysis of two other gene expression datasets was performed (55, 56), in conjunction with the initial discovery and validation datasets. A major ligand of LRP8 and VLDLR, reelin, was co-expressed along with the receptors (Table 1). The other major ligand, apolipoprotein E (APOE), was highly overexpressed along with LRP8 and VLDLR, in 3 of the 4 datasets. The intracellular adapter protein, DAB1, was also co-expressed at lower levels. The 2 receptors identified from the siRNA screen, LRP8 and VLDLR and their ligands APOE and reelin, are co-expressed in human triple-negative breast cancer.

3.5. Validation of siRNA screen results through confirmation of target mRNA and protein down-regulation

To confirm that the actual levels of the identified targets, LRP8 and VLDLR, were modulated by the siRNAs, transient transfection was performed with the same siRNA oligonucleotides used in the siRNA screen. 4 unique siRNAs targeting LRP8 and 4 unique siRNAs targeting VLDLR were tested separately at 25 and 50 nM. Target mRNA levels, protein levels, and viability of 4 different LRP8 and VLDLR-expressing TNBC cell lines were measured. mRNA and protein levels decreased after siRNA transfection, in the 4 siRNA oligonucleotides (Figure 1 and 2). A dose-dependent decrease in the viability of TNBC cell lines was observed compared to a non-targeting siRNA control oligonucleotide (Figure 3).

A

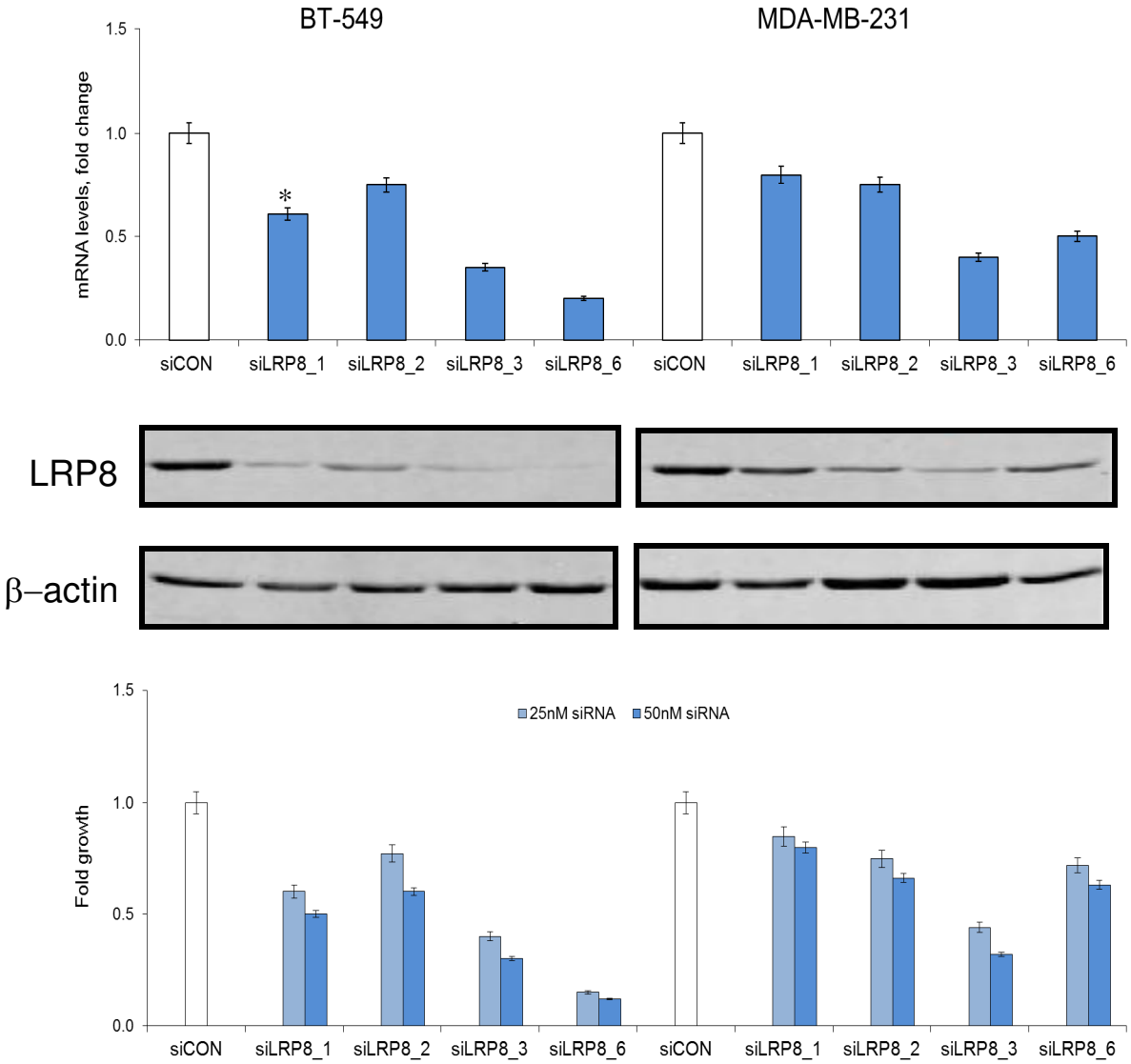
BT-549
MDA-MB-231
mRNA levels, fold change
1.5
1.0
0.5
0.0
*
siCON
siLRP8_1
siLRP8_2
siLRP8_3
siLRP8_6
LRP8
β–actin
25nM siRNA
50nM siRNA
Fold growth

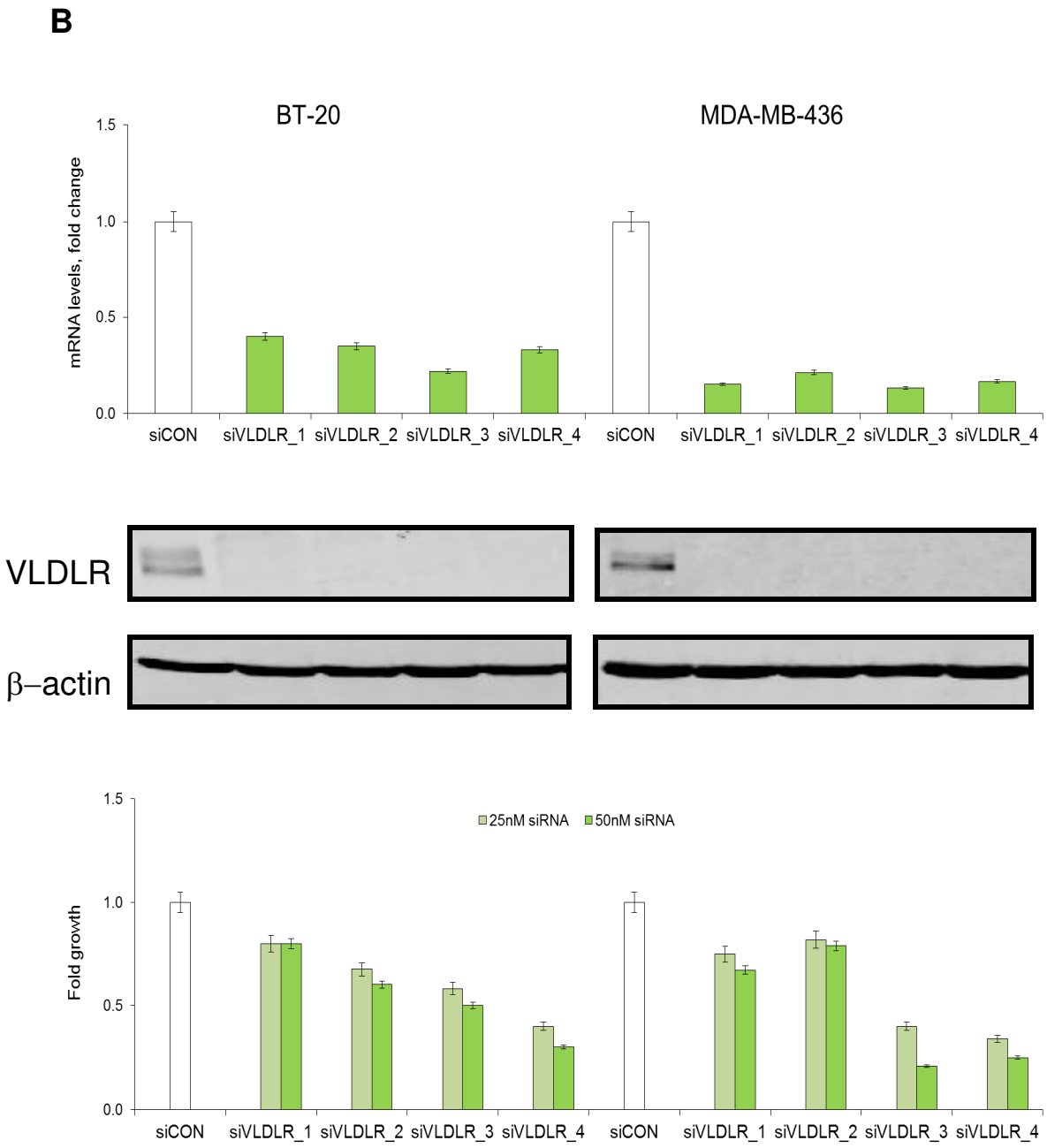

Figure 3. Confirmation of siLRP8 and siVLDLR downregulation of target mRNA, protein, and growth inhibition. (A) Top panel represents fold mRNA change in LRP8 after treatment with each of 4 siLRP8 oligonucleotides (denoted siLRP8_1, siLRP8_2, siLRP8_3, siLRP8_6). The middle panel represents protein change in LRP8 after each of 4 siLRP8 in comparison to β–actin. The bottom panel represents fold growth in LRP8 after siLRP8 treatment in comparison to siCON. (B) Data is shown from siVLDLR testing in the same order as panel A. *$p<0.001$, paired t-test when compared to siCON, error bars indicate standard error.

3.6. Validation of siRNA screen results through siRNA-resistant plasmid rescue of the phenotype

To confirm that the siRNA screen hits, LRP8 and VLDLR, were specific and not a result of off-target effects, plasmid rescue experiments were performed. siRNA resistant plasmids were constructed by introducing silent wobble mutations in the siRNA binding region of plasmids encoding for either LRP8 or VLDLR. If the siRNA is unable to bind to this siRNA-resistant copy of the gene of interest, the phenotype is rescued. This indicates that the loss of phenotype is specific to the target gene knockdown and not an artifact of off-target effects. The co-transfection of siRNAs and siRNA-resistant plasmid rescued the loss of viability, similar to the measured levels of viability for siRNA-resistant plasmid alone and compared to siRNA transfection alone (Figure 4). This was observed for each of the 4 siRNAs targeting LRP8 and VLDLR.

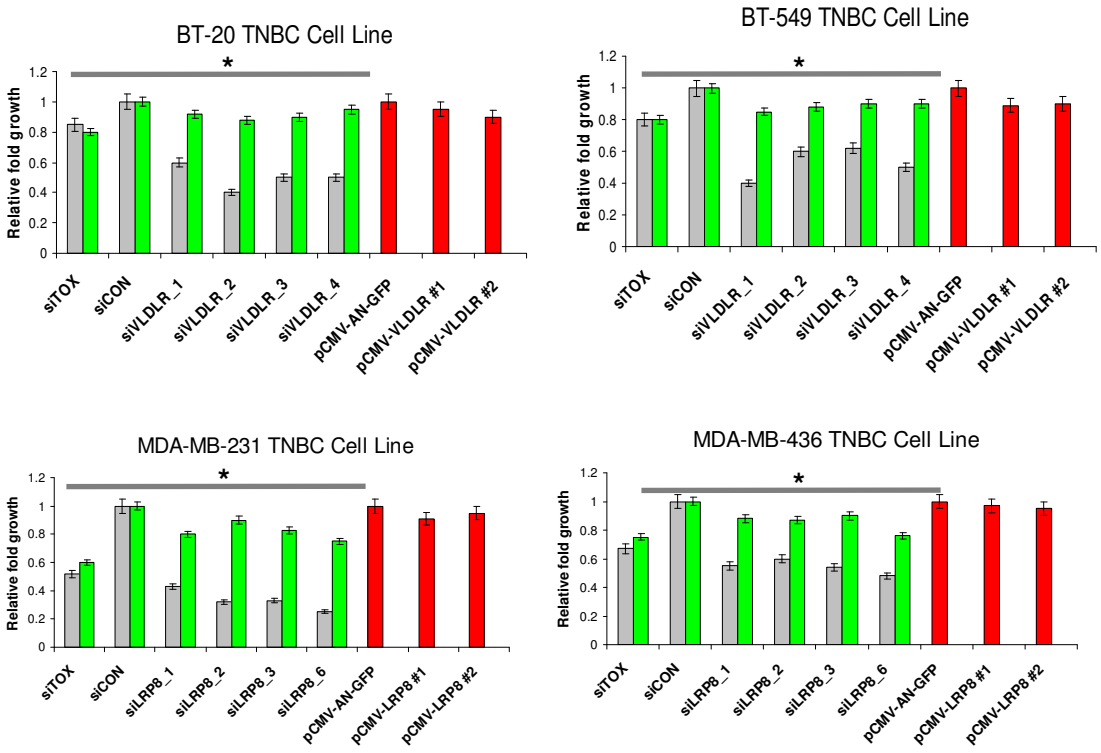

Figure 4. Plasmid rescue experiments used in validating siRNA screen results. Plasmid rescue validation experiments confirmed that growth inhibition was due to siRNA-mediated downregulation of LRP8 or VLDLR. TNBC cells were transfected with siLRP8 or siVLDLR alone (gray), LRP8 or VLDLR rescue plasmid with silent mutations in the siRNA binding region alone (red), or the combination of siLRP8 or siVLDLR and rescue plasmid (green). TNBC cell viability was rescued with the combination of siLRP8 or siVLDLR and rescue plasmid. Representative data from replicate experiments in four TNBC cell lines, BT-20, BT-549, MDA-MB-231, and MDA-MB-436.*$p<0.01$ with paired t-test when compared to siRNA alone, error bars indicate standard error.

3.7. Functional importance of LRP8-APOE signaling in triple-negative breast cancer

In order to investigate how LRP8 signaling affects the ability of TNBC tumors to proliferate, the combination of in vitro ligand stimulation and loss-of-function studies with siRNA and shRNA against LRP8 were completed in LRP8-expressing TNBC cell lines. The global gene expression, protein, and metabolic changes that were induced as a result of LRP8 signaling were studied using transcriptomic, proteomic, and metabolomics arrays. The study ends with investigations into the effect of LRP8 knockdown on TNBC tumor xenograft growth, the tissue expression level of LRP8, and the frequency of the ApoE4 genotype in early and late onset breast cancer patients.

3.8. Triple-negative breast cancer cell lines express LRP8 and VLDLR and their cognate ligands, reelin and APOE

To validate siRNA screen findings and investigate functional importance of LRP8 and VLDLR, several breast cancer cell lines were identified from their sensitivity to growth inhibition after siLRP8 and siVLDLR in the initial siRNA screen and their level of LRP8 and VLDLR mRNA and protein expression. To determine the breast cancer cell lines which could serve as model systems for the investigation of LPR8 and VLDLR signaling, the target mRNA and protein levels were measured in our panel of 18 breast cancer cell lines. We also interrogated a publicly available gene expression dataset of 51 breast cancer cell lines (46).

In the breast cancer cell line panel, triple-negative breast cancer cell lines had co-expression of LPR8, VLDLR, and APOE of mRNA (Table 1). At least 1 non-triple

negative breast cancer cell line had high gene expression of APOE with lower expression of LRP8 and VLDLR. In the publicly available gene expression dataset of 51 breast cancer cell lines, the TNBC cell line group had higher co-expression of LPR8, VLDLR, and APOE, compared to the non-TNBC cell line group (Table 1). mRNA and protein co-expression of the 2 target receptors, LRP8 and VLDLR, was observed for several TNBC cell lines (Figure 5 and 6). BT-20, BT-549, MDA-MB-231, and MDA-MB-468 cell lines were chosen for validation and functional studies based on co-expression of LRP8 and VLDLR, as well as their cognate ligands, Reelin and ApoE.

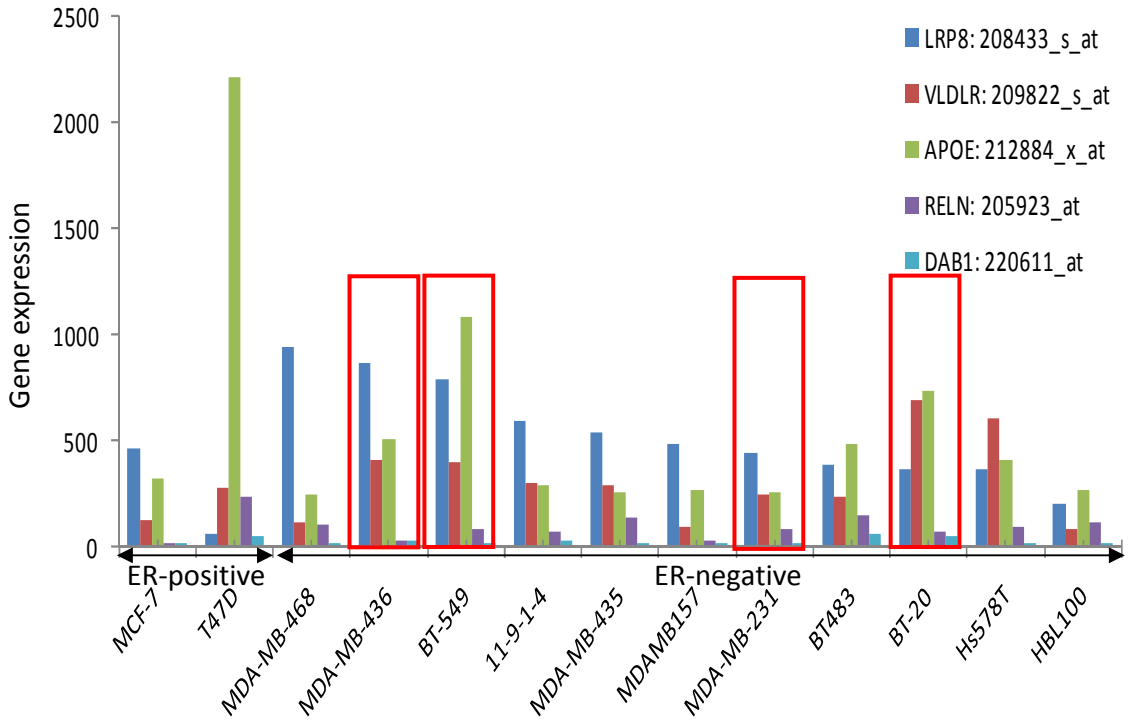

Figure 5. Co-expression of LRP8/VLDLR receptor - ligand system in breast cancer cell line data set. The probe set with the highest mean value and greatest variance was selected to compare normalized gene expression values of the two receptors (LRP8 and VLDLR), two ligands (APOE and RELN), and major intracellular adaptor protein, DAB1.

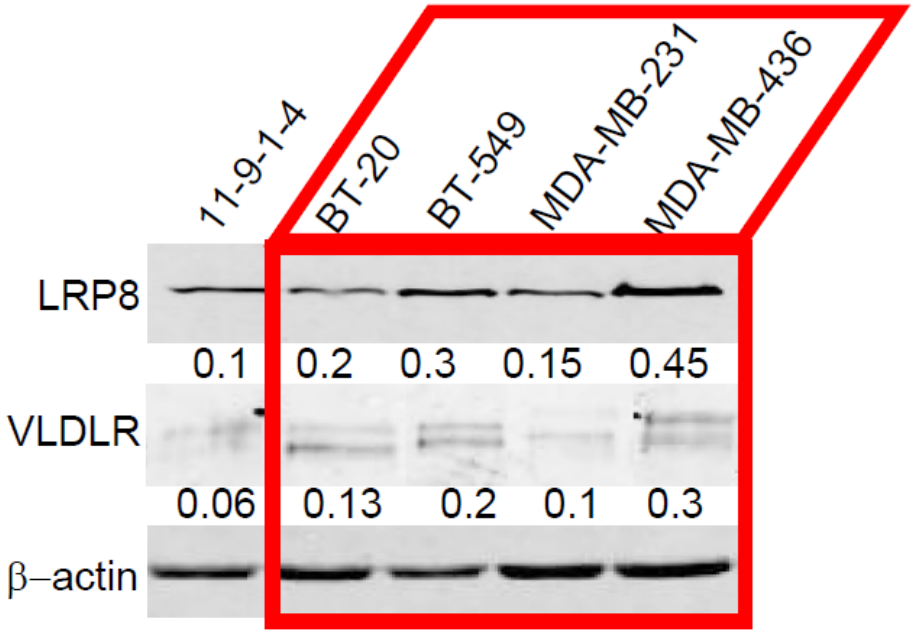

Figure 6. Protein expression of LRP8 and VLDLR in triple-negative breast cancer cell lines. Target protein levels in TNBC cell lines were assayed using Western immunoblotting. Relative protein levels were normalized to β–actin. 4 TNBC cell lines, shown in red, co-express both receptors, LRP8 and VLDLR, and were chosen for further validation experiments.

Table 1. Class comparison test between ER-negative and ER-positive breast cancer for the LRP8/VLDLR receptor - ligand system.

Table 1. Class comparison test between ER+/HER2- and ER-/HER2- breast cancer

		LRP8 (Probe set: 208433_s_at)							VLDLR (Probe set: 209822_s_at)						
	Number of samples	*P*-value*	*FDR*†	ER+/HER2-			ER-/HER2-		*P*-value*	*FDR*†	ER+/HER2-			ER-/HER2-	
Data set	(ER+HER2-/ER-HER2-)			Average		SD‡	Average	SD‡			Average		SD‡	Average	SD‡
MDACC/MAQC	133/65	<'0.001	<'0.001	296.8	±	181.0	558.4	± 227.4	<'0.001	<'0.001	252.8	±	176.8	491.8	± 258.0
Wang	178/56	<'0.001	<'0.001	137.9	±	108.0	296.8	± 130.4	<'0.001	<'0.001	250.5	±	129.6	460.1	± 277.1
TRANSBIG	124/46	<'0.001	<'0.001	215.6	±	126.8	421.9	± 271.0	<'0.001	<'0.001	236.1	±	129.1	389.6	± 205.0
Mainz	155/23	<'0.001	<'0.001	110.8	±	61.2	266.6	± 122.3	<'0.001	<'0.001	307.0	±	167.7	636.0	± 503.6
51 cell line	13/25	0.493	0.638	919.1	±	401.8	1060.9	± 784.1	0.135	0.422	439.0	±	218.4	680.2	± 1179.1
19 cell line	2/11	0.776	0.166	1069.2	±	277.0	1145.0	± 688.2	0.386	0.815	339.1	±	16.7	469.2	± 322.5

		RELN (Probe set: 205923_at)							DAB1 (Probe set: 220611_at)						
	Number of samples	*P*-value*	*FDR*†	ER+/HER2-			ER-/HER2-		*P*-value*	*FDR*†	ER+/HER2-			ER-/HER2-	
Data set	(ER+HER2-/ER-HER2-)			Average		SD‡	Average	SD‡			Average		SD‡	Average	SD‡
MDACC/MAQC**	133/65	0.130	0.163	109.9	±	100.5	133.9	± 282.7	0.936	0.936	32.0	±	39.6	31.7	± 33.0
Wang***	178/56	0.678	0.689	160.7	±	125.5	153.9	± 355.6	0.689	0.689	21.2	±	16.3	20.4	± 22.7
TRANSBIG****	124/46	0.224	0.280	83.4	±	152.9	68.2	± 87.8	0.051	0.0846	14.6	±	15.3	11.9	± 9.1
Mainz*****	155/23	0.563	0.692	87.3	±	70.6	78.5	± 245.3	0.692	0.692	10.0	±	6.5	7.0	± 3.5
51 cell line^	13/25	0.510	0.638	190.3	±	178.6	229.4	± 196.3	0.169	0.422	67.3	±	32.1	53.0	± 30.8
19 cell line	2/11	0.716	0.815	71.2	±	149.3	86.7	± 39.9	0.878	0.815	30.5	±	24.2	28.7	± 15.3

		APOE (Probe set: 212884_x_at)						
	Number of samples	*P*-value*	*FDR*†	ER+/HER2-			ER-/HER2-	
Data set	(ER+HER2-/ER-HER2-)			Average		SD‡	Average	SD‡
MDACC/MAQC	133/65	<'0.001	<'0.001	1549.0	±	1363.3	2160.3	± 2759.1
Wang	178/56	0.034	0.056	1943.8	±	1110.7	2278.7	± 2009.1
TRANSBIG	124/46	0.471	0.471	1609.0	±	711.1	1529.9	± 666.8
Mainz	155/23	<'0.001	<'0.001	1397.9	±	629.7	2037.0	± 1716.3
51 cell line	13/25	0.883	0.883	632.3	±	1236.2	654.1	± 1006.8
19 cell line	2/11	0.111	0.279	846.6	±	1337.9	384.7	± 226.0

ER: Estrogen Receptor; HER2: Human Epidermal Growth Factor Receptor 2
**P*-value was based on normal distribution. *P*-values less than .05 were considered statistically significant.
†FDR: False Discovery Rates
‡SD: Standard Deviation
**MDACC/MAQC GSE16716
***Wang GSE2034
****TRANSBIG GSE7390
*****Mainz GSE11121
^ArrayExpress accession number E-TABM-157

3.9. Triple-negative breast cancer cell lines express apolipoprotein E isoform 4

Separate capture ELISA experiments revealed that BT-549 and MDA-MB-436 express ApoE4 and all other forms of APOE (isoforms 2 and 3 represented by total APOE), within the cell and also extruded the lipoproteins into the media, as evidenced by binding signals of samples taken from the total cellular lysate and isolated culture supernatant (Figure 7). Cells grown in regular media expressed and secreted the highest levels of ApoE4 and total ApoE in the media (possibly from non-specific binding of lipids from fetal bovine serum in regular media). Cells grown in OptiMem expressed the most ApoE4 and total ApoE internally (possibly due to up-regulation of lipid production).

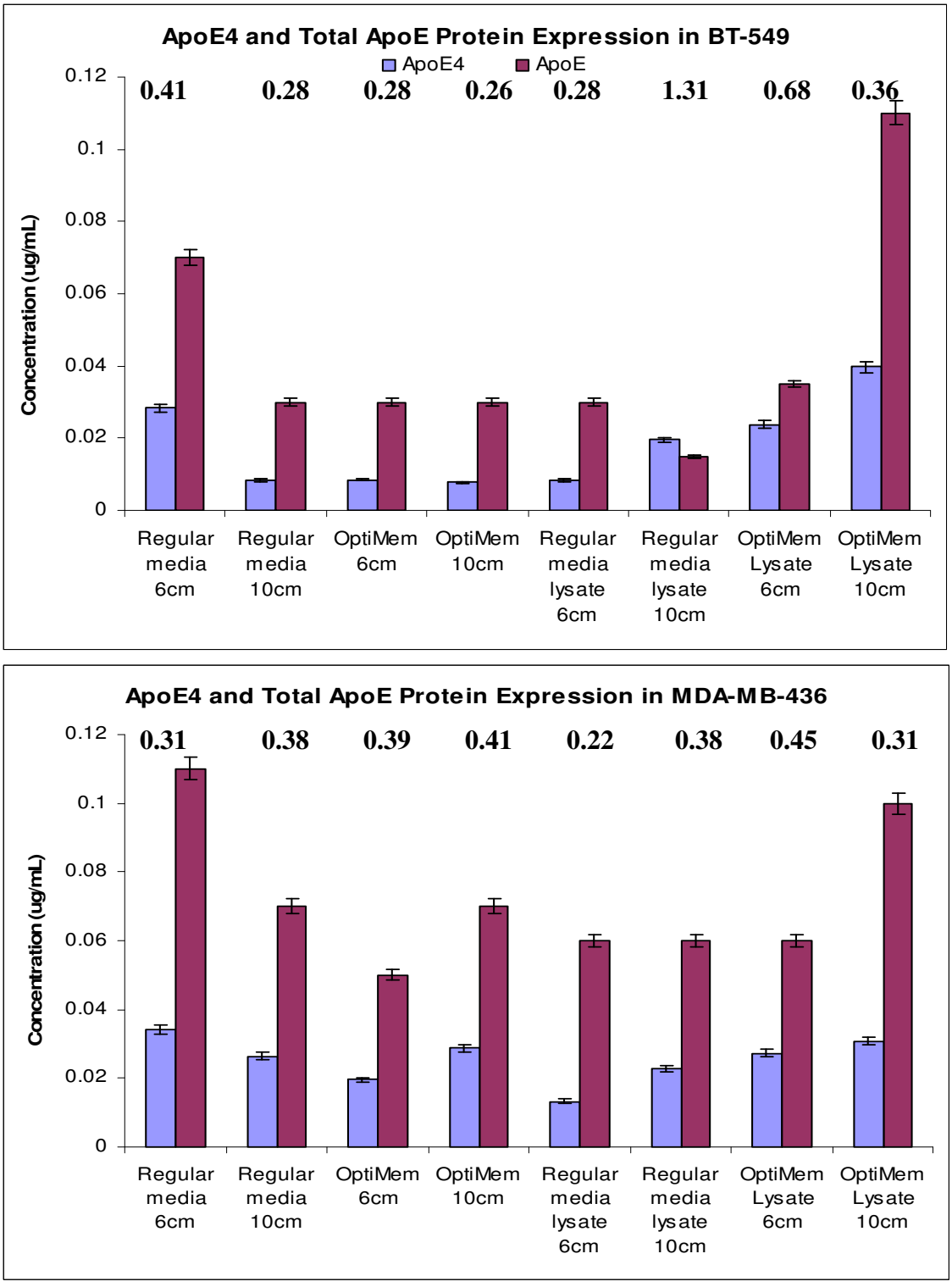

Figure 7. ApoE4 and total APOE protein expression in BT-549 and MDA-MB-436 triple-negative breast cancer cell lines. Detection of ApoE4 and total APOE (ApoE2, ApoE3, ApoE4) was performed using ELISA antibody detection.

3.10. Reelin stimulates the growth of triple-negative breast cancer cell lines

Reelin stimulation increases viability of BT-549 and MDA-MB-231 at 96 hours after treatment (Figure 8). Reelin stimulation increases viability of MDA-MB-436 at 48 hours after treatment (Figure 8). The BT-20 cell line was not stimulated by reelin treatment (Figure 8). This effect is more pronounced in cell lines which express higher levels of both LRP8 and VLDLR protein. Reelin treatment results in lower transient stimulation of BT-20 at 48 hours, which expresses higher protein levels of VLDLR. This suggests that reelin binds to LRP8 with greater affinity than VLDLR.

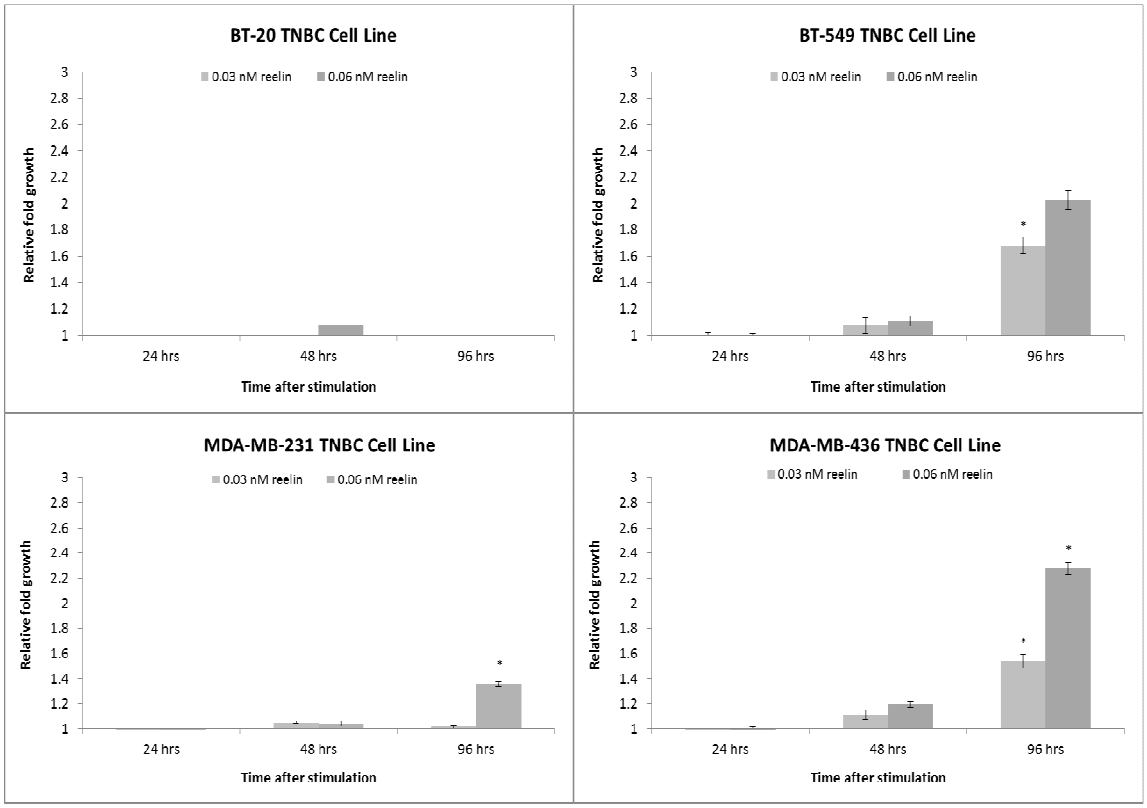

Figure 8. Effect on proliferation of reelin treatment on TNBC cell lines. TNBC cell lines were treated with 0.03 nM or 0.06 nM reelin for 24, 48, or 96 hours and their relative rate of growth assessed with the MTS assay. *p<0.01 with paired t-test when compared to untreated control, error bars indicate standard error.

3.11. Stimulatory effect of apolipoprotein E is isoform-dependent

TNBC cell lines were treated with increasing concentrations of human TNBC cell lines that co-express LRP8 and VLDLR were treated with reelin and the 3 isoforms of ApoE; ApoE2, ApoE3, and ApoE4. ApoE isoform 2 inhibited TNBC cell growth in a dose-dependent manner, ApoE isoform 3 did not affect growth, and ApoE isoform 4 promoted growth of TNBC cell lines (Figure 9). This effect was observed with varying lots of recombinant human APOE isoforms from 2 different manufacturers (Figure 9). The effects of apolipoprotein E on TNBC viability and growth was isoform dependent, with ApoE4 stimulating growth from 2 to 4 fold of mock treated cells. The ligands of LRP8 and VLDLR, Reelin and ApoE4, stimulated TNBC cells and increased cell viability. Transient knockdown of either receptor resulted in the abrogation of the ApoE4-mediated stimulatory response, indicating that growth signals were dependent on the interaction between ApoE4 and either LRP8 or VLDLR (Figure 10).

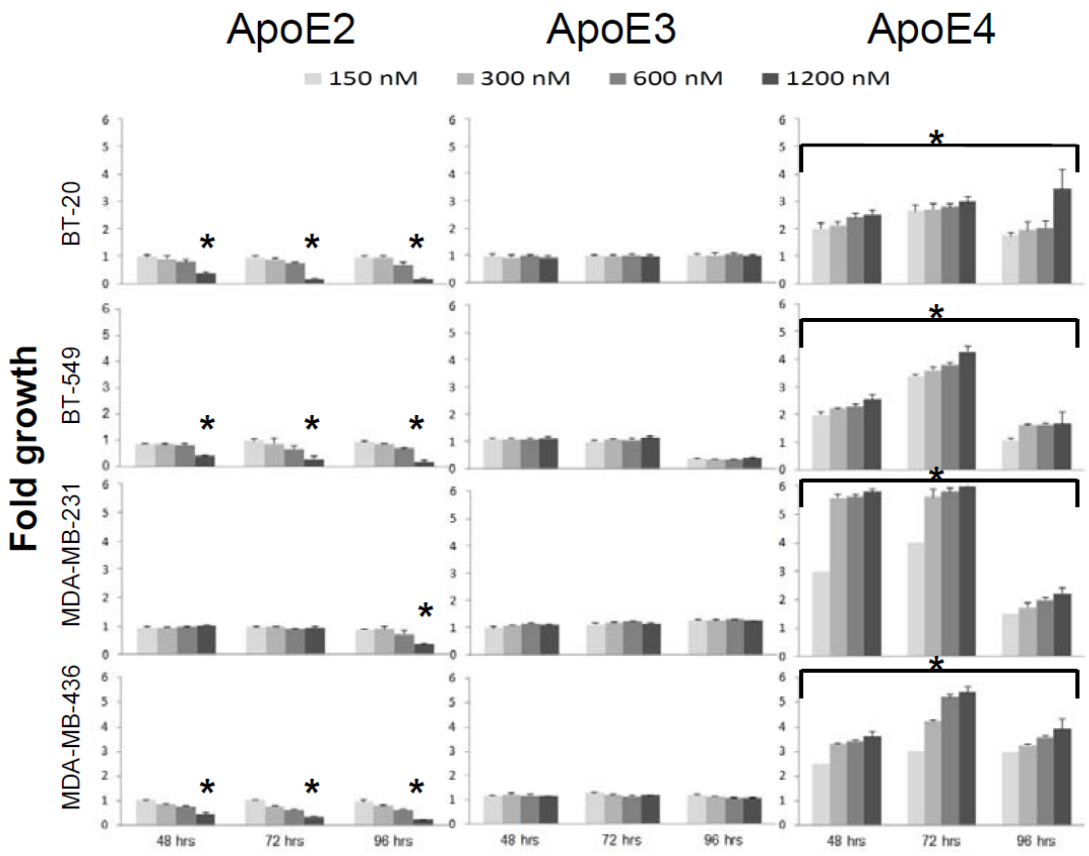

Figure 9. Differential growth effects of apolipoprotein E isoforms on proliferation of TNBC cell lines. BT-20, BT-549, MDA-MB-231, and MDA-MB-436 were treated with ApoE2, ApoE3, and ApoE4 isoforms and the effect on proliferation assessed through the MTS growth assay. ApoE2 inhibited growth, ApoE3 had an overall null effect on growth, and ApoE4 stimulated growth from 1.5 to 6-fold of untreated control. *$p<0.01$ with paired t-test when compared to untreated control, error bars indicate standard error.

A

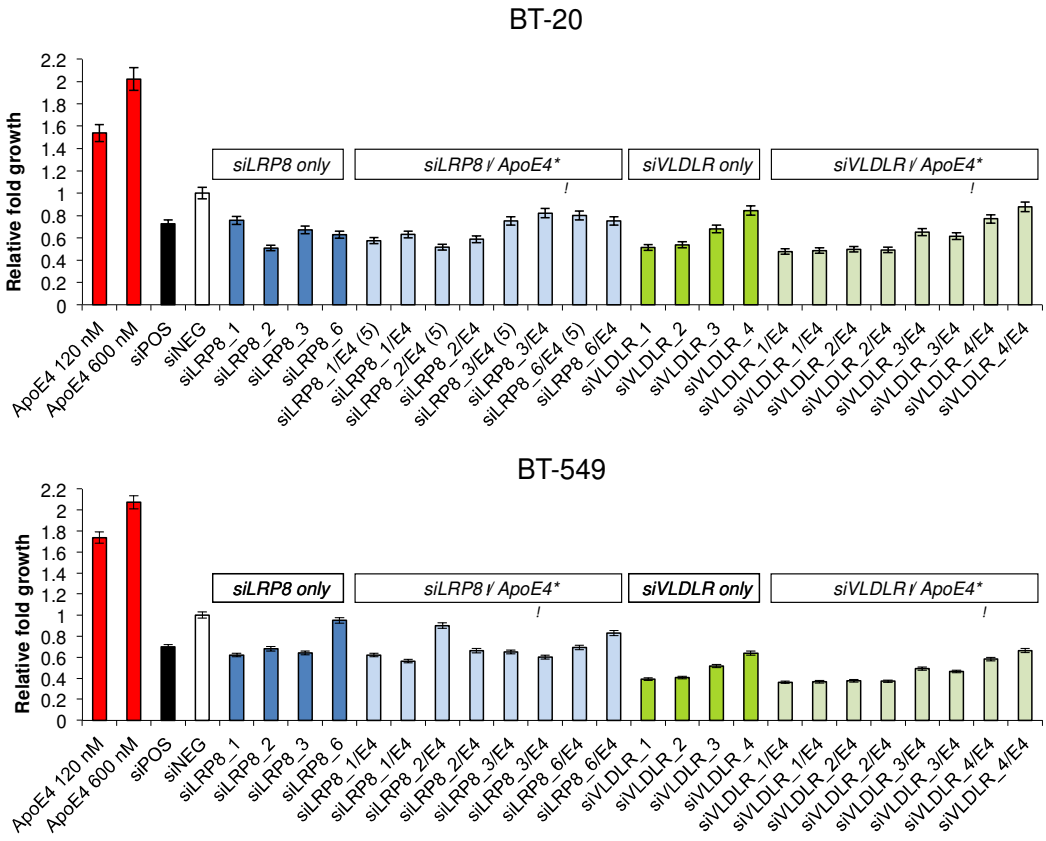
BT-20
Relative fold growth
2.2
2
1.8
1.6
1.4
1.2
1
0.8
0.6
0.4
0.2
0
siLRP8 only
siLRP8 / ApoE4*
siVLDLR only
siVLDLR / ApoE4*
!
!
ApoE4 120 nM
ApoE4 600 nM
siPOS
siNEG
siLRP8_1
siLRP8_2
siLRP8_3
siLRP8_6
siLRP8_1/E4 (5)
siLRP8_1/E4
siLRP8_2/E4 (5)
siLRP8_2/E4
siLRP8_3/E4 (5)
siLRP8_3/E4
siLRP8_6/E4 (5)
siLRP8_6/E4
siVLDLR_1
siVLDLR_2
siVLDLR_3
siVLDLR_4
siVLDLR_1/E4
siVLDLR_2/E4
siVLDLR_3/E4
siVLDLR_4/E4
BT-549
Relative fold growth
2.2
2
1.8
1.6
1.4
1.2
1
0.8
0.6
0.4
0.2
0
siLRP8 only
siLRP8 / ApoE4*
siVLDLR only
siVLDLR / ApoE4*
!
!
ApoE4 120 nM
ApoE4 600 nM
siPOS
siNEG
siLRP8_1
siLRP8_2
siLRP8_3
siLRP8_6
siLRP8_1/E4
siLRP8_1/E4
siLRP8_2/E4
siLRP8_2/E4
siLRP8_3/E4
siLRP8_3/E4
siLRP8_6/E4
siLRP8_6/E4
siVLDLR_1
siVLDLR_2
siVLDLR_3
siVLDLR_4
siVLDLR_1/E4
siVLDLR_2/E4
siVLDLR_3/E4
siVLDLR_4/E4

B

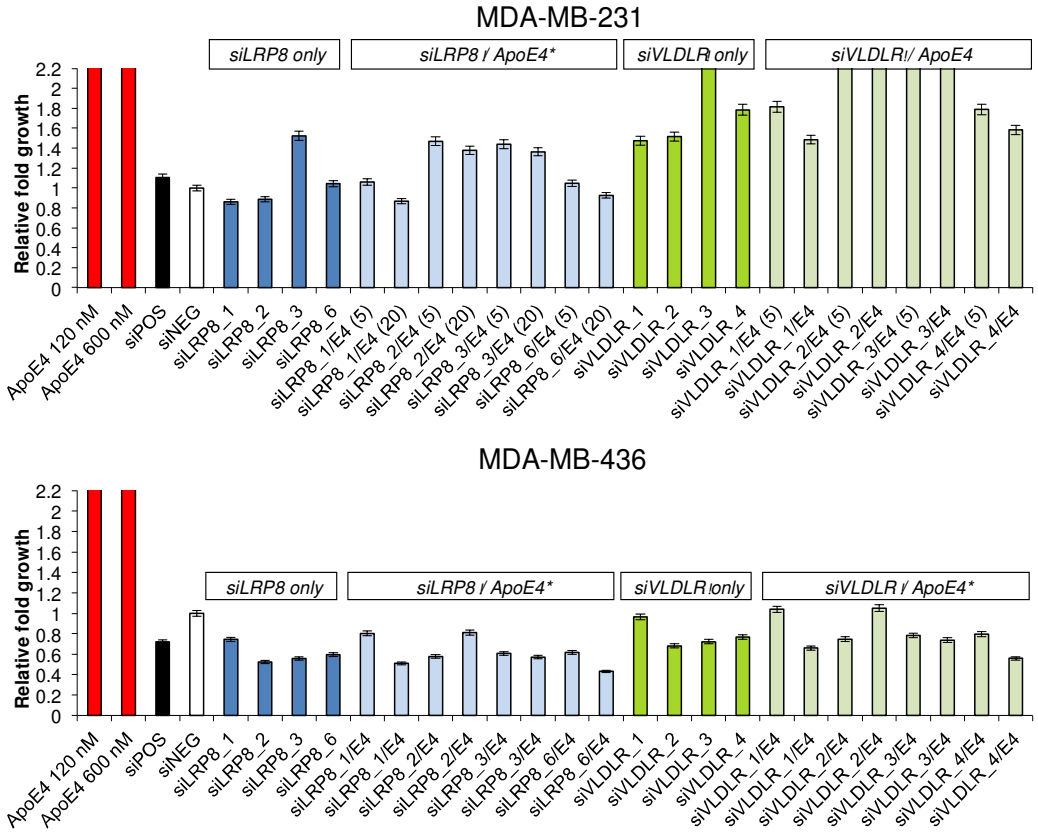

Figure 10. siLRP8 and siVLDLR abrogates ApoE4 stimulation of TNBC cells. Each of siRNAs against LRP8 and VLDLR were applied to TNBC cells alone or with ApoE4. siLRP8 or siVLDLR reversed ApoE4 stimulation and reduced growth to that of untreated controls. Dark bars indicate ApoE4 or siRNA alone. Lighter colored bars represent the combination of siLRP8/ApoE4. *$p<0.01$ with paired t-test when compared to ApoE4 alone and error bars indicate standard error.

3.12. LRP8 and VLDLR mediate the stimulatory effect of apolipoprotein E isoform 4 on TNBC cell lines

To differentiate between amplified proliferation and reduced apoptosis, TNBC cells were treated with 600 and 1200 nM of ApoE4. The level of BrdU incorporation increased with increasing ApoE4 concentrations, with no change in caspase-3/7 activity (Figure 11 and 12). siLRP8 and siVLDLR cell lines were treated with ApoE4, however, there was no change in BrdU incorporation or apoptotic activity, indicating the stimulatory effects of ApoE4 are mediated through LRP8 and VLDLR.

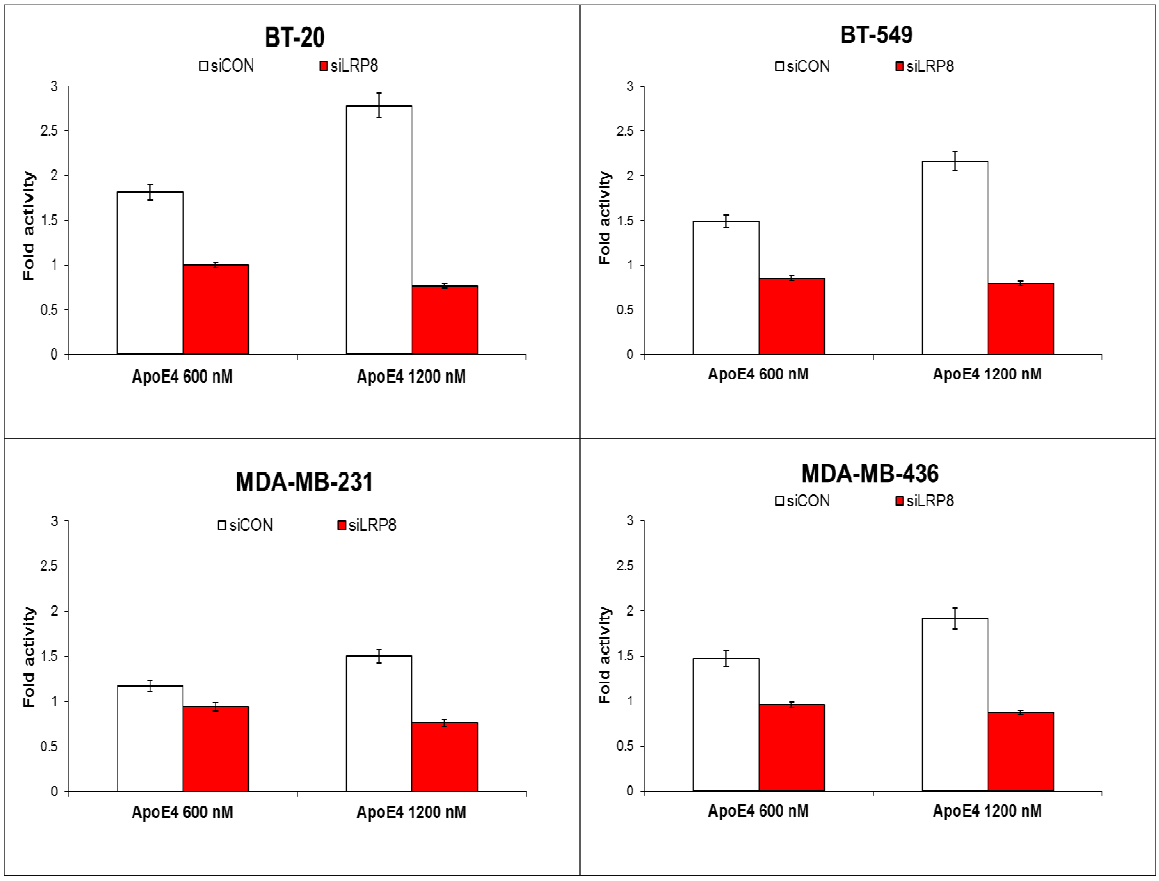

Figure 11. Apolipoprotein E isoform 4 stimulation increases the rate of BrdU incorporation – process mediated by LRP8. ApoE4 increased BrdU incorporation in siCON cells after 48 hours of treatment, increasing in activity from 600 or 1200 nM of ApoE4. siLRP8 reduced the level of BrdU incorporation. *$p<0.01$ with paired t-test when compared to siCON alone, error bars indicate standard error.

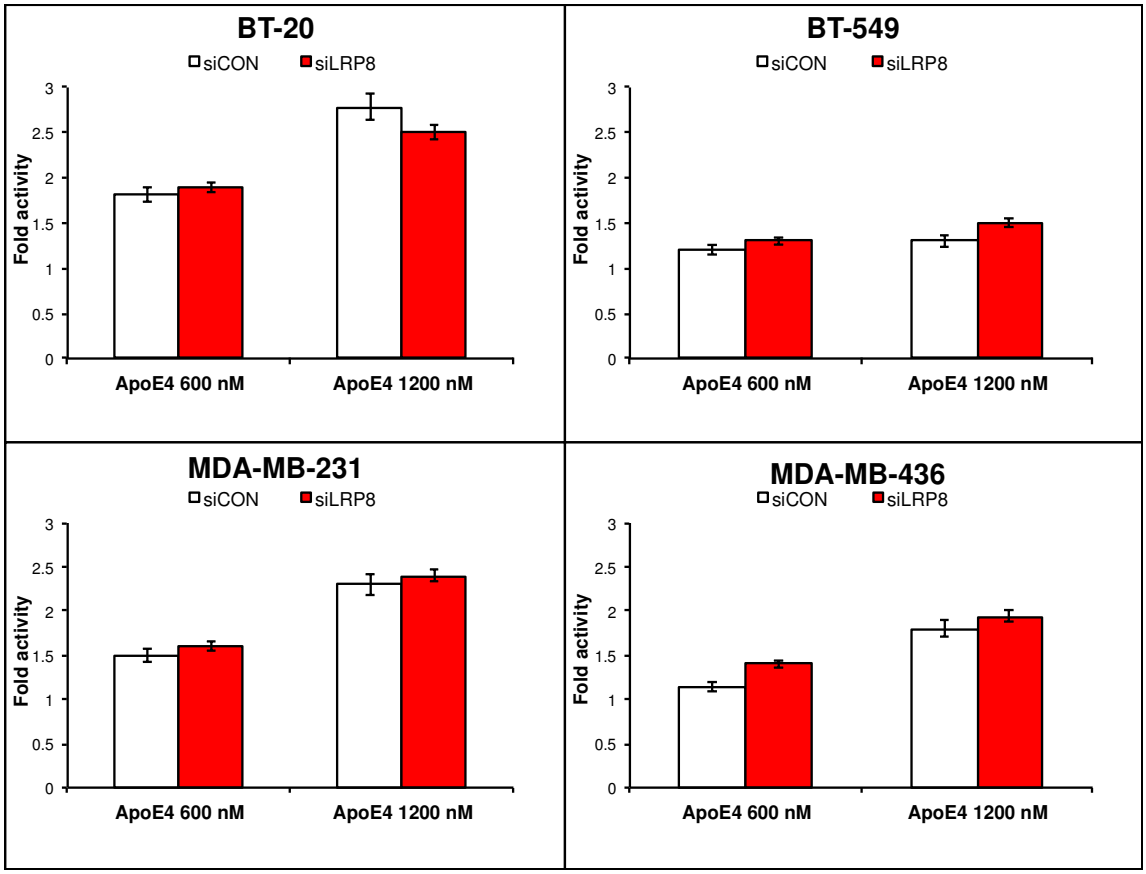

Figure 12. siLRP8 does not affect the level of caspase-3/7 proapoptotic activity. siCON (white bars) and siLRP8 (red bars) TNBC cells were treated with 600 or 1200 nM of ApoE4. Caspase-3/7 apoptotic activity was measured after 48 hours of treatment.

3.13. Non-triple negative breast cancer cell lines are not stimulated by Reelin or apolipoprotein E isoform 4

To investigate if the differential stimulation effects of the 3 different ApoE isoforms were unique to TNBC cells, receptor-positive cell lines were treated with the 500 nM of each APOE isoform. BT-474 (ER+/HER2+), MCF-7 (ER+/HER2-), and SK-BR-3 (ER-/HER2+) were treated and their viability was not affected by the APOE isoforms (Figure 13).

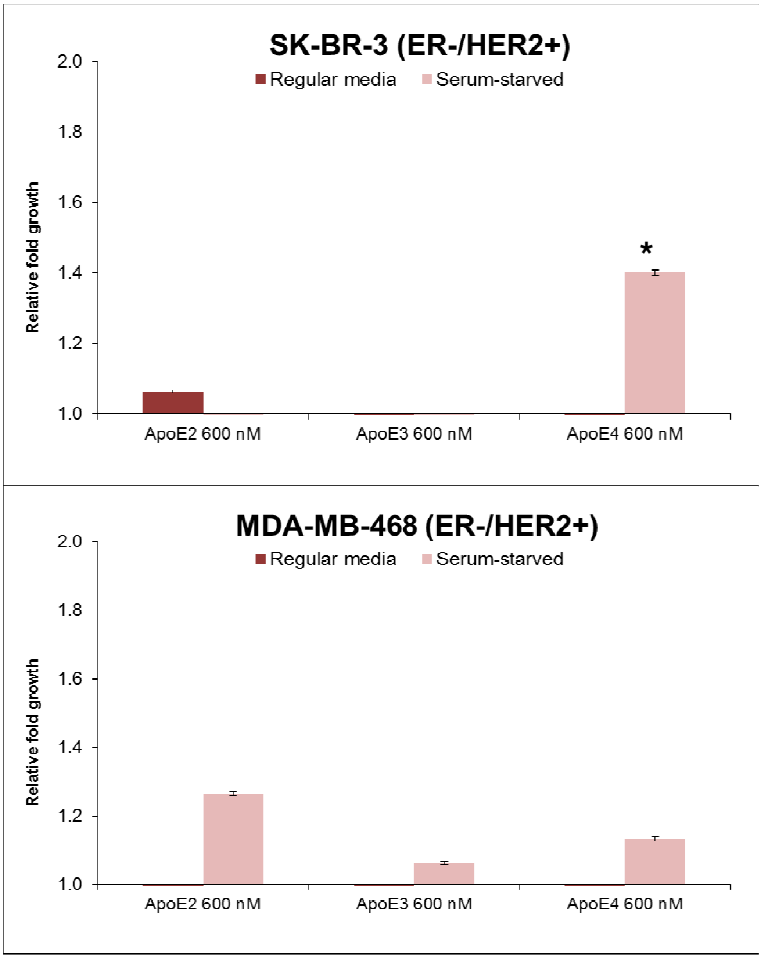

Figure 13. Apolipoprotein E isoform 4 has no significant effect on proliferation of non-TNBC cell lines. Non-TNBC cell lines with varying receptor status were treated with the three ApoE isoforms at 600 nM. There were no significant differences in growth from untreated controls when testing in regular or serum-starved media, with the exception of SK-BR-3.

3.14. ApoE4 stimulation results in cell cycle progression of triple-negative breast cancer cell lines

Two doses of ApoE4 were given and FACS analysis was performed to ascertain the potential changes in cell cycle distribution given the growth stimulatory properties of ApoE4. BT-20 and BT-549 were pushed into the synthesis phase, while MDA-MB-231 and MDA-MB-436 were pushed into the G2/M phase (Figure 14). BT-20 and BT-549 cell lines had an S phase increase, for BT-20 18% in mock treated control cells to 24% in 600 nM ApoE4 and 30% in 1500 nM ApoE4. For MDA-MB-231 and MDA-MB-436 cells, the G2/M fraction increased with ApoE4 treatment.

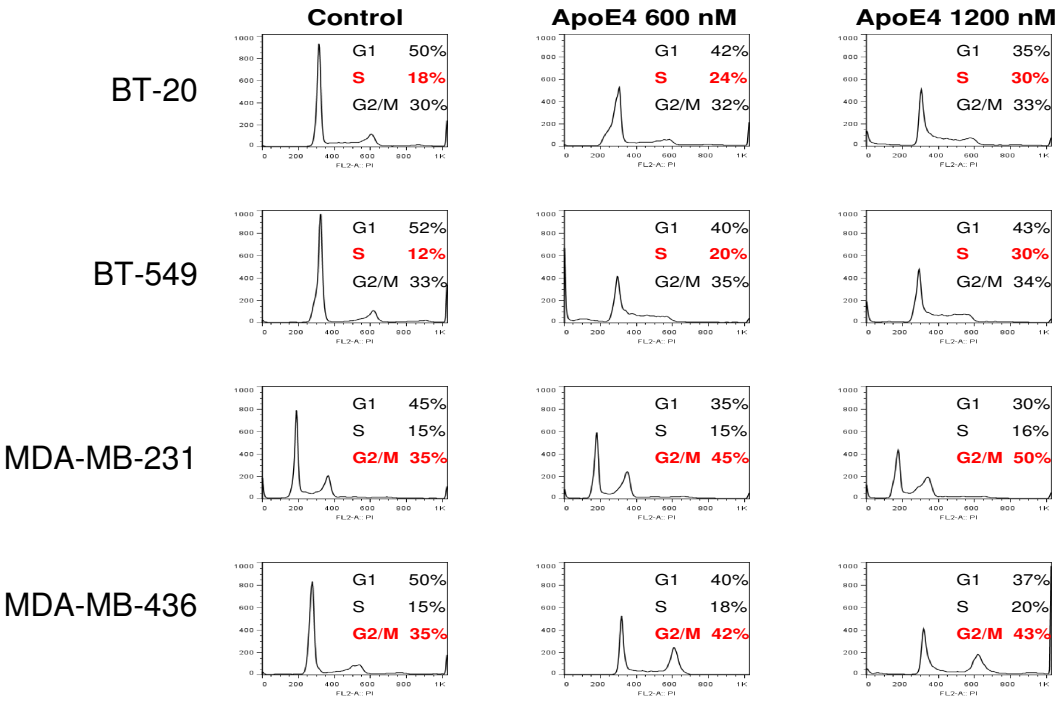

Figure 14. Apolipoprotein E isoform 4 stimulation mediates S- and G2/M-phase cell cycle progression in TNBC cells. BT-20 and BT-549 cell lines shifted from G1 to S phase, while the G2/M fraction increased in MDA-MB-231 and MDA-MB-436 cells. *p<0.05 with paired t-test when compared to untreated controls, error bars indicate standard error.

3.15. Inhibition of apolipoprotein E binding abolishes the growth stimulatory effect on triple-negative breast cancer cell lines

To test whether the stimulatory effect on viability was a result of ApoE binding to LRP8/VLDLR, LRP8 and VLDLR expressing breast cancer cell lines were treated with ApoE4 alone or the combination of ApoE4 and RAP1, an endogenous inhibitor of ApoE binding to LRP8/VLDLR. The addition of RAP1 abolished the stimulatory effect previously observed at 72 hours (Figure 15).

To test whether commercial antibodies that target different regions of LRP8 can inhibit binding of ApoE4 to its cognate receptor, LRP8. Previously, treatment of LRP8-expressing breast cancer cell lines with the ApoE4 isoform resulted in greater cell viability (MTS assay – reduction of NADPH produced in cell culture, measure of metabolic activity). The objective of this experiment was to (i) develop a custom, solid phase binding assay for LRP8 and ApoE4, (ii) identify commercial antibodies that may inhibit the binding interaction between LRP8 and ApoE4, and (iii) identify potential binding domains on LRP8 which may be targeted. A mouse monoclonal antibody against LRP8 reduced the binding affinity of recombinant human LRP8 and ApoE4 using an ELISA binding assay (Figure 16). In comparison, a mouse polyclonal antibody against the intracellular C-terminal region of LRP8 and mouse IgG antibody did not affect the binding of recombinant LRP8 and ApoE4 (Figure 16).

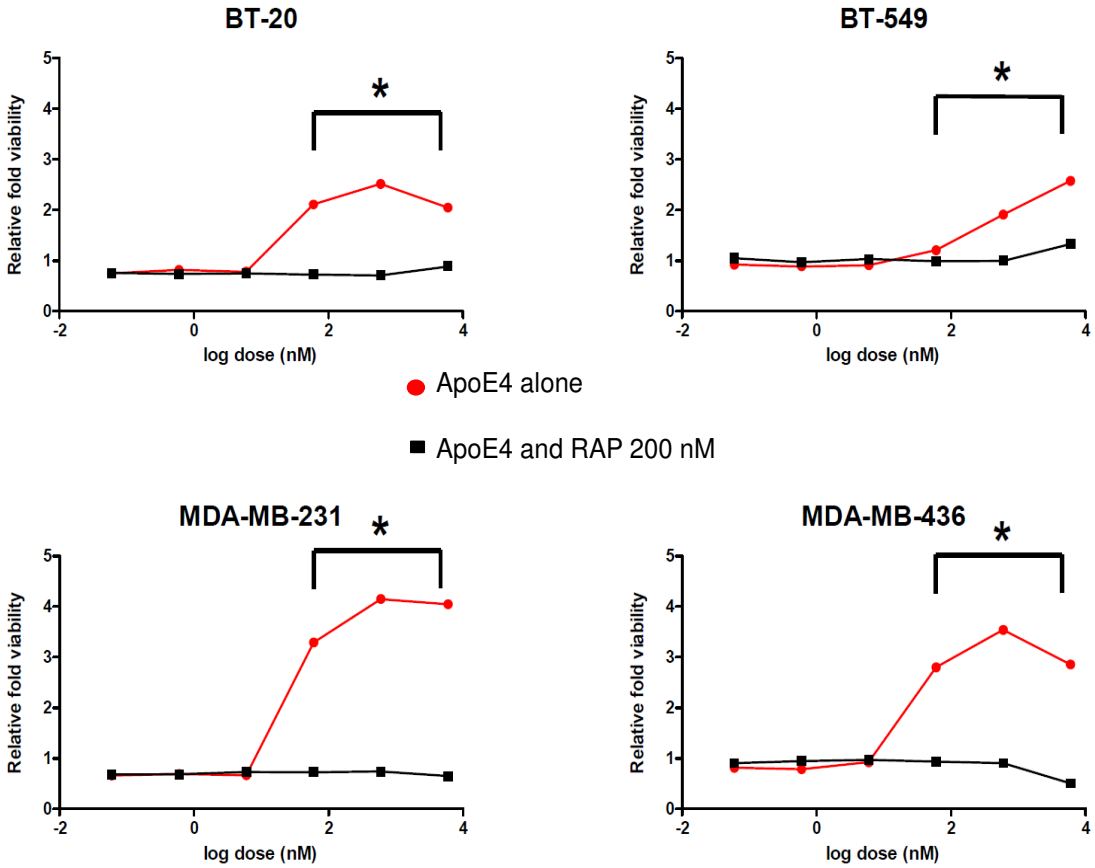

Figure 15. RAP1-induced abolishes proliferative effect of ApoE4 on TNBC cell lines. RAP treatment (black lines) abolished the ApoE4 stimulatory effect (red lines) when 200 nM of RAP was combined with greater than 150 nM of ApoE4 after 48 hours of treatment. *p<0.001 with paired t-test when compared to ApoE4 alone, error bars indicate standard error.

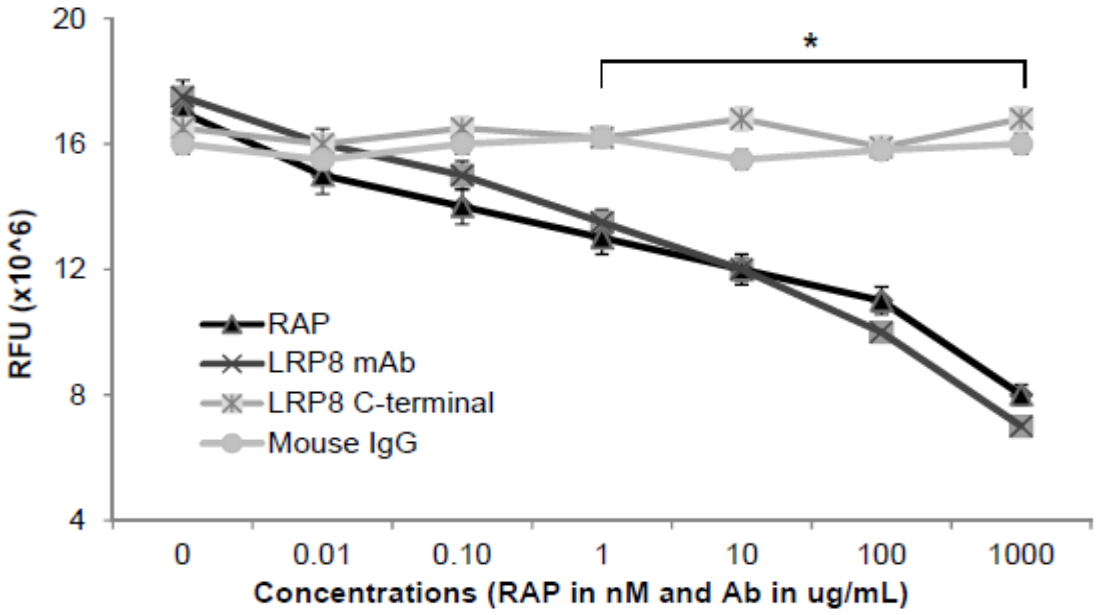

Figure 16. LRP8 monoclonal antibody abrogates binding between LRP8 and ApoE4. In an ELISA solid-phase binding assay, RAP and a monoclonal antibody targeting the ApoE4 binding region of LRP8 reduced the binding activity level between recombinant human LRP8 and ApoE4. *$p<0.05$ with paired t-test when compared to mouse IgG alone, error bars indicate standard error.

3.16. ApoE4 stimulation rescues TNBC cells from serum-starvation effects by down-regulating members of lipid biosynthesis

To investigate the mechanisms controlling the robust growth effect after ApoE4 stimulation, transcriptional, proteomic, and metabolic profiling was performed using the same experimental schema described in the Methods section. Global profiling was performed in the BT-549 and MDA-MB-436 cell lines, which had the most consistent proliferative effects in response to ApoE4 stimulation as well as higher expression of LRP8 and VLDLR according to Western blotting. During serum starvation, most of the gene expression changes occurred between 8 and 48 hours of treatment, with the highest number of common probe sets occurring during the entire 48 hour treatment period (Table 2, Control T00 vs. T48). Likewise, ApoE4-induced gene expression changes were concentrated at the 48 time point, indicating that gene expression changes after 8 hours of treatment are responsible for the transcriptional changes related to serum starvation and ApoE4 stimulation. Each set of triplicate clustered together with a second level of separation occurring between the group of T0/T8 and the group at T48, with this effect being more obvious with BT-549 than MDA-MB-436 (Figure 17). For these reasons, further analyses focused on the 48 hour time point comparisons.

Serum-starvation induced the upregulation of steroid biosynthesis and lipid and amino acid metabolism pathways, while downregulating pathways associated with mitotic division and nucleotide metabolism (Figure 18). The lipid biosynthesis network connecting the upregulated starvation-induced genes centered around SREBF2 (Figure 19). ApoE4 stimulation increased expression of genes associated with chemokine signaling, while downregulating members of steroid biosynthesis pathways (Figure 19).

This dampening or normalization of starvation-induced steroid biosynthesis rescues TNBC cells from starvation by supplying them with an exogenous energy source mediated by ApoE4.

Table 2. Global profiling changes after serum-starvation and ApoE4 treatment in TNBC cell lines

Serum-starvation regulated genes		BT-549	MDA-MB-436	Common probe sets
Control T00 vs. T08	Threshold	p<0.005	p<0.005	
	Up	226	219	4
	Down	304	295	64
Control T08 vs. T48	Threshold	FDR 0.01	p<0.005	
	Up	427	362	94
	Down	405	225	50
Control T00 vs. T48	Threshold	FDR 0.01	p<0.005	
	Up	696	315	108
	Down	663	201	67
ApoE4 regulated genes		**BT-549**	**MDA-MB-436**	**Common probe sets**
Treated vs. Control (T08)	Threshold	FDR 0.05	p<0.005	
	Up	167	132	7
	Down	123	114	1
Treated vs. Control (T48)	Threshold	FDR 0.05	p<0.005	
	Up	638	113	16
	Down	589	167	38

Common to BT-549 and MDA-MB-436

Serum-starvation genes Control T00 vs. T48		ApoE4 genes Treated vs. Control (T48)	
Up-regulated	Down-regulated	Up-regulated	Down-regulated
ABCD4	ABCF2	CAV2	ACAT2
ACAT2	ACP1	CTSB	ACLY
ANK2	ARD1A	CXCL2	AP1M2
ANXA4	BCLAF1	CXCL3	C14orf1
AP1M2	BOP1	CYR61	CYP51A1
ARG2	C8orf33	FOSL1	DBI
ASNS	CCDC56	GPX1	DHCR24
BNIP3L	CCND1	KPNB1	DHCR7
BST2	CTPS	NEDD4L	EBP
C14orf1	CYP1B1	PLAU	FADS1
C6orf62	DDX18	SEPW1	FASN
CAPRIN2	DNAJC9	TBL1X	FDFT1
CAST	EIF2B3	TGFBI	

CCNG1	EMG1		FDPS
CEP170	FHL2		HMGCS1
CHP	FOSL1		HSD17B12
CYP51A1	GLRX3		HSD17B7
DCAF6	GYG1		IDI1
DDIT4	HSP90AB1		INSIG1
DHCR7	HSPD1		LDLR
DZIP1	IMPDH2		LIPA
EBP	KPNB1		LPIN1
EGFR	LSG1		LSS
FADS1	MCM7		MICA
FADS2	MRPS33		NEU1
FASN	MT1X		NPC2
FDFT1	MT2A		NSDHL
FDPS	NME1		S100A10
FTL	NOL7		SC4MOL
G6PD	NOLC1		SCD
GARS	PFAS		SLC25A1
GGPS1	PLAU		SQLE
HERC5	POP4		TMEM97
HEXB	PPIF		TUBA1A
HMGCR	PPIH		ZC3HAV1
HMGCS1	PRPF4		
HSD17B7	PSMD3		
HSP90B1	PUF60		
IDH1	RANBP1		
IDI1	RANGAP1		
IFI44	RFTN1		
IFI6	RRM2		
IFIH1	RRP9		
IFIT1	SEPW1		
IFIT3	SERPINE1		
INSIG1	SRM		
ISG15	SRRT		
ISG20	TH1L		
ITGB5	TOMM70A		
JUND	TPM1		
KIAA0430	VDAC3		
LAMB2			
LDLR			
LPIN1			
MAGED1			
NNT			
NPC1			
NPC2			
NSDHL			
OAS1			
PHGDH			
PMAIP1			
PNMA2			

POFUT2 RHOQ RSAD2 SC4MOL SCD SLC2A3 SLC38A2 SQLE SREBF2 STX16 TCF7L2 TMX1 TPBG TPD52L1 TRADD TRIB3 TTC3 TUBA1A WARS WSB1			

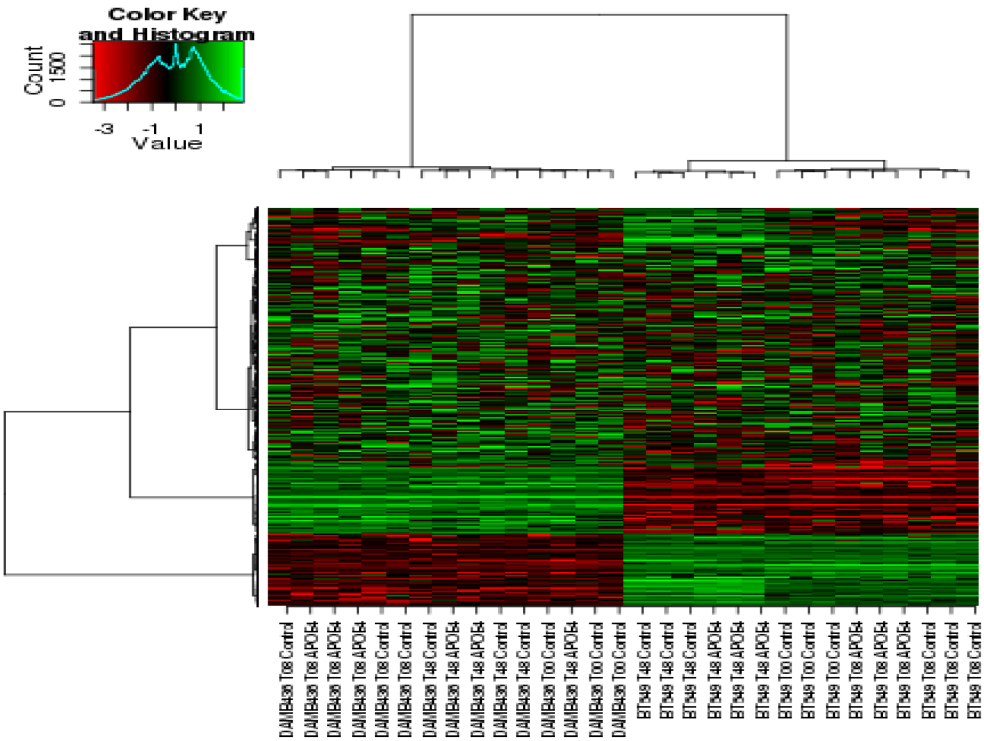

Figure 17. Global profiling changes in BT-549 and MDA-MB-436 cell lines shows modulation of lipid biosynthesis during serum-starvation and after ApoE4 treatment. Untreated control and ApoE4 treated cells were assayed at baseline, 8 hours, and 48 hours of treatment in triplicate (T00 Control, T08 Control, T48 Control, T48 ApoE4, T48 ApoE4). A heatmap of hierachical clustering of the samples is shown, using top 20% variable probe sets (probe sets = 4457), measured by median absolute deviation, and using Pearson distance and Ward linkage.

Upregulated pathways after serum-starvation

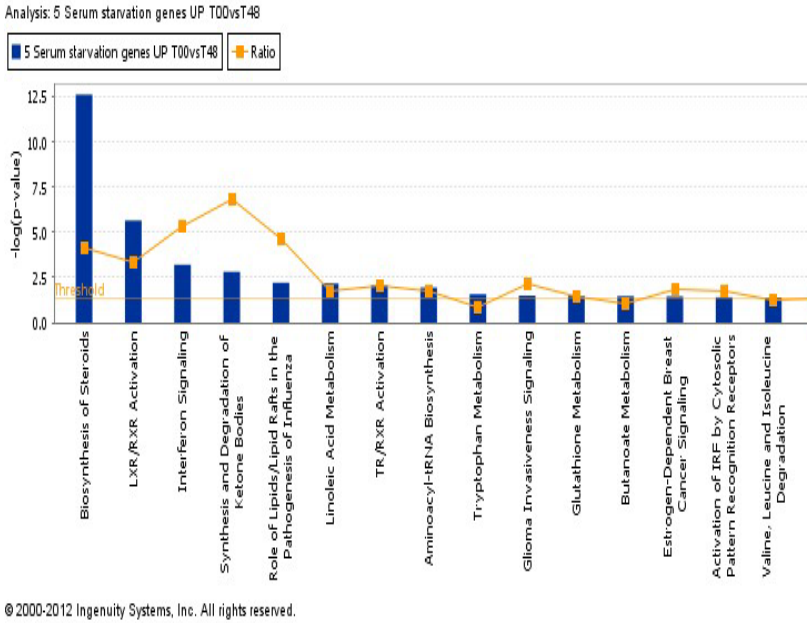

Downregulated pathways after ApoE4 stimulation

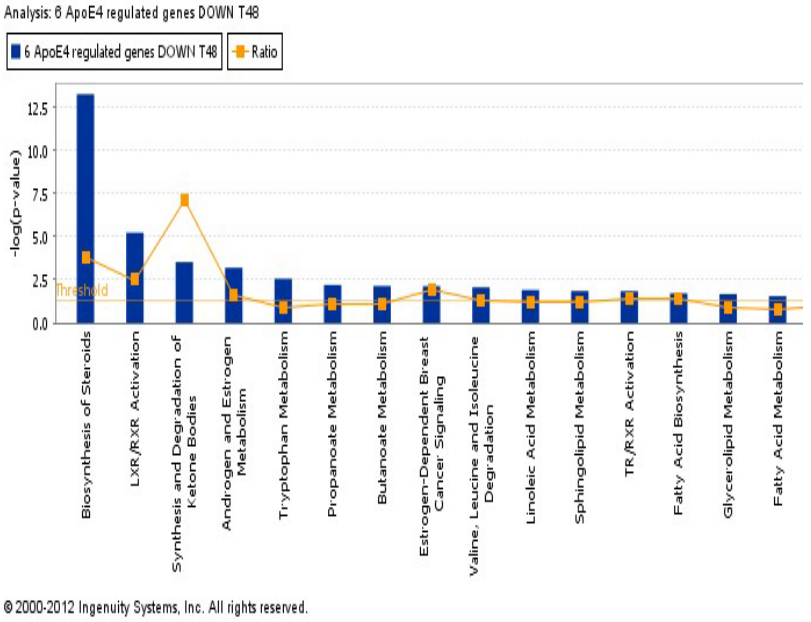

Figure 18. Significantly differentially regulated canonical pathways of TNBC cells at baseline and with 48 hours of serum-starvation vs. ApoE4 treatment. Serum-starvation and ApoE4 regulated genes that were common to both BT-549 and MDA-MB-436 were imputed into Ingenuity Pathway Analysis for canonical pathway analysis and the results are as depicted (Table 3). At time point 48, serum-starvation induced the upregulation of pathways involved in steroid biosynthesis and lipid metabolism. ApoE4 treatment rescued this starvation-induced effect and reduced the activation of steroid biosynthesis pathways.

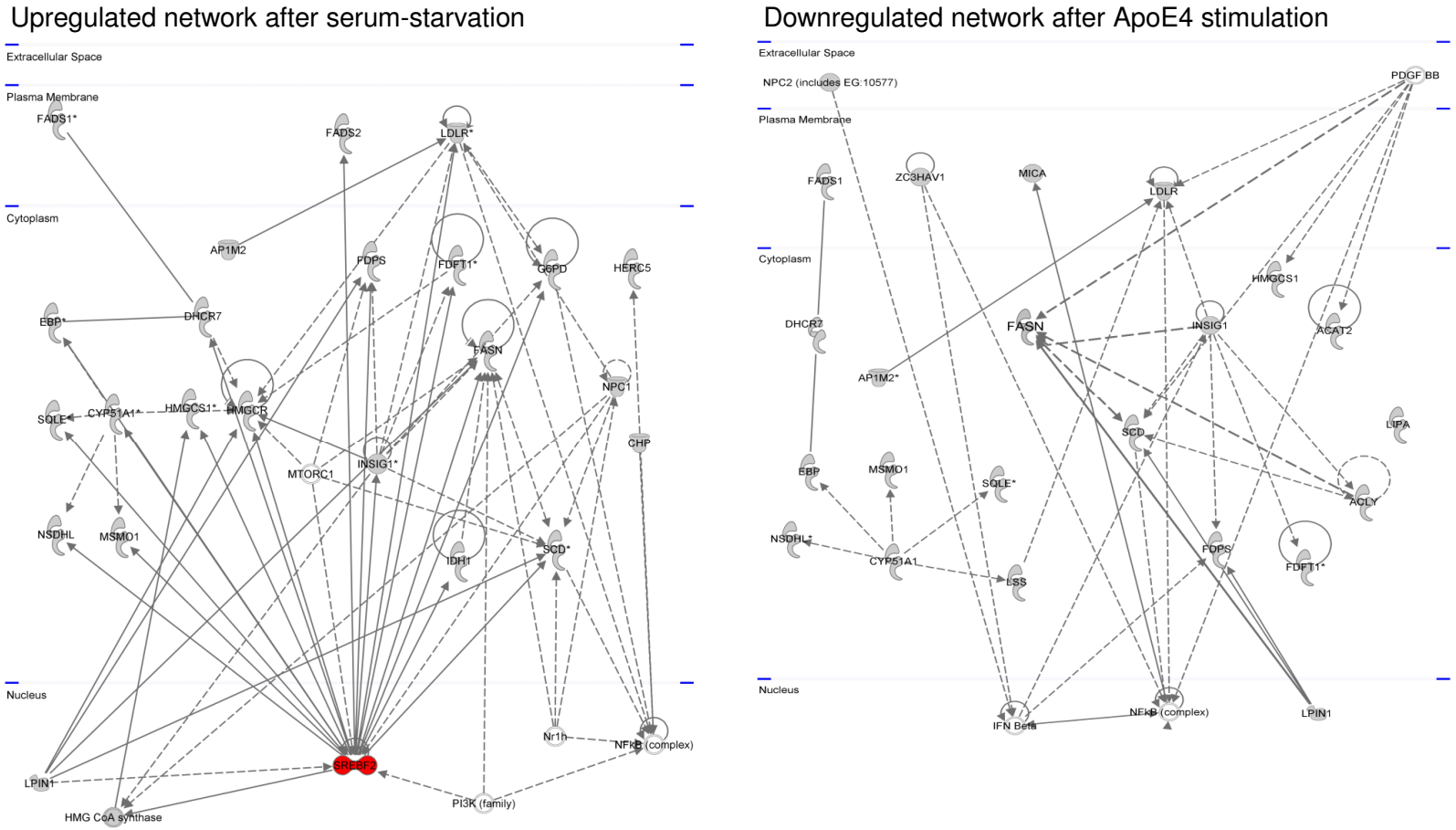

Figure 19. Major regulated transcriptional networks in TNBC cells with 48 hours of serum-starvation vs. ApoE4 treatment. The serum-starvation regulated genes belong to an interacting network centered on the transcriptional regulator, SREBF2. ApoE4 treatment rescues TNBC cells from starvation conditions by downregulating interacting steroid biosynthesis factors, which are responsible for growth and survival during serum-starvation conditions.

3.17. MAPK signaling mediates ApoE4 downstream signaling for TNBC cell proliferation To determine the protein mediators of proliferation after ApoE4 stimulation, reverse phase protein array was performed after 48 hours of ApoE4 treatment in BT-549 and MDA-MB-436. Consistent protein changes occurred at time point 48, consistent with the results from gene expression profiling (Figure 20). Ingenuity Pathway Analysis showed that the activated proteins were interconnected through the MAPK signaling network (Figure 21, Table 3). Proteins repressed after ApoE4 treatment were involved in ribosomal assembly and protein translation (Figure 21, Table 3).

Table 3. Perturbation of oncogenic protein expression after ApoE4 treatment

Serum-starvation regulated proteins		BT-549	MDA-MB-436	Common
Control T00 vs T08	Threshold	FDR 0.05	FDR 0.05	
	Up	60	14	3
	Down	31	16	8
Control T08 vs T48	Threshold	FDR 0.05	FDR 0.05	
	Up	21	67	17
	Down	25	62	16
Control T00 vs T48	Threshold	FDR 0.05	FDR 0.05	
	Up	66	31	24
	Down	45	34	20
ApoE4 regulated proteins		**BT-549**	**MDA-MB-436**	**Common**
Treated vs Control (T08)	Threshold	p<0.05	p<0.05	
	Up	13	18	5
	Down	12	10	1
Treated vs Control (T48)	Threshold	FDR 0.05	FDR 0.05	
	Up	59	51	12
	Down	53	36	12

ApoE4 upregulated proteins (n=5) Treated vs Control (T08)	ApoE4 upregulated proteins (n=12) Treated vs Control (T48)	
HIF1a	Caspase-7_cleavedD198	MAPK14_pT180/182
p53	CDKN1B	p53
PKC-alpha_pS657	ERRFI1	PTGS2
Snail	HIF1a	PTK2
VEGF	HistoneH2AX_pS139	Rab25
	MAP2K1	Snail

ApoE4 downregulated proteins (n=1) Treated vs Control (T08)	ApoE4 downregulated proteins (n=12) Treated vs Control (T48)	
AMPK_pT172	AR	HER2
	Chk2_pT68	RPS6_pS235/236/240/244
	C-Raf_pS388	RPS6KB1 (p70S6K_pT389)
	CyclinD1	SPARC
	EGFR	Stat3_pY705
	EIF4EBP1_pS65/T70	YAP

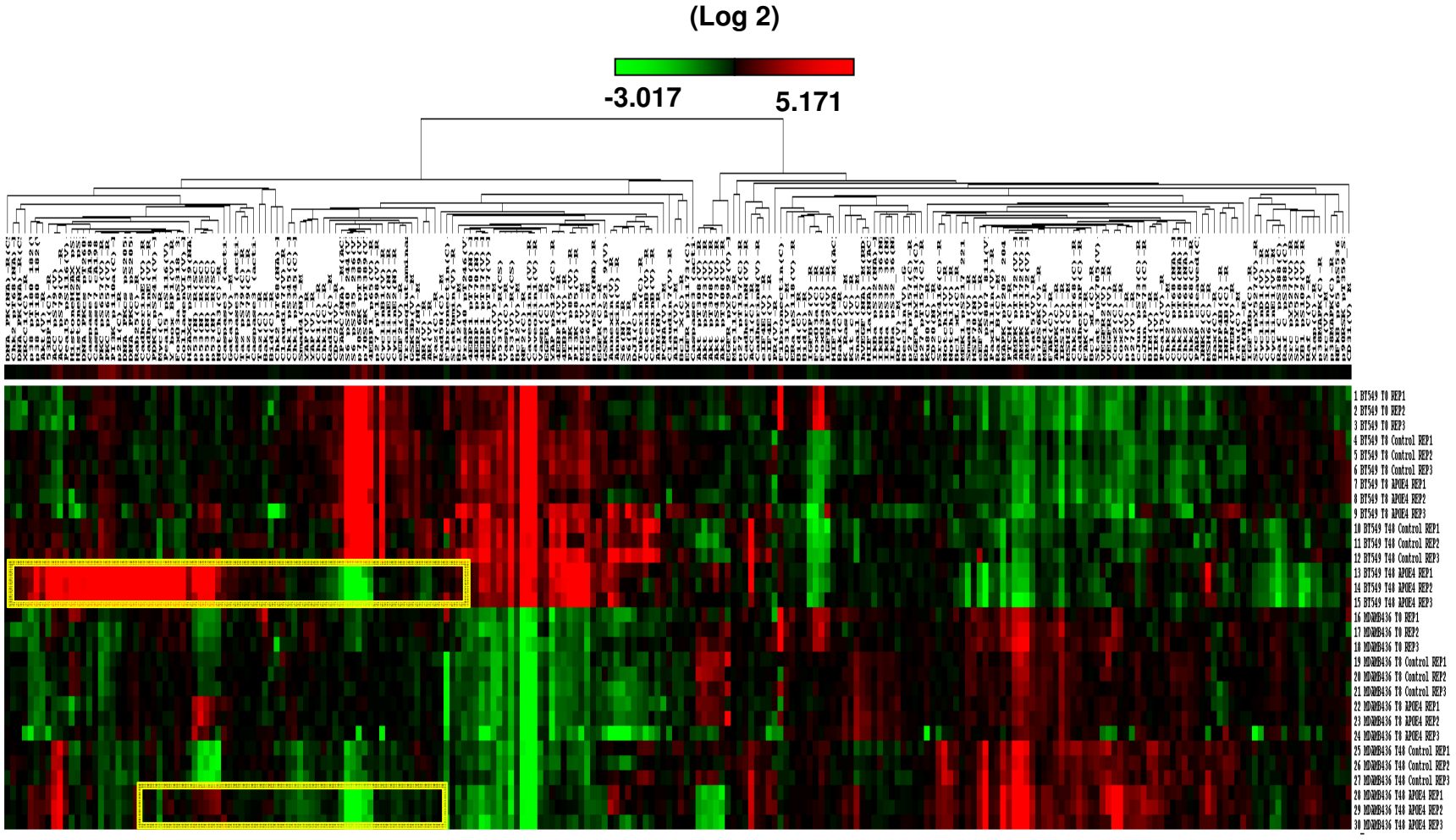

Figure 20. RPPA heatmap of hierarchical clustering of control and ApoE4 treated experimental samples using samples arranged in order (n=230 antibodies, clustering performed using Pearson distance and median centered). A heatmap depicting samples arranged in order (rows) is shown with antibodies (columns) listed in the top row (median centered array). Yellow boxes highlight antibody signals which changed significantly between the control and ApoE4 treated samples at 48 hours.

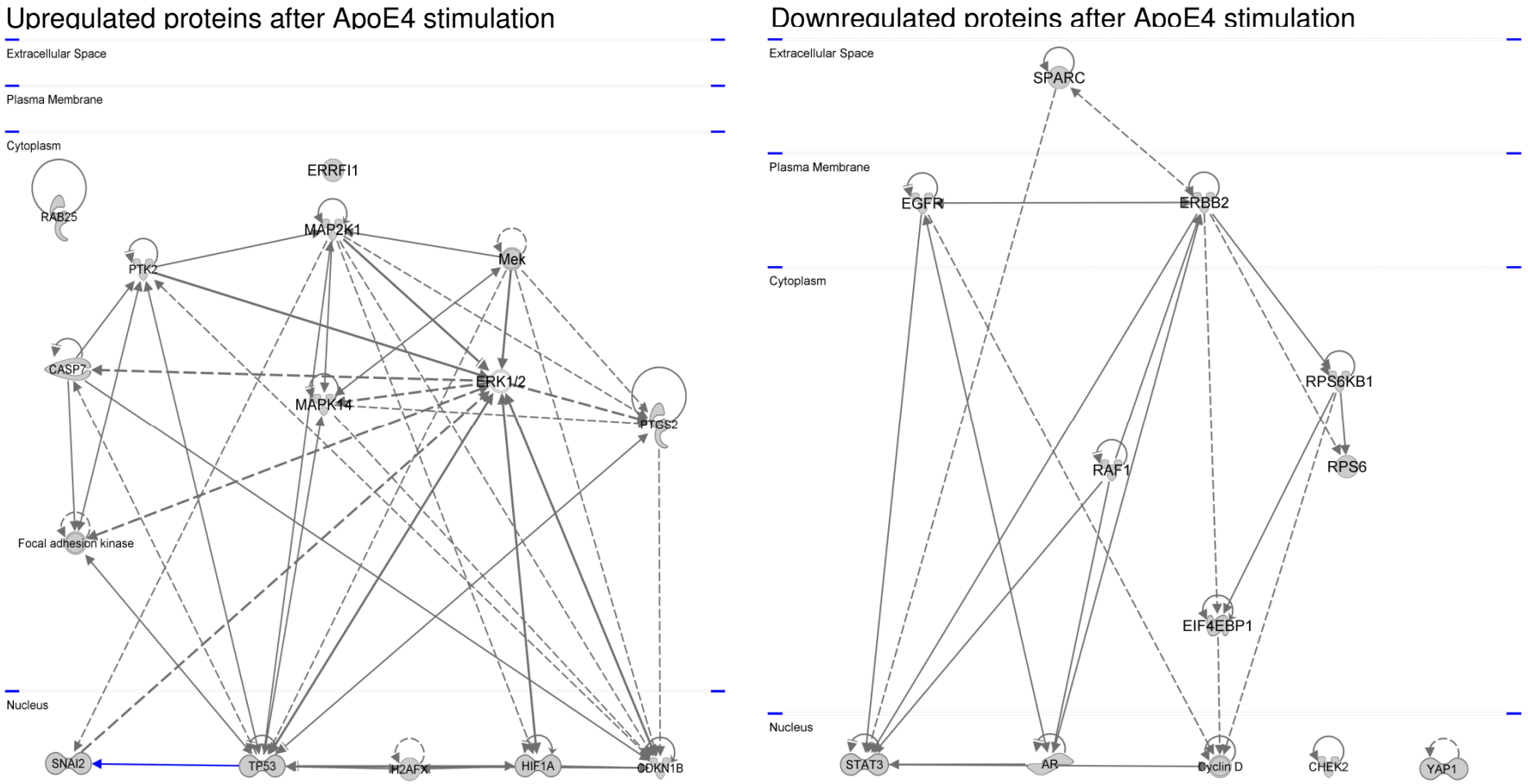

Figure 21. Major regulated protein networks in TNBC cells with 48 hours of serum-starvation vs. ApoE4. Proteins from Table 4 were imputed into Ingenuity Pathways Analysis for canonical pathway and molecular network analyses and the results are as shown. ApoE4 activated proteins are involved in the transmittal of exogenous growth signals through cytoplasmic MAPK signaling to further activate transcriptional regulators such as p53 and CDKN1B. ApoE4 represses proteins involved in protein translation.

To confirm the RPPA array findings, Western immunoblotting of the ApoE4 activated proteins was performed (Figure 22). Transient and stably transfected LRP8 knockdown cell lines were established to test if ApoE4 stimulation affects TNBC cells with lower levels of ApoE's cognate receptor. The MDA-MB-231 shLRP8 stable knockdown cell line was used to establish the nude mice xenografts. LRP8 knockdown efficiency was similar in both BT-549 and MDA-MB-231 LRP8 knockdown cell lines. In BT-549 parental cells, ApoE4 increased the protein levels of phosphorylated serine-473 of histone H2AX, COX2, Rab25, and Snail. In BT-549 siLRP8 cells, this increase was reduced for phosphorylated serine-473 of histone H2AX. In BT-549 siCON and siLRP8 cells, there were no detectable levels of COX2, Rab25, or Snail. In MDA-MB-231 parental cells, there were minimal increases in phosphorylated serine-473 of histone H2AX and Snail after ApoE4 treatment. In MDA-MB-231 shLRP8 cells, both proteins were slightly reduced in comparison to shCON.

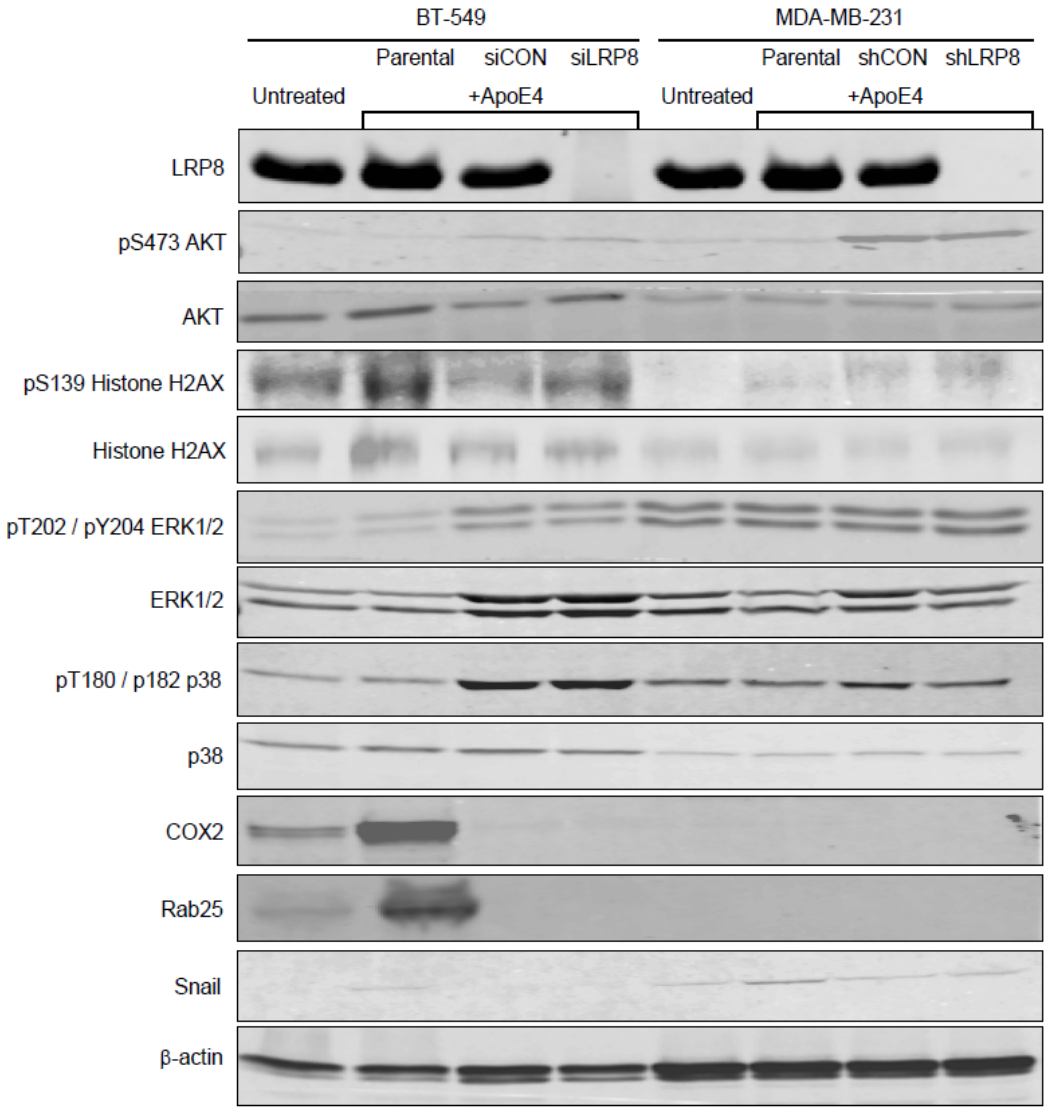

Figure 22. Western immunoblotting validation of RPPA results. Western blot confirmation of key activated proteins is depicted. BT-549 and MDA-MB-231 cell lines were treated with 600 nM ApoE4 for 48 hours. BT-549 cells transiently transfected with siLRP8 and a stably transfected shLRP8 MDA-MB-231 cell line were treated concurrently. The increased protein levels of phosphorylated histone H2AX (S139), COX2, RAB25, and SNAIL were confirmed for BT-549. The results for MDA-MB-231 were less consistent with the RPPA results.

3.18. Metabolomic profiling indicates that TNBC cells use alternative metabolic pathways during serum starvation and coordinate LRP8-ApoE4 signaling to rescue cells from cellular stress

BT-549 cells were treated with ApoE4 for 48 hours and GC/MS and LC/MS/MS profiling platforms were used by Metabolon, Inc. to determine the metabolic biochemical changes that mediate growth and survival of ApoE4 activated cells. Three comparisons were focused upon, the effects of serum-starvation (serum-free cells at 48 hours / regular media cells at 48 hours), the rescue effects of ApoE4 treatment (ApoE4 treated cells at 48 hours / serum-free cells at 48 hours), and the rescue effects potentially reversed by LRP8 knockdown (siLRP8+ApoE4 at 48 hours / siCON at 48 hours). Serum-starvation resulted in the activation of Warburg metabolism, with increased tryptophan and reduced NAD+ levels (Table 4). Glycolysis intermediates, such as fructose-6-phosphate and 3-phosphoglycerate, were increased in serum-starved cells. Reduced glutathione and hydroxycholesterol metabolites generated by reactive oxygen species were also elevated (Figure 23 and 24).

In response to ApoE4 treatment, the cells had decreased levels of the previously activated glycolysis intermediates and reduced levels of some oxidative stress chemicals and cholesterol metabolites (Figure 24). In response to LRP8 knockdown, cells reversed some of the rescue effects and reconstituted levels of key chemicals in nucleic acid metabolism and lipid metabolites and re-entered the pentose phosphate pathway to produce nucleotide precursors and intermediates (Figure 25).

Table 4. 192 of 273 changing metabolites in BT-549 and MDA-MB-436 in response to serum-starvation and ApoE4/siLRP8 treatment

Super Pathway	Sub Pathway	Biochemical Name	KEGG	SF-48 / REG-48	APO-48 / SF-48	LRP-48 / CTRL-48	A/L-48 / CTRL-48
Amino acid	Glycine, serine, threonin metabolism	serine	C00065	1.15	1.28	1.24	1.5
		threonine	C00188	1.13	1.33	1.18	1.54
		N-acetylthreonine	C01118	1.01	1.29	1.25	1.28
	Alanine and aspartate metabolism	aspartate	C00049	0.82	0.81	0.92	1.03
		asparagine	C00152	1.92	1.14	1.26	1.29
		beta-alanine	C00099	0.37	1.25	1.13	1.1
		N-acetylalanine	C02847	1.2	0.99	0.95	0.91
	Glutamate metabolism	glutamine	C00064	3.36	1.33	2.09	2.11
		pyroglutamine*		1.84	1.05	1.11	1.1
		gamma-aminobutyrate (GABA)	C00334	0.19	1.31	1.18	1.55
		N-acetylglutamate	C00624	1.85	0.72	1.04	0.77
		N-acetyl-aspartyl-glutamate (NAAG)	C12270	1.3	1	0.99	0.9
	Histidine metabolism	histidine	C00135	1	1.1	1.28	1.46
		imidazole propionate		0.38	0.89	0.98	1.3
	Lysine metabolism	lysine	C00047	1.13	1.35	1.32	1.63
		2-aminoadipate	C00956	0.21	0.68	1	0.68
	Phenylalanine & tyrosine metabolism	phenylalanine	C00079	1.13	1.34	1.19	1.42
		tyrosine	C00082	1.18	1.35	1.18	1.5
		3-(4-hydroxyphenyl)lactate	C03672	2.41	1.06	1.18	1.05
		phenylacetylglycine	C05598	1.23	0.57	0.84	0.74
	Tryptophan metabolism	kynurenine	C00328	0.43	1.03	1.12	1.21
		tryptophan	C00078	25.51	1.64	1.25	1.55
	Valine, leucine and isoleucine metabolism	isoleucine	C00407	1.13	1.26	1.17	1.3
		leucine	C00123	1.11	1.31	1.23	1.41
		valine	C00183	1.2	1.3	1.2	1.38
		isobutyrylcarnitine		0.69	1	1	1
		2-methylbutyrylcarnitine (C5)		0.07	1.3	0.87	0.68
		isovalerylcarnitine		0.08	1	1	1
	Cysteine, methionine, SAM, taurine metabolism	cystathionine	C02291	1.62	1.16	1.18	1.18
		methionine sulfoxide	C02989	2.19	0.69	1.11	0.85
		hypotaurine	C00519	0.26	1.33	1.14	1.24
		S-adenosylhomocysteine (SAH)	C00021	1.07	0.87	1.09	1.1

		methionine	C00073	1.23	1.32	1.19	1.41
		N-acetylmethionine	C02712	1.55	1.16	1.13	1.31
		homocysteine	C00155	1.45	0.83	1.31	1.12
	Urea cycle; arginine-, proline-, metabolism	dimethylarginine (SDMA + ADMA)	C03626	2.12	1.39	1.19	1.79
		arginine	C00062	1.4	1.34	1.39	1.69
		N-acetylornithine	C00437	0.66	1.07	0.97	1.05
		trans-4-hydroxyproline	C01157	0.45	0.82	1.34	1.26
		argininosuccinate	C03406	0.69	1.65	0.86	1.3
	Creatine metabolism	creatine	C00300	0.53	1.03	1.1	1.11
		creatinine	C00791	0.45	1.35	1.1	1.04
	Polyamine metabolism	putrescine	C00134	0.34	0.67	0.41	0.42
		spermidine	C00315	1.27	0.9	0.95	0.88
		spermine	C00750	1.58	2.34	0.67	0.99
	Glutathione metabolism	glutathione, reduced (GSH)	C00051	1.21	1.08	0.93	0.95
		5-oxoproline	C01879	1.66	1.09	1.16	1.3
		S-lactoylglutathione	C03451	1.78	0.31	1.99	0.48
Peptide	Dipeptide	glycylglycine	C02037	1.35	1.11	1.3	1.42
		glycylproline		1.4	1.67	1	1.36
		pro-hydroxy-pro		0.35	1.64	1.21	1.47
		phenylalanylglutamate		1.25	1.4	1.18	1.32
		cysteinylglycine	C01419	1.38	0.94	1.03	1.08
		isoleucylglycine		1.71	1.08	1.05	0.84
		isoleucylserine		3.14	1.29	0.77	0.97
		leucylglycine		2.2	1.26	1.11	1.23
		prolylglutamate		1.36	1.13	1.04	1.32
	gamma-glutamyl	gamma-glutamylvaline		1.72	1.17	1.01	1.03
		gamma-glutamylleucine		1.34	1.1	1.12	1.11
		gamma-glutamylglutamate		1.43	0.96	0.81	0.85
		gamma-glutamylphenylalanine		1.47	1.04	1.27	1.2
Carbo-hydrate	Aminosugars metabolism	erythronate*		1.21	0.9	1.01	0.93
	Fructose, mannose, galatose, starch, sucrose	lactose	C00243	1.33	0.94	1.2	1.17
		6'-sialyllactose	G00265	1.17	0.84	1.07	0.95
		mannitol	C00392	0.45	0.84	1.27	1.95
	Glycolysis, gluconeogenesis, pyruvate metabolism	glucose 1-phosphate	C00103	0.81	0.66	0.97	0.79
		Isobar: fructose 1,6-diphosphate, glucose 1,6-diphosphate, myo-inositol 1,4		2.35	0.16	1.82	0.4
		3-phosphoglycerat	C00597	1.84	0.5	0.92	0.73

		e					
		dihydroxyacetone phosphate (DHAP)	C00111	1.69	0.33	1.46	0.48
		pyruvate	C00022	2.16	0.71	1.1	0.81
		lactate	C00186	1.18	0.95	1.09	1.03
	Nucleotide sugars, pentose metabolism	6-phosphogluconate	C00345	0.76	1.05	1.04	1.03
		sedoheptulose-7-phosphate	C05382	0.7	1.21	1.2	2.19
		ribose	C00121	1.79	0.52	1.43	1.26
		ribose 5-phosphate	C00117	1.17	0.52	1.6	1.25
		Isobar: ribulose 5-phosphate, xylulose 5-phosphate		1.2	0.54	1.89	1.49
		UDP-glucose	C00029	1.18	0.75	1.05	0.79
		UDP-glucuronate	C00167	0.95	0.92	0.82	0.69
		xylitol	C00379	2.63	0.52	1.48	1.52
		xylonate	C05411	1.81	0.9	0.96	0.94
	Krebs cycle	succinate	C00042	1.68	0.77	1	0.91
		fumarate	C00122	1.94	0.96	1.04	1.25
		malate	C00149	0.94	0.83	0.98	0.88
Lipid	Essential fatty acid	linoleate (18:2n6)	C01595	0.54	1.17	1.16	1.34
		linolenate [alpha or gamma; (18:3n3 or 6)]	C06427	0.39	1.04	0.92	0.97
		dihomo-linolenate (20:3n3 or n6)	C03242	0.23	1.14	1.6	2.1
		eicosapentaenoate (EPA; 20:5n3)	C06428	0.53	1.06	1.14	1.08
		docosapentaenoate (n3 DPA; 22:5n3)	C16513	0.35	1.09	1.63	1.8
		docosapentaenoate (n6 DPA; 22:5n6)	C16513	0.22	1.36	1.68	2.59
		docosahexaenoate (DHA; 22:6n3)	C06429	0.26	1.29	1.42	2.02
	Medium chain fatty acid	heptanoate (7:0)	C17714	1.27	1.23	0.83	0.99
		caprylate (8:0)	C06423	1.36	0.9	1.15	1.25
		laurate (12:0)	C02679	1.32	1.07	1.15	1.11
	Long chain fatty acid	myristate (14:0)	C06424	1.1	1.15	1.07	1.09
		myristoleate (14:1n5)	C08322	1.4	1.17	1.03	1.06
		10-heptadecenoate (17:1n7)		0.48	2.2	1.29	3.16
		oleate (18:1n9)	C00712	0.85	1.15	1.29	1.67
		10-nonadecenoate (19:1n9)		0.55	3.18	1.3	5.14
		eicosenoate (20:1n9 or 11)		0.97	1.03	1.21	1.41
		dihomo-linoleate	C16525	0.57	1.05	1.34	1.72

		(20:2n6)					
		mead acid (20:3n9)		0.42	0.94	1.03	1.21
		arachidonate (20:4n6)	C00219	0.16	1.3	1.69	2.43
		docosadienoate (22:2n6)	C16533	0.86	0.87	1.15	1.11
		2-hydroxystearate	C03045	3.11	0.57	1.02	0.76
		2-hydroxypalmitate		3.94	0.51	0.98	0.67
	Fatty acid, dicarboxylate	2-hydroxyglutarate	C02630	1.66	0.71	0.87	0.58
	Fatty acid, amide	stearamide	C13846	0.61	2.04	1.53	1.55
	Endocannabinoid	oleic ethanolamide		1.33	1.27	1.24	1.9
		palmitoyl ethanolamide		1.29	1.22	1.2	1.49
	Fatty acid metabolism (also BCAA metabolism)	propionylcarnitine	C03017	0.12	0.76	0.63	0.39
		butyrylcarnitine		0.17	1.22	1.72	1.51
	Carnitine metabolism	deoxycarnitine	C01181	0.51	1.06	1.06	1.07
		carnitine	C00318	0.1	1.26	1.29	1.2
		3-dehydrocarnitine *		0.31	1	1	1
		acetylcarnitine	C02571	0.16	1.19	1.28	1.01
	Glycerolipid metabolism	choline phosphate	C00588	4.21	0.67	1.32	0.92
		ethanolamine	C00189	0.96	1.37	1.19	2.51
		phosphoethanolamine	C00346	0.49	1	1.84	1.83
		choline	C00114	1.02	1.23	1.32	1.65
		glycerophosphorylcholine (GPC)	C00670	1.59	0.74	1.15	0.57
		cytidine 5'-diphosphocholine	C00307	1.13	0.7	0.95	0.75
Lipid	Inositol metabolism	scyllo-inositol	C06153	0.19	0.94	0.8	0.86
	Ketone bodies	3-hydroxybutyrate (BHBA)	C01089	1.15	1.07	1.31	1.27
	Lysolipid	1-palmitoylglycerophosphoethanolamine		1.55	1	1.07	1.19
		2-palmitoylglycerophosphoethanolamine*		0.89	1.26	1.61	1.57
		2-palmitoleoylglycerophosphoethanolamine*		1.48	1.04	1.26	1.03
		1-stearoylglycerophosphoethanolamine		1.5	0.64	1.28	0.95
		1-oleoylglycerophosphoethanolamine		1.3	0.8	1.1	0.96
		2-linoleoylglycerop		1.07	1.02	1.42	1.09

		hosphoethanolamine*					
		2-arachidonoylglycerophosphoethanolamine*		0.92	1.11	1.33	1.06
		2-docosapentaenoylglycerophosphoethanolamine*		0.66	1.2	1.38	0.97
		2-docosahexaenoylglycerophosphoethanolamine*		0.74	1.18	1.31	1.1
		2-myristoylglycerophosphocholine*		0.79	1.29	1.4	1.24
		2-palmitoylglycerophosphocholine*		0.72	1.11	1.51	1.01
		1-linoleoylglycerophosphocholine	C04100	0.49	1.04	1.42	0.85
		2-linoleoylglycerophosphocholine*		0.53	1.05	1.47	0.87
		2-arachidonoylglycerophosphocholine*		0.41	1.04	1.43	0.96
		1-docosapentaenoylglycerophosphocholine*		0.36	1.03	1.07	0.71
		2-docosapentaenoylglycerophosphocholine*		0.27	1.31	1.64	1.27
		2-docosahexaenoylglycerophosphocholine*		0.3	1.05	1.38	1.12
		1-stearoylglycerophosphoinositol		0.66	1.18	1.2	0.94
		1-palmitoylplasmenylethanolamine*		1.51	0.55	1.13	0.87
	Monoacylglycerol	1-linoleoylglycerol (1-monolinolein)		0.67	0.99	1.28	1.11
	Sphingolipid	sphinganine	C00836	1.52	1.07	1.31	1.27
		sphingosine	C00319	0.77	1.31	1.46	1.74
		palmitoyl sphingomyelin		0.6	0.84	1.04	0.84
		stearoyl sphingomyelin	C00550	0.41	1.23	1.12	1.13
	Sterol/Steroid	lathosterol	C01189	2.98	1.51	1.1	1.47
		cholesterol	C00187	0.76	0.89	1.12	0.99
		7-dehydrocholesterol	C01164	1.58	1.44	1.08	1.35
		7-alpha-hydroxycholesterol	C03594	2.04	0.46	1.09	0.59

		7-beta-hydroxycholesterol	C03594	1.65	0.6	1.09	0.69
		lanosterol	C01724	9.64	0.73	1.04	0.77
Nucleotide	Purine metabolism, xanthine containing	hypoxanthine	C00262	1.37	1.07	1.33	1.99
		inosine	C00294	2.67	0.61	1.45	1.49
	Purine metabolism, adenine containing	adenosine	C00212	0.67	1.12	1.7	2.22
		adenosine 2'-monophosphate (2'-AMP)	C00946	1.04	0.99	1.2	1.43
		adenosine 3'-monophosphate (3'-AMP)	C01367	1.53	0.82	1.41	1.35
		adenosine 5'-monophosphate (AMP)	C00020	1.37	0.91	1.48	1.14
		adenosine 5'-diphosphate (ADP)	C00008	1.13	0.76	1.02	0.74
		adenosine 5'-triphosphate (ATP)	C00002	1.43	0.88	0.84	0.62
	Purine metabolism, guanine containing	guanine	C00242	1.01	1.28	1.31	2.07
		guanosine	C00387	1.7	0.61	1.77	1.58
		guanosine 5'-triphosphate	C00044	1.67	1.13	0.83	0.77
		guanosine 5'-diphospho-fucose		1.11	1.18	1.17	1.33
	Pyrimidine metabolism, cytidine containing	cytidine	C00475	5.69	0.23	0.72	0.56
		cytidine 5'-monophosphate (5'-CMP)	C00055	1.32	0.83	1.05	0.9
	Pyrimidine metabolism, thymine containing	thymidine	C00214	1	1	1	1.66
	Pyrimidine containing, uracil containing	uridine	C00299	3.26	0.71	1.33	1.37
		pseudouridine	C02067	0.58	1.29	1	1.23
		uridine monophosphate (5' or 3')		1.53	0.65	1.38	1.1
		uridine 5'-diphosphate (UDP)	C00015	1.25	0.74	0.95	0.7
		uridine 5'-triphosphate (UTP)	C00075	1.32	1.01	0.73	0.71
Cofactors and vitamins	Ascorbate and aldarate metabolism	glucarate (saccharate)	C00818	0.94	0.83	0.62	0.57
	Folate metabolism	5-methyltetrahydrofolate (5MeTHF)	C00440	1.83	1.13	1.33	1.23
		folate	C00504	1	1.86	1.95	4.2
		nicotinamide adenine dinucleotide (NAD+)	C00003	0.75	1.16	0.73	0.92
		nicotinamide adenine dinucleotide reduced (NADH)	C00004	1.16	0.53	1.08	0.43
		nicotinate adenine	C00857	0.85	1.56	1.15	2.18

		dinucleotide (NAAD+)					
		nicotinamide riboside*	C03150	0.89	0.48	1.25	0.61
		adenosine 5'diphosphoribose	C00301	0.3	1.1	0.88	0.94
		1-methylnicotinamide	C02918	1.84	0.88	1.42	1.32
	Pantothenate and CoA metabolism	pantothenate	C00864	0.88	0.78	0.93	0.84
		coenzyme A	C00010	1.8	0.9	0.95	0.89
	Riboflavin metabolism	flavin adenine dinucleotide (FAD)	C00016	1.18	1.03	1.1	1.16
		riboflavin (Vitamin B2)	C00255	1.22	1.29	1.97	1.97
		flavin mononucleotide (FMN)	C00061	0.72	2	1.38	2.43
	Thiamine metabolism	thiamin (Vitamin B1)	C00378	0.88	0.99	2.16	3.43
Xenobiotics	Chemical	HEPES		1.19	1.04	1.09	1.1
		phenol red	C12600	1.11	1.18	1.41	1.61
	Drug	penicillin G	C05551	0.8	1.12	1.39	1.17
	Sugar, sugar substitute, starch	erythritol	C00503	0.59	1.05	1.04	1.05

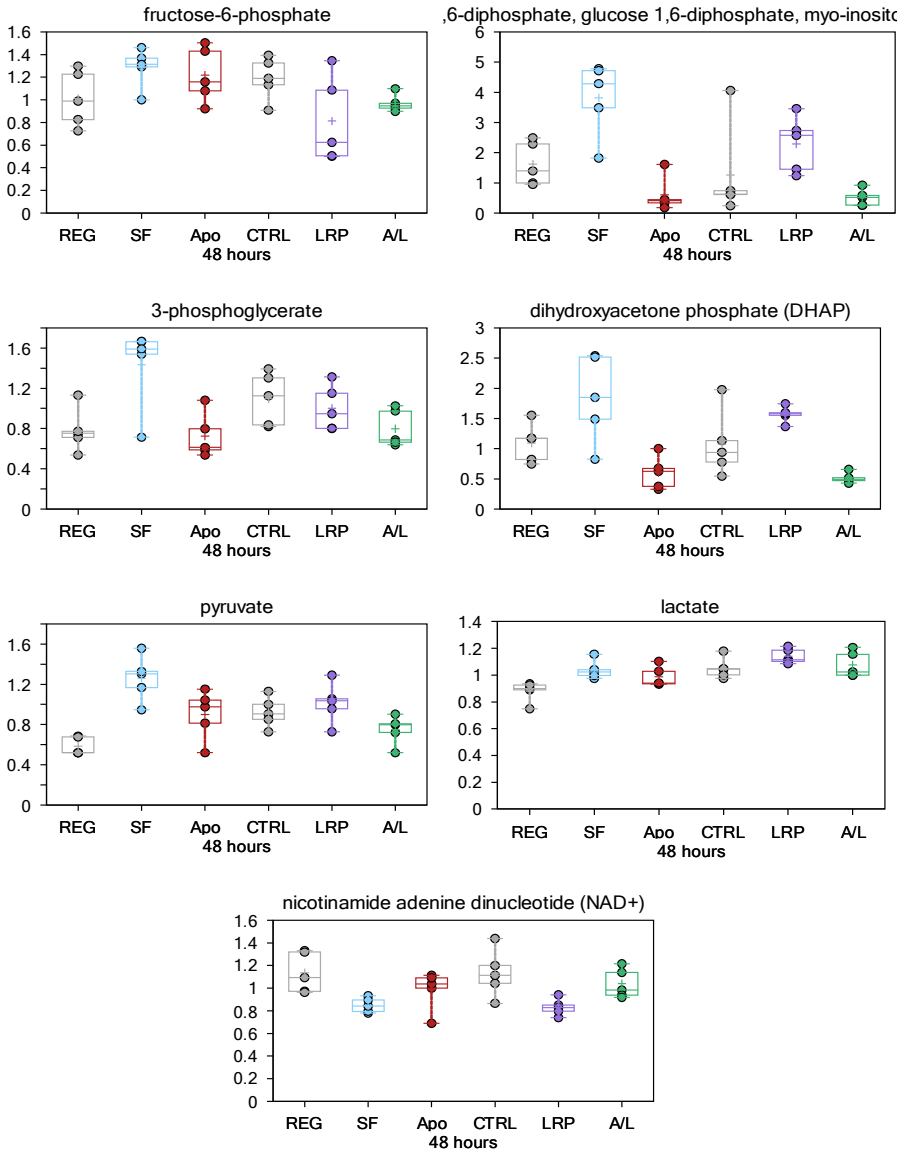

Figure 23. Glycolytic metabolism in serum-starved BT-549 cells. The increase in glycolytic intermediates indicates that serum-starved TNBC cells utilize the Warburg metabolism program to subsist and grow in the face of reduced nutrient content. The reduction in pentose phosphate pathway intermediates indicates that TNBC cells reduce anabolic reactions through this pathway. ApoE4-induced rescue of serum starvation resulting in improved oxidative homeostasis and reduced the production of glycolytic intermediates to downregulate Warburg metabolism.

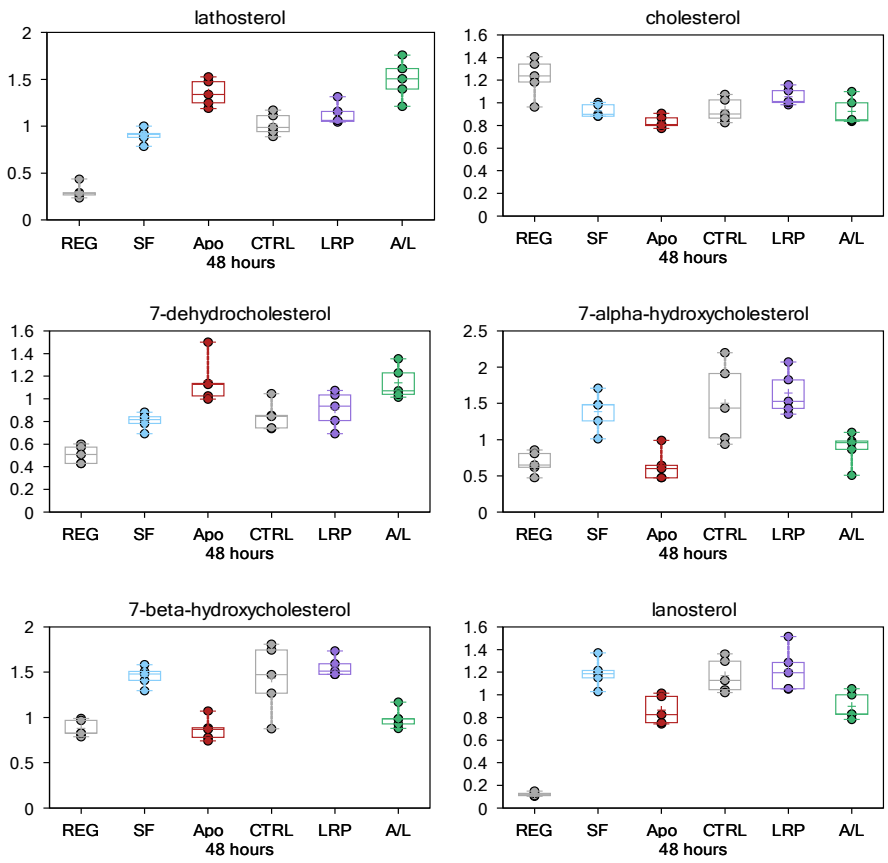

Figure 24. ApoE4-induced rescue of serum starvation resulting in reduction of cholesterol and fatty acid metabolites. As noted in gene expression profiling and confirmed in metabolic profiling, serum starvation affected levels of several cholesterol metabolites. ApoE4 rescued effects of serum starvation on likely oxidative stress metabolites 7α-hydroxycholesterol and 7β-hydroxycholesterol and the cholesterol precursor lanosterol. ApoE4 effects on cholesterol metabolism is related to the role of ApoE4 in regulation of cholesterol transport and metabolism.

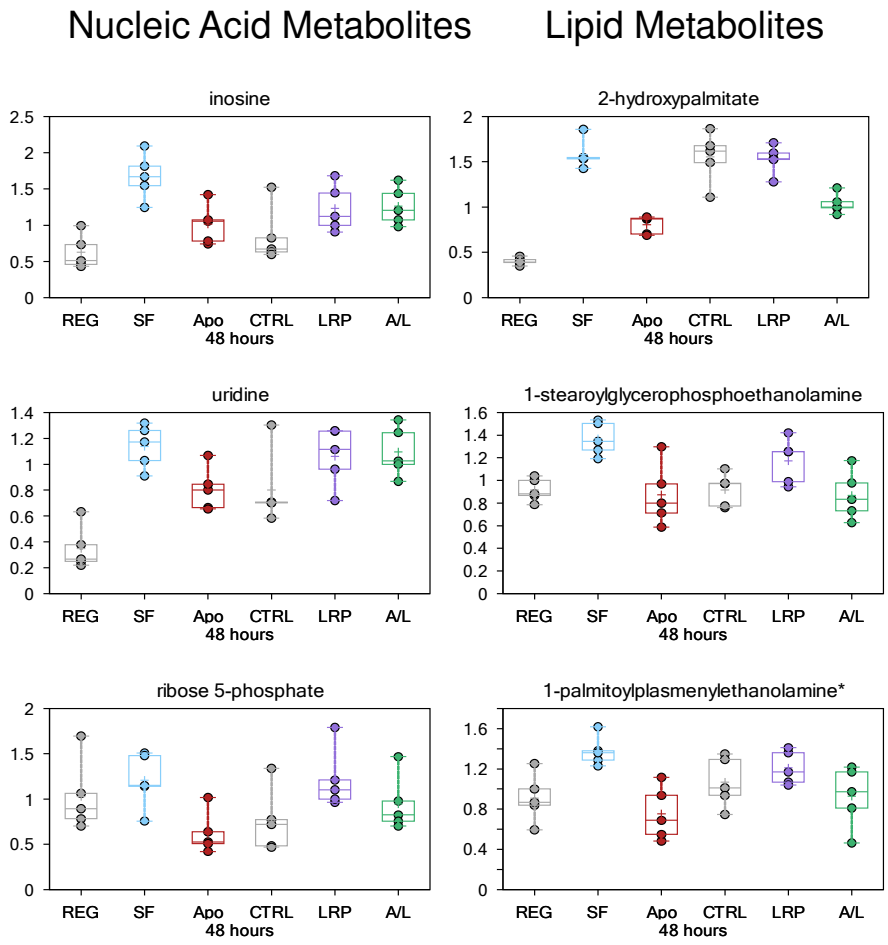

Figure 25. LRP8 knockdown reverses ApoE4-induced growth and restores pentose phosphate pathway. Nucleic acid metabolites, inosine, guanosine and uridine were more abundant in cells with serum-free media relative to regular media, and LRP knockdown further increased the levels of these nucleosides, while ApoE4 addition had the opposite effect. Intermediates to nucleotide synthesis that are components of the pentose phosphate pathway (ribose-5-phosphate and the ribulose-5-phosphate isobar) also had similar patterns. This pattern suggests that LRP8 may block ApoE rescue by impinging upon the pentose phosphate pathway and reverting the cellular response to serum-free metabolic responses.

3.19. Reduced tumor growth in shLRP8 MDA-MB-231 mouse xenografts

shLRP8 stable knockdown cell lines were used to establish xenografts in the mammary glands of nude mice. Significant differences in tumor volume were observed 3 weeks after tumor cell injection and persisted until 6 weeks after injection (Figure 26). The number of noted lymphovascular invasions was elevated in the shLRP8 group, in comparison to the one observed in the parental group (Figure 26). The percent of necrotic cells was significantly elevated in the shLRP8 group.

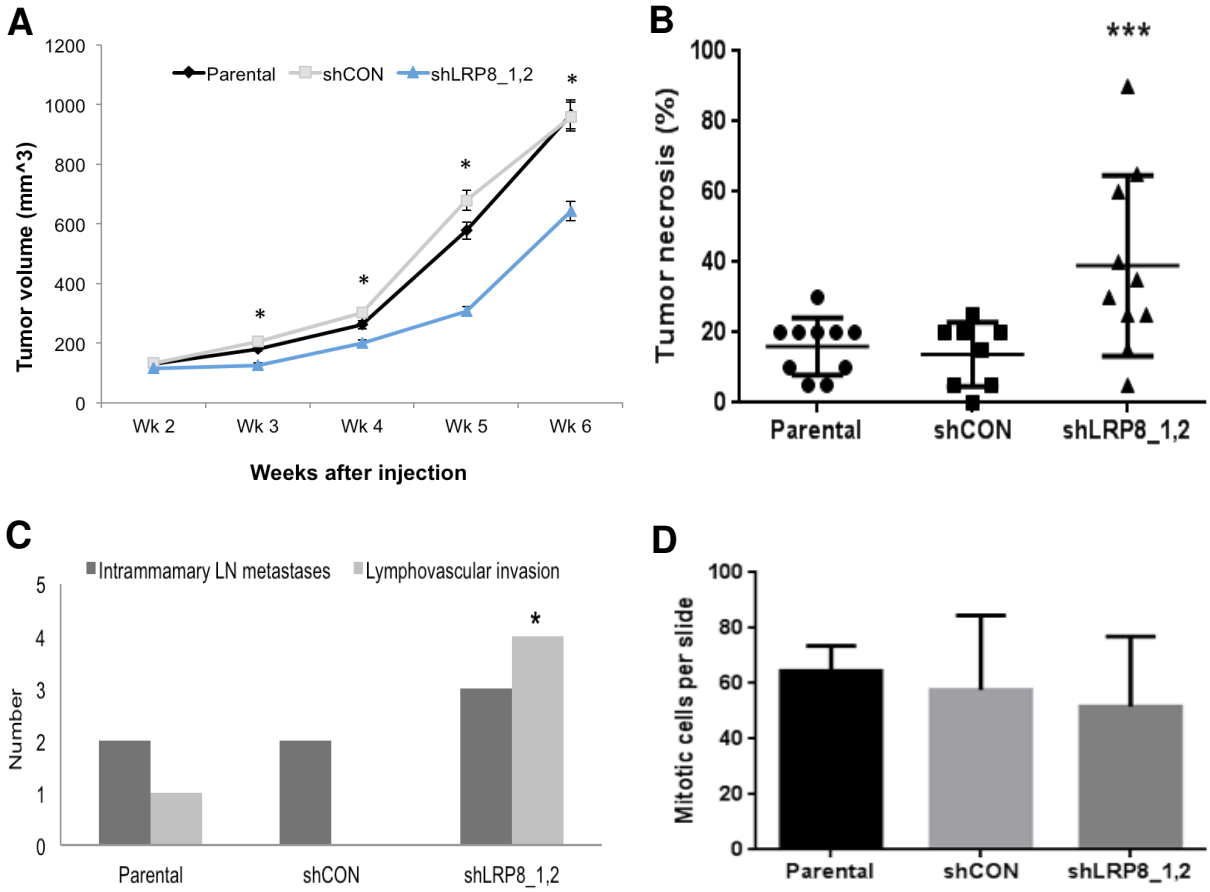

Figure 26. shLRP8 MDA-MB-231 xenograft study. (A) MDA-MB-231 parental, shCON, and shLRP8 xenografts were established in 4 week old nude mice (n=12 per group). (B) Tumor necrosis as a percentage of total tumor section per slide is shown. (C) Tumor sections were examined for the presence of intramammary lymph node metastases and sectioned nodes were examined for lymphovascular invasion. Raw number count is depicted in the first graph. (D) Mitotic cells were counted and the mean counts were tested. Mean tumor quantities of the three groups were tested with one-way ANOVA analysis. In all panels, * indicates $p<0.05$ and *** indicates $p<0.01$.

3.20. High Ki67 and LRP8 expression in human breast tumors

Immunohistochemical staining of LRP8 and VLDLR was performed in receptor-negative and receptor-positive human breast tumor samples to assess the relative level of protein expression. 59 tumor samples were stained for LRP8 or VLDLR. For LRP8, there were a total of 49 IHC readings that were interpretable (13 strongly staining, 11 moderately staining, 20 weakly staining, 5 negatively staining). 10 readings were discounted for the following reasons: 3 cases with no tumor cells present, 1 case with tissue floated, 2 cases needing H&E slide, and 4 cases with conflicting accession numbers between the slide label and IHC reading.

There were 31 grade III/IV tumors positive for LRP8 protein expression, in comparison to 3 grade III/IV tumors that were LRP8 negative (Table 5). The positive trend between high grade tumors and LRP8 protein expression did not reach statistical significance. High Ki67 expression was significantly associated with positive LRP8 staining (Figure 27).

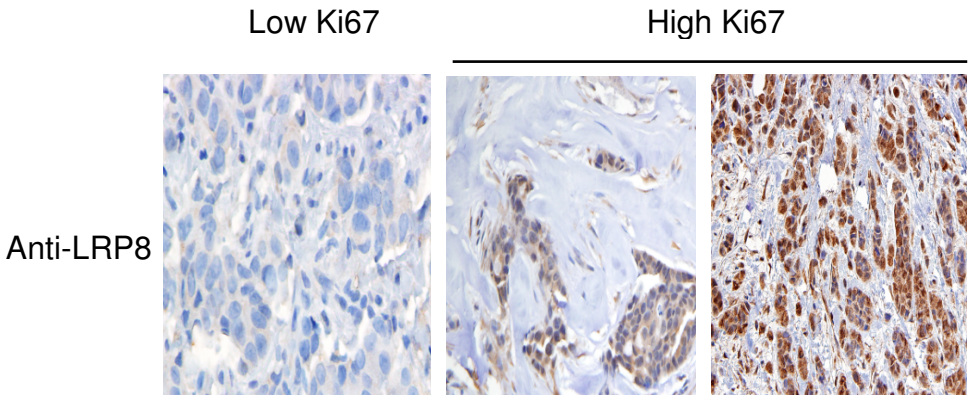

Figure 27. LRP8 staining in human breast tumor samples. Low Ki67 expression and negative LRP8 staining is shown on the left tissue sample. High Ki67 expression was significantly correlated with positive LRP8 expression and is shown on the two right panels.

Table 5. LRP8 protein expression and its relation to clinicopathologic variables of breast cancer patients

		Number	LRP8 positive* n (%)	LRP8 negative* n (%)	p-value***
All cases		49	44 (90)	5 (10)	
Age	<50	19	17 (39)	2 (40)	1
	≥50	30	27 (61)	3 (60)	
ER	positive	25	23 (52)	2 (40)	1
	negative	23	21 (48)	2 (40)	
	unknown	1	0	1 (20)	
HER2**	positive	13	13 (30)	0	0.5627
	negative	35	31 (70)	4 (80)	
	unknown	1	0	1 (20)	
Stage	I	3	2 (5)	1 (20)	0.2343
	II-III	45	42 (95)	3 (60)	
	unknown	1	0	1 (20)	
T	T0-T1	32	29 (66)	3 (60)	1
	T2-3	16	15 (34)	1 (20)	
	unknown	1	0	1 (20)	
N	NX-N1	41	36 (82)	5 (100)	0.5751
	N2-N3	8	8 (18)	0	
Nuclear grade	I-II	14	13 (30)	1 (20)	1
	III-IV	34	31 (70)	3 (60)	
	unknown	1	0	1 (20)	
Ki67**	High	24	23 (52)	1 (20)	0.025
	Low	3	1 (3)	2 (40)	
	unknown	22	20 (45)	2 (40)	

*LRP8 positive was considered strong and moderate immunostaining on IHC. LRP8 negative was considered weak immunostaining.

**HER2 positive was considered >2+ score on IHC. Ki67 high expression was considered >10% immunostaining.

***p-values are based on Fisher's exact test with n ≤ 5. Two-sided, 95% confidence interval, α<0.05.

3.21. ApoE genotyping of serum samples from human breast cancer

Previous studies reported that genotypic expression of ApoE4 (E3/E4 and E4/E4) is higher in early onset breast cancer (35). To further investigate this finding, we compared the rate of apolipoprotein E4 carrier genotype between women with (i) ER-negative / ER-positive breast cancer who are < 50 years and those (ii) who are >70 years of age. We hypothesized that ApoE4 carrier status (E4/E4, E3/E4, E2/E4) is more frequent among patients with young onset breast cancer compared to older patients women. The rate of ApoE4 carrier status was not significantly different amongst the three test cohorts, with 34% ApoE4 carrier status in the TNBC <50 years of age group, 28% in the non-TNBC <50 years of age group, and 29% in the all receptor status >70 years of age group (Table 6). This suggests that ApoE4 carrier status is not related to estrogen or progesterone receptor or HER2 status or age in the tested cohorts and that ApoE4 may be one signaling factor in the multifactorial development of TNBC.

Table 6. Frequency of differential APOE genotype in breast cancer subpopulations

		APOE Genotype, n (%)		
Patient group	Total	ApoE2	ApoE3	ApoE4
TNBC <50 years of age	50	4 (8)	29 (58)	17 (34)
Non-TNBC <50 years of age	50	8 (16)	28 (56)	14 (28)
Receptor positive Race-matched >70 years of age	50	10 (20)	26 (51)	15 (29)

Chapter 4 – Discussion

4.1. Target discovery and validation process

The study investigates the LRP8 - ApoE4 receptor - ligand system in the growth of triple-negative breast cancer. The systematic investigation of this receptor system started with target identification from human breast cancer samples and led to experimental analysis of the growth promoting properties in vitro and in vivo. LRP8 and VLDLR belong to the LDL receptor family, which are most notable for their roles in neuronal intracellular signaling after brain injury and for cholesterol uptake and metabolism through LRP8 and VLDLR membrane receptors in the periphery. This study examines a previously defined receptor – ligand system for its role in the context of triple-negative breast cancer.

Initial identification of the overexpressed genes in TNBC was performed using datasets from The University of Texas M. D. Anderson Cancer Center (initial discovery, n = 294) and from the Erasmus Medical Center in Rotterdam the Netherlands (validation set, n = 286). The total patient population represents patients across all age categories, race, and ethnicities. The total TNBC patient population in the initial discovery set was 73, which was comparable to the 56 patients in the validation dataset. The discovery dataset were comprised of fine-needle aspiration samples, which contain little or no contaminating stoma. These specimens represent an ideal tissue to define inherent molecular differences between breast cancer subsets. The additional filter (<2.0 fold overexpression) was introduced to confirm the initial discovery results and add confidence to the results obtained through sequential analysis of the initial discovery and validation datasets. The concurrent identification of amplified segments of DNA was performed for a smaller subset of 103 cases (35 of which were TNBC cases) from the

M. D. Anderson Cancer Center, which had matching CGH and transcriptional profiling results. These results confirm large-scale molecular differences between TNBC and other cancers.

Subsequent re-analysis of two additional datasets for the co-expression of the major ligands Reelin and APOE, receptors LRP8 and VLDLR, and intracellular adapter protein DAB1, was performed to assess whether the signaling system was consistently present across several transcriptomic datasets. This decreases the likelihood that the initial identification resulted in spurious results. The third database from the TRANSBIG study contained 170 samples, 46 TNBC and 124 non-TNBC and the fourth database from the Mainz study contained 178 samples, 23 TNBC and 155 non-TNBC (44, 45). The same interrogation of 2 cell line gene expression databases did not result in significant overexpression of the members of LRP8 – APOE signaling axis, however, the sample numbers were much lower, 51 and 19 cell lines respectively.

There were a number of advantages to the siRNA screen that ultimately identified the candidate genes that sustain the proliferation of TNBC cell lines. This high throughput screen has several advantages, (i) allows one to separate phenotypic markers from potential drivers of cancer cell growth by assessing how transient knockdown of a candidate gene affects growth in vitro, (ii) ability to compare growth inhibition in several cell lines so that an entire subset of breast cancer cell lines can be assessed to another, (iii) identifies key regulatory sequences in candidate genes that may serve as sites of downregulation in future transient or stable knockdown experimentation (based on the most effective siRNA target sequences), and (iv) the resulting dataset serves as a functional repository of annotated genes, many of which have unknown functions in

cellular biology. There are limitations of a large siRNA screen that were mitigated, at least in part, by the data normalization methods and the optimization of the transfection process for each cell line described herein.

As previously described, LRP8 and VLDLR are family members of the LDL receptor family and share similar structural motifs borne from similar DNA sequences. The siRNA target regions for LRP8 and VLDLR were unique regions that mapped to independent regions of each gene, indicating that the siRNA top tier hit results were not duplicated based on their sequence homology. Additionally, the plasmid rescue experiments performed separately for LRP8 and VLDLR in 2 independent breast cancer cell lines helps to rule-out off-target effects and supports their independent contributions to TNBC cell growth.

Validation that the loss-of-phenotype, i.e., reduction in viability, was due to a loss of LRP8 and VLDLR mRNA and protein further supports that the top tier hits from the initial siRNA screen could be promoted to the next step of evaluation, functional evaluation of the role of LRP8 and VLDLR in TNBC. There were some differences in the optimal time point to evaluate mRNA and protein levels amongst the TNBC cell lines that were chosen for further validation with a standardized concentration of 50 nM of siRNA oligonucleotide. There were also differences in the level of target knockdown that was achieved. This reflects differences in the growth rate independent to each cell line in common use.

The ligand stimulation studies revealed important lessons about LRP8 signaling in TNBC. Reelin exposure stimulated TNBC cell growth, but to a lesser extent than the ApoE isoform 4. It should be noted that mouse reelin was used, as recombinant human

reelin was not available commercially. The central fragment that was used in cell culture mediates receptor binding to LRP8 and VLDLR and shares 95% sequence homology with human reelin. The differential binding effects of the APOE isoforms contrasted rather starkly to one another, with ApoE isoform 2 resulting in reduced growth and viability of TNBC cells and ApoE isoform 4 resulting in profound stimulation of growth and the overall viability of TNBC cells. To confirm that the ApoE isoform results were reproducible, several lots of recombinant human ApoE isoforms from 2 different manufacturers was used. The trend was consistent amongst different lots and protein manufacturer. However, there were experimental variations in viability values that were observed amongst the 5 replicate experiments. Lots of ApoE isoforms that were rehydrated and stored for longer periods of time resulted in reduced stimulation in ligand binding studies, suggesting that a minimal level of protein degradation occurs.

The ELISA binding assays between recombinant human LRP8 and ApoE4 serve as proof of principle that biologics may be active against the long extracellular binding region of LRP8. Additionally, ApoE4 stimulation resulted in robust proliferative signal at 48 hours and the addition of RAP abolished the stimulatory effect, indicating that the two components compete for the LRP8 associated binding regions with higher RAP concentrations. RAP is not a probable candidate for therapeutic inhibition due to the promiscuous binding to multiple LDL receptor family members and high potential for off-target cardiovascular effects. Likewise, this study concentrated on the LRP8 membrane receptor due to the restriction of its tissue distribution to the testes and brain, reducing the possibility of systemic off-target effects during the use of targeted therapeutics in most patients with breast cancer.

High-throughput analyses of the ApoE4 stimulatory effects on TNBC growth revealed several lessons about LRP8- and VLDLR-expressing TNBC cells, (i) transcriptomic and metabolomic results indicate that TNBC cells amplify internal synthesis of steroids and lipids as energy sources and utilize glycolysis during environmental stress, (ii) ApoE4 restores the cell's response to external signals and triggers the metabolism of supplied ApoE4, and (iii) the downstream mediators of growth are members of the MAPK signaling network, which integrate the ApoE4 stimulatory signal at the membrane surface into protein changes required for growth. Interestingly, human fibroblasts preferentially utilize external sources of LDL cholesterol and keep biosynthesis at reduced levels for energy conservation (51).

This study is the first to investigate LRP8 – ApoE4 signaling in breast cancer. It supports previous findings that ApoE4 may mediate higher affinity binding to LRP8 and VLDLR and relates it to the activation of growth promoting signaling pathways for triple-negative breast cancer. The study may explain the well-documented association between obesity and breast cancer (52-55). It refines the existing knowledge by detailing that *APOE* genotype (ε4) may regulate LRP8- and VLDLR- expressing tumor cells in their unique metabolism that adapts well to nutrient-rich and serum-starved conditions.

4.2. Coordination of proliferative and metabolic pathways in TNBC

The aggressive phenotype of triple-negative breast cancer is well established (56, 57). The disease phenotype is typified by a high rate of proliferative activity and increased rates of metastases. However, the underlying biology is not completely understood for triple-negative tumors. Two prognostic signatures comprised of 264 and 26 probe sets were identified from supervised analysis of triple-negative breast cancers. *IL-8-related, VEGF-related,* and *histone-related* were identified as the major regulatory metagenes associated with poor prognosis (58). These signatures relate that triple-negative tumors may be driven by high inflammatory activity and aided by low functioning B-cell humoral responses.

Oncogenic mechanisms involving AKT activation, MYC-mediated carcinogenesis, and MAP kinase signaling result in altered metabolic pathways that are specific to the cancer cell and contribute to the observation that Otto Warburg made; cancer cells have increased dependence on glycolysis (59). Akt mediates growth factor signaling to change proliferation, growth, and survival in response to changes in the extracellular environment. Akt is also a major regulator of glucose homeostasis and works by increasing GLUT1 transport, hexokinase activity, and phosphofructokinase activity to mediate activation of glycolysis (60). Further, AKT1 enhances Glu-4 expression and activates the hexokinase to phosphorylates glucose to glucose 6-phosphate in the first step of glycolysis (60). Akt may also be important in the regulation of *de novo* fatty acid synthesis, by elevating gene expression of enzymes for cholesterol and fatty acid biosynthesis such as ATP citrate lyase, HMG-CoA reductase, fatty acid synthase, and stearoyl-CoA desaturase (61). However, the transcription of these enzymes

requires members of the stearoyl-regulatory element-binding protein (SREBP) family of transcription factors. The activities of the SREBP family are mediated downstream by the mitogen-activated protein kinase pathway (62).

Myc has been implicated in the carcinogenesis of most common human cancers. In terms of the glycoloytic switch mechanisms, Myc activation stimulates pyruvate dehydrogenase kinase, isozyme 1 (PDK1) and lactate dehydrogenase A (LDH-A), which prevents pyruvate conversion to acetyl CoA to produce lactate (63-65). The Sp family of transcription factors has been shown to integrate proliferative signals and altered metabolism through upregulation of fatty acid synthase (FAS) through Sp1 (66). Sp1 is also regulates CDC25A, indicating that transcription factors may play a role in integrating proliferation and metabolic factors in breast cancer (66).

Oncogenes are not the only actors in the altered metabolic schema. Tumor suppressor pathways support or restrict metabolic activity. For example, *TP53* induces the expression of *TP53*-induced glycolysis and apoptosis regulator (TIGAR) to inhibit glycolysis and shunt precursors to the pentose phosphate pathway after DNA damage, or represses the activity of the rate limiting enzyme of this pathway, glucose 6-phosphate dehydrogenase (67). p53 mutations are a frequent event in TNBC and may result in reduced senescence and apoptosis, which is promoted by upregulation of cyclin-dependent kinase inhibitor 2A (CDKN2A, p16Ink4A) and inhibition of cyclin-dependent kinase 2 (68). The functional consequence of p53 mutations in breast cancer is still unclear, but a working hypothesis involves cell cycle deregulation that promotes accelerated proliferation and reduced DNA repair pathway mechanisms that promote tumorigenesis (69, 70). The coordination of multiple cellular signals require signaling

centers that can integrate and regulate cellular responses; Akt, p53, HIF-1, NF-κB, and Myc are integrators that can channel signals and orchestrate the interaction between proliferation and metabolic pathways (71-73).

The high rate of proliferation in TNBC cells, enabled by oncogenic mechanisms, is the basis for the metabolic differences between normal cells and cancer cells (74-80). High demand for cell cycle biomolecules requires a shift into anabolic metabolism, a transition from the normal catabolic mechanisms that breakdown glucose, fats, and amino acids into ATP energy-rich molecules (81-82). Signs of anabolic metabolism are high rates of glycolysis, the production of lactic acid, and the production of necessary macromolecules to be used in constructing new plasma membranes and in membrane remodeling as a result of increased growth factor signaling at the cellular periphery (83-84). The ability to maximize on the limited supply of energy biomolecules through increased glycolytic flux and fatty acid metabolism under low nutrient and anaerobic conditions allows TNBC cells to grow and persist despite high energy demands and compromised nutrient conditions (85-86).

Increased glucose uptake occurs at the cellular plasma membrane and enhances the synthesis of cholesterol and fatty acids, nucleic acids, and the process of gluconeogenesis to support high energy demands of TNBC cells (87-88). The glycolysis pathway is the convergence point of proliferation and metabolism. TNBC cells have increased glycolytic flux and dependence on the Warburg metabolism to generate ATP, albeit inefficiently (89). To supplant this deficiency, serine biosynthesis is increased to fuel anaplerotic contributions of serine into the tricarboxylic acid (TCA) cycle (90). In ER-negative cell lines, *PHGDH* is overexpressed as a result of DNA amplifications and

encodes for 3-phosphoglycerate dehydrogenase: the key enzyme that bridges the gap between glycolysis and the serine synthesis pathway (85, 86). Serine biosynthesis is essential for protein and nucleotide biosynthesis and further indicates that anabolic metabolism is important in the growth and survival of cells receptor-negative tumor cells with high energy demand. The detachment of MCF-10A cells from the surrounding matrix is energized by ATP produced from fatty acid β-oxidation and not glucose metabolism, suggesting that the transition from a normal cellular state to a state of cancer is mediated by altering the pathways for energy production and increasing the per molecule yield of ATP (91). The shift from epithelial to a mesenchymal phenotype occurs with loss of fructose-1,6-bisphosphatase (FBP1) and increased glycolytic flux and lactate production in TNBC cell lines (65).

In the clinic, there is an association between patients with triple-negative breast cancer and metabolic syndrome. Metabolic syndrome manifests as central obesity, insulin resistance, and dyslipidemia (92, 93). Experimental models using cell lines and mice indicate that the insulin-leptin metabolic axis is perturbed and contributes to tumorigenesis of breast cancer (94, 95). However, the exact mechanisms involved are still unclear, but the following data encapsulates what is currently known. The upregulation of insulin may increase breast cancer cell proliferation through insulin-receptor signaling (94, 95). Conversely, insulin-mediated intracellular signaling may reduce the bioavailability of binding factors for insulin-like growth factors and effectively increase insulin bioavailability (94, 95). Unbound insulin in the plasma increases the level of insulin-like growth factor 1 (IGF-1) through positive feedback (96). The administration of Metformin or insulin inhibits the proliferative and colony

formation ability of TNBC cells, reduces tumor growth in TNBC xenograft mice, and is associated with reduced cancer burden in patients with type 2 diabetes mellitus (95, 97). The regulatory hormone for hunger, leptin, has been shown to increase hunger signals to the hypothalamus and increase IGF-1 receptor activity leading to increased phosphorylation of the leptin receptor in a feed-forward mechanism of action (95). Crosstalk between the IGF and EGFR pathways increased proliferation and migration of TNBC cells, amplifying the downstream activities of mitogen-activated protein kinases (MAPK), signal transducer and activator of transcription 3 (STAT3), cyclin D1, vascular endothelial growth factor (VEGF), and protein kinase B (Akt) (leptin). Approximately 70% of TNBC tumors overexpress EGFR and clinical trials are currently underway that test the efficacy of several EGFR inhibitors (95). The combination of EGFR inhibitors and chemotherapeutic regimens using carboplatin plus cetuximab and irinotecan/carboplatin plus cetuximab has been shown to have some initial therapeutic value. However, there was no improvement in objective response rate, progression-free survival, or overall survival for metastatic TNBC patients (99, 100).

Despite the understanding that metabolism and proliferation are interconnected, the critical molecular regulators of amplified proliferative activity in triple-negative breast cancer have not been identified. The central goal of this study was to identify and validate potential new targets for TNBC. In this study, LRP8 and one of its ligands, ApoE4, were found to stimulate breast cancer cell lines and its downregulation in TNBC mouse xenografts reduced tumor incidence and volume. The LRP8 – ApoE4 signaling axis may represent one path towards amplified proliferation and altered metabolism for the growth and survival of triple-negative cells.

4.3. Significance of LRP8 – ApoE4 signaling to TNBC tumor biology

In light of the previously discussed results, there are genes that are important to proliferative signaling and activation of the metabolic switch of TNBC. The underlying biology that drives TNBC growth and survival integrates proliferation and metabolic pathways. These pathways are dependent on key regulatory genes that are currently untargeted.

The identification and characterization of molecular targets of TNBC has been limited by (i) availability of enough TNBC cases, (ii) validation in more than one experimental model system, and (iii) the heterogeneity of TNBC. TNBC cases comprise between 20 to 25% of all breast cancer cases. Therefore, triple-negative tumors represent a small proportion for a given gene expression study. The recent increase of molecular profiling of human breast tumors has created a rich repository of gene expression data and enabled the discrimination of overexpressed genes in a statistical study that can be powered for accurate discovery. This study identified 681 genes that may contribute to TNBC proliferation from a discovery data set of 294 breast tumors with 73 receptor-negative cases and a validation data set of 286 breast tumors with 56 receptor-negative cases. *In vitro* validation in multiple TNBC cell lines, MDA-MB-231 tumor xenografts, and additional analysis of 2 separate gene expression data sets provides a competitive basis to confirm the role of LRP8 in TNBC biology. TNBC tumor heterogeneity has been reported as one reason for the reduced efficacy of cetuximab, an anti-EGFR antibody (100-102). It is likely that a subtype of TNBC that overexpress EGFR is sensitive to anti-EGFR treatment. However, the clinical success of targeting EGFR may be dependent on the discovery of genes that drives proliferation and contributes to altered metabolism, the

reproducibility of *in vitro* and *in vivo* experiments, patient selection for treatment regimens, and targeting the critical amplifiers of tumor growth.

Lipid metabolism has been associated with estrogen receptor-negative breast cancers. Lipidomic profiling of 257 primary breast tumors identified a candidate list of 24 genes involved in lipid metabolism (103). Several phosphocholines, phosphatidylethanolamines, phosphatidylinositols, and sphingomyelins were upregulated in ER-negative tumors of high grade (103). These membrane phospholipids are responsible for incorporating newly synthesized fatty acid chains into the plasma membrane (103). Acetyl-CoA carboxylase 1 (ACACA), stearoyl-CoA desaturase-1 (SCD), fatty acid synthase (FASN), sterol regulatory element-binding protein 1 (SREBP-1), and insulin-induced gene 1 (INSIG1) were highly expressed in ER-negative tumors. siRNA silencing of ACACA, FASN, and INSIG1 in MDA-MB-468 cells reduced cell viability and induced apoptosis, suggesting that lipid biosynthesis and metabolism plays a critical role in TNBC cell survival (103). Increased suppression of cell viability was observed for breast cancer cells with higher expression of lipogenic genes. Interestingly, siRNA-mediated reduction of proliferation was higher in MDA-MB-468 vs. MCF-10A cells, but the expression level of lipogenic genes was not different between cancer and normal cells. This suggests that (i) normal and receptor-negative cancer cells have different metabolic circuitry that drives growth, (ii) there are external triggers that may activate or inhibit lipid metabolism to modulate growth signals, and (iii) initiating target discovery in primary tumor samples may be more relevant to tumor biology. Further, in this study, ACACA, FASN, and INSIG1 were highly upregulated in low-lipid, serum-starvation conditions, recapitulating the *in vivo* shift into anabolic conditions of active

storage of lipid biomolecules. These studies suggest that *de novo* fatty acid synthesis and membrane phospholipids restructuring occur together in ER-negative cells. Further, the function of fatty acid synthase (FASN) may be modulated according to metabolic needs during the long-course of tumor progression (104).

In this study, LRP8 – ApoE4 signaling was identified as a potential mediator of environmental conditions that trigger internal metabolic changes to permit a high level of metabolic adaptability for growth and survival during times of reduced nutrient availability in TNBC cells. LRP8 – ApoE4 signaling resulted in stimulation of growth of triple-negative breast cancer cell lines and LRP8 silencing reduced TNBC cell growth *in vitro* and *in vivo*. This suggests that extracellular ligands, such as members of the apolipoprotein family, engage cognate lipoprotein receptors to increase cell proliferation. This process is regulated by the amount of nutrients in the surrounding environment. In low serum conditions, TNBC cells grew more slowly, exhibited signs of anabolic metabolism by increasing *de novo* synthesis of lipids by upregulation of fatty acid desaturase 1 and 2 (FADS1, FADS2), FASN, and LDLR, and increased the levels of key glycolytic intermediates (fructose-6-phosphate, fructose 1,6-diphosphate, 3-phosphoglycerate, pyruvate, and lactate) to participate in Warburg metabolism (59, 93). A downstream effect is the increase in TCA cycle intermediates (succinate and fumarate). This process is inefficient and costly in comparison to normal oxidative respiration, evidenced by the increase in reactive oxygen species such as reduced glutathione (GSH) and the strong signature of oxidative stress. Interestingly, the levels of long chain fatty acids were less abundant in low serum, while the levels of medium chain fatty acids were increased. This suggests that the breakdown of fatty acids, fueled by the increased *de*

novo synthesis of lipids, was active and used to fuel energy demands as part of a metabolic response to low nutrient conditions.

In response to the introduction of apolipoprotein E isoform 4, one of two potential ligands for LRP8, TNBC cells converted the intracellular signaling response. ApoE4 stimulation downregulated many of the same members of the lipid biosynthesis family (FASN and LDLR), reduced levels of glycolysis and TCA intermediates, increased the levels of MAP2K1, and increased phosphorylation of threonine 180 and tyrosine 182 to activate MAPK14. The lipid biogenesis activity was centered around SREBF2, a transcription factor that stimulates transcription of sterol-regulated genes. The restoration of exogenous growth signals from ApoE4 rescued TNBC cells from a fasted state of serum starvation and allowed them to re-establish high levels of proliferation. This data suggests that triple-negative cells are capable of switching their metabolic programming to accomodate the absence or presence of extracellular growth factors. During times of low nutrient content in the extracellular milieu, triple-negative cells actively build lipids using acetyl-coA stores that remain in the cell to feed themselves. This anabolic process is temporary as cells and tissues become depleted of energy equivalents. In the body, the process of proteolysis and lipolysis from existing protein and fat mass eventually leads to extreme anabolic shock and metabolic acidosis and renal dysfunction followed by multi-organ failure, without exogenous nutrient supplementation (starvation). However, once nutrients are restored, exemplified by the addition of ApoE4 to triple-negative cells, cells reduce their anabolic response and use the lipid signal to activate downstream signaling for amplified proliferation.

Perhaps, as a triple-negative tumor grows in mass and constructs new blood vessels there is a period of time whereby cells are starved of growth factors and oxygen (angiogenesis triple-negative). The metabolic switch into anabolism allows them to grow and survive for a short period of time. The arrival of growth factors and oxygen through newly established vessels allow triple-negative cells to re-enter catabolic metabolism. This metabolic adaptation enables triple-negative cells to adapt and thrive irrespective of the changing metabolic environment.

The added knowledge that LRP8 – ApoE4 signaling initiates metabolic switching in TNBC cells (i) identifies biological mediators that integrate proliferation and metabolism pathways, (ii) introduces a membrane receptor – ligand pair that could be targeted using new or existing compounds, and (iii) contributes to the need for rational design of therapeutic regimens that incorporate metabolic responses.

4.4. Further credentialing of LRP8-ApoE4 signaling in TNBC

There are several limitations to this study that should be further investigated. It is unclear how TNBC cells function in the presence of full serum and ApoE4 ligands. There is some inconsistent data that suggests ApoE4 stimulation is present, but blunted in the presence of other ligands in full serum culture conditions. In addition, there is some data suggesting that miRNAs targeting ApoE contributes to invasion and metastatic endothelial recruitment, indicating that ApoE is an anti-angiogenic factor (miRNA ApoE). The elevated number of intramammary lymph node metastases and lymphovascular invasions were higher in shLRP8 MDA-MB-231xenografts, suggesting that the loss of LRP8 signaling results in reduced tumor cell proliferation, but also that

the loss of ApoE-mediated anti-angiogenic signaling through LRP8 increases the invasive potential of triple-negative tumor cells. Further, in the human body, it is unclear how chylomicron-bound ApoE4 associates with LRP8 / VLDLR to induce tumor cell growth in the mammary gland. It is also unclear whether ApoE4 dissociates from chylomicrons to engage LRP8 and how this occurs during fluctuating states of tumor cell growth. Further, the stable integration of shLRP8 in the MDA-MB-231 cell line was quite difficult to sustain, indicating that TNBC cells may have robust compensatory growth mechanisms that maintain LRP8 expression levels, which may require rational combinations of chemotherapy and targeted therapeutics against LRP8.

The primary focus of future studies in TNBC utilizing the LRP8 – ApoE4 signaling axis will be to define (i) how to target the LRP8 – ApoE4 signaling axis, (ii) the exact signaling mechanisms that occur after LRP8 – ApoE4 after inhibition, (iii) whether inhibition of signaling can reduce proliferation *in vivo*, and (iv) the potential effects on lipid biosynthesis and metabolism after inhibition.

4.5. Potential impact of targeting LRP8 - ApoE4 in TNBC

The potential impact of targeting LRP8 signaling in TNBC revolves around the (i) effects on lipid and cholesterol metabolism and trafficking, (ii) off-target effects of tissues that express LRP8, and (iii) potential to complement existing chemotherapeutics and synergistically attack proliferation and metabolism.

There may be some effects on lipid and cholesterol metabolism. *Reelin* knockout mice display neurological defects in neuronal migration during development, decreased size of the cerebellum, and reduced synaptic activity (29). However, there is no indication

of dyslipidemias or hypercholesterolemia, suggesting that Reelin and ApoE4 signaling is not cooperative. Conversely, ApoE knockout mice have reduced ability to lower plasma cholesterol levels and develop vascular lesions (105). LRP8 was chosen as the primary target of this study due to its restricted tissue expression distribution in the testes and brain. VLDLR has a wide tissue expression distribution and is expressed throughout the body specifically in the liver, heart, skeletal muscle, and adipose tissue. Therefore, targeting LRP8 may reduce the level of off-target systemic toxicities due to the presence of the blood brain barrier. The potential synergistic effects of using chemotherapeutics and compounds targeting metabolic mediators or cholesterol have been shown for metastatic colorectal cancer (106, 107). A chemosensitizing effect was observed in myeloma and lymphoma, suggesting that the combination of existing chemotherapeutics and drugs targeting lipid or cholesterol synthesis may be potentially beneficial (107).

Appendix

Appendix Table A1. ER and HER2 status of 18 breast cancer cell line panel tested in siRNA screen

	ER status			HER2 status			
Cell line	GEV[1]	Cutoff	Distribution	GEV	Cutoff	Distribution	Binary[2]
11-9-1-4	7.03	N	N	9.42	N	N	1
AU565	7.20	N	N	15.29	P	P	0
BT20	7.53	N	N	9.33	N	N	1
BT483	6.63	N	N	11.52	N	N	1
BT549	7.66	N	N	8.62	N	N	1
HBL100	7.15	N	N	8.92	N	N	1
HS578T	6.83	N	N	8.74	N	N	1
MCF7	11.45	P	P	9.57	N	N	0
MDAMB157	7.10	N	N	8.87	N	N	1
MDAMB231	7.32	N	N	9.29	N	N	1
MDAMB361	10.70	P	P	12.98	P	P	0
MDAMB435	7.76	N	N	8.69	N	N	1
MDAMB436	7.16	N	N	8.48	N	N	1
MDAMB453	7.75	N	N	12.83	P	P	0
MDAMB468	6.94	N	N	11.81	N	P	0
SKBr3	7.55	N	N	14.69	P	P	0
T47D	10.14	N	P	8.92	N	N	0
ZR751	10.22	P	P	15.08	P	P	0

[1]Gene expression value
[2]0 = non-TNBC, 1 = TNBC

Appendix Table A2. siRNAs with preferential growth inhibition in TNBC cell lines

Product.Id	Product.Name	NCBI.gene.symbol	Gene.Description	pval	Num.TN.cell.line.inhibited
SI02780022	Hs_ADCY7_5	ADCY7	adenylate cyclase 7	0.017256223	6
SI00293391	Hs_AGPAT5_1	AGPAT5	1-acylglycerol-3-phosphate O-acyltransferase 5 (lysophospl	7.07E-05	7
SI03031329	Hs_AKT3_13	AKT3	v-akt murine thymoma viral oncogene homolog 3 (protein ki	0.000349851	6
SI04199503	Hs_ANKRD11_7	ANKRD11	ankyrin repeat domain 11	0.008425566	6
SI03067568	Hs_ANXA1_11	ANXA1	annexin A1	0.001596206	6
SI04149621	Hs_APBA2_5	APBA2	amyloid beta (A4) precursor protein-binding, family A, memb	0.000202072	7
SI04138498	Hs_ARHGEF9_5	ARHGEF9	Cdc42 guanine nucleotide exchange factor (GEF) 9	0.002323237	7
SI04350829	Hs_ARL4C_5	ARL4C	ADP-ribosylation factor-like 4C	2.27E-06	8
SI02776956	Hs_ASNS_5	ASNS	asparagine synthetase	0.002997599	5
SI04354364	Hs_ATP11A_8	ATP11A	ATPase, class VI, type 11A	1.55E-05	8
SI00094066	Hs_BTN3A2_3	BTN3A2	butyrophilin, subfamily 3, member A2	0.00352236	6
SI00093681	Hs_BTN3A3_4	BTN3A3	butyrophilin, subfamily 3, member A3	4.43E-05	8
SI03038343	Hs_BTN3A3_5	BTN3A3	butyrophilin, subfamily 3, member A3	0.011282511	7
SI04375924	Hs_C11orf75_3	C11orf75	chromosome 11 open reading frame 75	0.00383842	5
SI04174002	Hs_C13orf15_2	C13orf15	chromosome 13 open reading frame 15	0.011098716	7
SI04286527	Hs_C18orf10_8	C18orf10	chromosome 18 open reading frame 10	2.26E-05	7
SI03495744	Hs_LOC727728_4	C1R	complement component 1, r subcomponent	0.011261178	8
SI00027363	Hs_C1S_2	C1S	complement component 1, s subcomponent	0.001147884	7
SI04278960	Hs_C21orf91_5	C21orf91	chromosome 21 open reading frame 91	6.09E-06	9
SI03190824	Hs_CALB2_6	CALB2	calbindin 2	0.000473104	6
SI04373166	Hs_CALD1_10	CALD1	caldesmon 1	0.008182397	5
SI04355764	Hs_CALU_8	CALU	calumenin	6.25E-05	8
SI00104517	Hs_CAPN6_3	CAPN6	calpain 6	0.002211935	8
SI04381510	Hs_CBFB_14	CBFB	core-binding factor, beta subunit	0.005021249	7
SI02777117	Hs_CBFB_9	CBFB	core-binding factor, beta subunit	0.01663954	6
SI02777166	Hs_CBS_6	CBS	cystathionine-beta-synthase	0.008660288	5
SI00079625	Hs_CCL8_3	CCL8	chemokine (C-C motif) ligand 8	0.000932998	7
SI02625889	Hs_CCR1_6	CCR1	chemokine (C-C motif) receptor 1	0.000224037	8
SI00024983	Hs_CCR1_4	CCR1	chemokine (C-C motif) receptor 1	0.011030667	6
SI03037419	Hs_CD44_8	CD44	CD44 molecule (Indian blood group)	0.010793521	4
SI00092946	Hs_CD86_3	CD86	CD86 molecule	0.00825734	6
SI02225720	Hs_CD97_9	CD97	CD97 molecule	0.005272821	5
SI00148498	Hs_CD97_4	CD97	CD97 molecule	0.007563179	6
SI02663941	Hs_CDH3_6	CDH3	cadherin 3, type 1, P-cadherin (placental)	0.004239063	7
SI00605087	Hs_CDKN2C_6	CDKN2C	cyclin-dependent kinase inhibitor 2C (p18, inhibits CDK4)	0.00585189	6
SI00122010	Hs_BM039_2	CENPN	centromere protein N	0.011778048	8
SI04331901	Hs_CHD1L_7	CHD1L	chromodomain helicase DNA binding protein 1-like	0.002614413	6
SI04348799	Hs_CHST2_9	CHST2	carbohydrate (N-acetylglucosamine-6-O) sulfotransferase 2	0.015315573	6
SI04214217	Hs_CHST3_8	CHST3	carbohydrate (chondroitin 6) sulfotransferase 3	0.013615294	5
SI00605381	Hs_CKS1B_4	CKS1B	CDC28 protein kinase regulatory subunit 1B	0.000421337	8
SI02663388	Hs_CKS2_10	CKS2	CDC28 protein kinase regulatory subunit 2	0.001922322	6
SI02660014	Hs_CKS2_8	CKS2	CDC28 protein kinase regulatory subunit 2	0.015321471	6
SI00028896	Hs_CLCN4_1	CLCN4	chloride channel 4	0.003007695	7
SI04314618	Hs_CREG1_7	CREG1	cellular repressor of E1A-stimulated genes 1	0.000735612	6
SI00355936	Hs_CSTB_2	CSTB	cystatin B (stefin B)	8.07E-08	8
SI02777313	Hs_CTSC_5	CTSC	cathepsin C	0.003592486	6
SI00076699	Hs_CXCL11_1	CXCL11	chemokine (C-X-C motif) ligand 11	0.004156138	7
SI00110082	Hs_CYLD_2	CYLD	cylindromatosis (turban tumor syndrome)	0.006213501	7
SI00015547	Hs_CYP27A1_3	CYP27A1	cytochrome P450, family 27, subfamily A, polypeptide 1	0.003327216	7
SI02634100	Hs_DAPK1_8	DAPK1	death-associated protein kinase 1	0.009051367	7
SI02637950	Hs_ASK_7	DBF4	DBF4 homolog (S. cerevisiae)	0.007069086	7
SI04370639	Hs_DDX39_7	DDX39	DEAD (Asp-Glu-Ala-Asp) box polypeptide 39	0.002723352	6
SI02631132	Hs_DEK_6	DEK	DEK oncogene	0.000140731	7

SI04345383	Hs_DNAJB6_10	DNAJB6	DnaJ (Hsp40) homolog, subfamily B, member 6	0.003205669	7
SI03081729	Hs_DNMT1_8	DNMT1	DNA (cytosine-5-)-methyltransferase 1	0.000106911	7
SI04244394	Hs_DONSON_6	DONSON	downstream neighbor of SON	5.36E-07	8
SI03138709	Hs_DSG2_5	DSG2	desmoglein 2	0.000265361	7
SI00030408	Hs_E2F3_1	E2F3	E2F transcription factor 3	8.61E-05	8
SI02638076	Hs_EHD1_6	EHD1	EH-domain containing 1	0.001997514	8
SI00379624	Hs_EN1_2	EN1	engrailed homeobox 1	0.000408735	5
SI03060771	Hs_EN1_5	EN1	engrailed homeobox 1	0.007756752	5
SI00063763	Hs_EPHB3_3	EPHB3	EPH receptor B3	3.58E-05	9
SI03249365	Hs_EPHB3_7	EPHB3	EPH receptor B3	0.009952099	6
SI02665166	Hs_EZH2_7	EZH2	enhancer of zeste homolog 2 (Drosophila)	0.004644741	6
SI04210948	Hs_FABP5_9	FABP5	fatty acid binding protein 5 (psoriasis-associated)	0.015310524	5
SI00094150	Hs_FAF1_3	FAF1	Fas (TNFRSF6) associated factor 1	0.001943792	6
SI03074771	Hs_FAM64A_3	FAM64A	family with sequence similarity 64, member A	0.010284817	6
SI04287346	Hs_FANCL_9	FANCL	Fanconi anemia, complementation group L	1.31E-05	8
SI02664424	Hs_FAT_8	FAT1	FAT tumor suppressor homolog 1 (Drosophila)	0.015924492	5
SI04164951	Hs_FBL_7	FBL	fibrillarin	5.77E-08	7
SI00026138	Hs_FOXC1_1	FOXC1	forkhead box C1	0.014855504	5
SI04261831	Hs_FOXM1_8	FOXM1	forkhead box M1	0.006384873	8
SI04374265	Hs_FXYD6_8	FXYD6	FXYD domain containing ion transport regulator 6	0.000558756	7
SI00052766	Hs_FZD7_3	FZD7	frizzled homolog 7 (Drosophila)	0.008792018	7
SI00103614	Hs_GABRP_4	GABRP	gamma-aminobutyric acid (GABA) A receptor, pi	0.001037336	7
SI04345089	Hs_GART_7	GART	phosphoribosylglycinamide formyltransferase, phosphoribos	0.007350319	6
SI04161339	Hs_GART_5	GART	phosphoribosylglycinamide formyltransferase, phosphoribos	0.012747425	4
SI04160065	Hs_GCSH_8	GCSH	glycine cleavage system protein H (aminomethyl carrier)	0.005961711	7
SI00114639	Hs_GPRC5B_2	GPRC5B	G protein-coupled receptor, family C, group 5, member B	0.000453029	6
SI03048570	Hs_GPX7_5	GPX7	glutathione peroxidase 7	0.000858056	6
SI04272961	Hs_ALF_9	GTF2A1L	general transcription factor IIA, 1-like	0.013072027	6
SI04339475	Hs_GTPBP2_8	GTPBP2	GTP binding protein 2	0.011128936	6
SI02639420	Hs_GTPBP4_5	GTPBP4	GTP binding protein 4	0.001120366	6
SI00099547	Hs_GTPBP4_2	GTPBP4	GTP binding protein 4	0.014894314	6
SI00060060	Hs_GZMB_4	GZMB	granzyme B (granzyme 2, cytotoxic T-lymphocyte-associate	0.013962594	5
SI04247425	Hs_HLA-DOB_6	HLA-DOB	major histocompatibility complex, class II, DO beta	2.62E-05	8
SI04435333	Hs_HLA-E_8	HLA-E	major histocompatibility complex, class I, E	0.015969332	6
SI03157952	Hs_HLA-G_5	HLA-G	major histocompatibility complex, class I, G	0.011367865	4
SI00445697	Hs_IFI16_4	IFI16	interferon, gamma-inducible protein 16	0.001850885	7
SI04238360	Hs_IFRD1_7	IFRD1	interferon-related developmental regulator 1	0.003231301	7
SI04193700	Hs_IFRD1_6	IFRD1	interferon-related developmental regulator 1	0.008214793	6
SI04138820	Hs_IGF2BP2_3	IGF2BP2	insulin-like growth factor 2 mRNA binding protein 2	2.28E-08	10
SI00033866	Hs_IL15RA_2	IL15RA	interleukin 15 receptor, alpha	0.001087714	6
SI00605269	Hs_IRAK1_6	IRAK1	interleukin-1 receptor-associated kinase 1	0.001946072	8
SI00034104	Hs_IRF1_4	IRF1	interferon regulatory factor 1	0.00035607	6
SI04332832	Hs_ITGB1BP1_8	ITGB1BP1	integrin beta 1 binding protein 1	0.000125386	7
SI04340406	Hs_IVNS1ABP_8	IVNS1ABP	influenza virus NS1A binding protein	0.001077805	6
SI00450002	Hs_JRKL_3	JRKL	jerky homolog-like (mouse)	0.014231613	6
SI04338222	Hs_ANKRD15_8	KANK1	KN motif and ankyrin repeat domains 1	0.001521885	7
SI04212075	Hs_KARS_7	KARS	lysyl-tRNA synthetase	0.013894209	5
SI00017885	Hs_KCNJ2_1	KCNJ2	potassium inwardly-rectifying channel, subfamily J, member	0.00047871	7
SI00017892	Hs_KCNJ2_2	KCNJ2	potassium inwardly-rectifying channel, subfamily J, member	0.013645724	6
SI03042858	Hs_KCNN4_6	KCNN4	potassium intermediate/small conductance calcium-activate	0.000559495	7
SI03099509	Hs_KIF4A_6	KIF4A	kinesin family member 4A	0.003691331	6
SI04161381	Hs_KLF5_6	KLF5	Kruppel-like factor 5 (intestinal)	0.000759331	6
SI04281074	Hs_KLF5_9	KLF5	Kruppel-like factor 5 (intestinal)	0.004553831	5
SI00463806	Hs_KLHL21_3	KLHL21	kelch-like 21 (Drosophila)	0.003126358	7

SI04305217	Hs_KLHL24_2	KLHL24	kelch-like 24 (Drosophila)	0.010870788	7
SI00071820	Hs_KLK7_2	KLK7	kallikrein-related peptidase 7	0.013649085	5
SI04353139	Hs_LAD1_7	LAD1	ladinin 1	2.04E-06	8
SI02780638	Hs_LAMP2_5	LAMP2	lysosomal-associated membrane protein 2	0.00427389	6
SI03067778	Hs_LBR_10	LBR	lamin B receptor	0.015791542	5
SI04227076	Hs_LILRB2_8	LILRB2	leukocyte immunoglobulin-like receptor, subfamily B (with T	0.002099815	6
SI00071043	Hs_LIMS1_3	LIMS1	LIM and senescent cell antigen-like domains 1	0.000664736	7
SI02639350	Hs_LPHN2_5	LPHN2	latrophilin 2	0.002001317	6
SI00066283	Hs_LRP8_3	LRP8	low density lipoprotein receptor-related protein 8, apolipopro	1.45E-05	8
SI03088204	Hs_LRP8_6	LRP8	low density lipoprotein receptor-related protein 8, apolipopro	0.000219115	6
SI00066269	Hs_LRP8_1	LRP8	low density lipoprotein receptor-related protein 8, apolipopro	0.001925051	5
SI03118787	Hs_LTBP1_10	LTBP1	latent transforming growth factor beta binding protein 1	0.01013516	5
SI00036505	Hs_LY75_3	LY75	lymphocyte antigen 75	1.48E-07	8
SI04157104	Hs_LY75_9	LY75	lymphocyte antigen 75	0.013131304	7
SI00605570	Hs_LYN_12	LYN	v-yes-1 Yamaguchi sarcoma viral related oncogene homolo	0.013114552	6
SI00626941	Hs_MAGED4_3	MAGED4B	melanoma antigen family D, 4B	0.004490425	7
SI00104251	Hs_MAPRE2_1	MAPRE2	microtubule-associated protein, RP/EB family, member 2	1.16E-05	7
SI03031812	Hs_MCAM_6	MCAM	melanoma cell adhesion molecule	0.015042133	6
SI00300818	Hs_MCM4_1	MCM4	minichromosome maintenance complex component 4	0.006453696	6
SI04151119	Hs_MCM4_8	MCM4	minichromosome maintenance complex component 4	0.007935719	5
SI00629076	Hs_MCM6_4	MCM6	minichromosome maintenance complex component 6	0.001220822	6
SI04163558	Hs_MCM6_6	MCM6	minichromosome maintenance complex component 6	0.012825369	7
SI04192041	Hs_MCM7_5	MCM7	minichromosome maintenance complex component 7	0.008077136	6
SI00629692	Hs_ME1_4	ME1	malic enzyme 1, NADP(+)-dependent, cytosolic	0.007937176	4
SI00629678	Hs_ME1_2	ME1	malic enzyme 1, NADP(+)-dependent, cytosolic	0.008998899	7
SI04313015	Hs_ME2_8	ME2	malic enzyme 2, NAD(+)-dependent, mitochondrial	0.016019221	5
SI02654897	Hs_MET_10	MET	met proto-oncogene (hepatocyte growth factor receptor)	0.001183407	7
SI00300874	Hs_MET_7	MET	met proto-oncogene (hepatocyte growth factor receptor)	0.003244267	8
SI00630805	Hs_MFGE8_3	MFGE8	milk fat globule-EGF factor 8 protein	5.53E-05	7
SI04306309	Hs_MIA_9	MIA	melanoma inhibitory activity	3.84E-05	7
SI03117933	Hs_MMP7_6	MMP7	matrix metallopeptidase 7 (matrilysin, uterine)	1.83E-05	7
SI04176788	Hs_EVA1_6	MPZL2	myelin protein zero-like 2	3.89E-05	8
SI04435900	Hs_MSH2_9	MSH2	mutS homolog 2, colon cancer, nonpolyposis type 1 (E. coli	0.010731906	7
SI03082856	Hs_MSLN_5	MSLN	mesothelin	0.005940165	7
SI04374461	Hs_PAPD1_7	MTPAP	mitochondrial poly(A) polymerase	0.00362102	7
SI04131715	Hs_NAB1_7	NAB1	NGFI-A binding protein 1 (EGR1 binding protein 1)	0.00260081	6
SI00133336	Hs_HCAP-G_3	NCAPG	non-SMC condensin I complex, subunit G	3.30E-05	8
SI02624993	Hs_NCK2_9	NCK2	NCK adaptor protein 2	0.006942703	5
SI04218543	Hs_NDRG2_5	NDRG2	NDRG family member 2	0.00314286	8
SI04222666	Hs_NDRG2_6	NDRG2	NDRG family member 2	0.00797214	6
SI03032197	Hs_NFIB_5	NFIB	nuclear factor I/B	0.005779657	7
SI04282719	Hs_NFIL3_7	NFIL3	nuclear factor, interleukin 3 regulated	0.001114907	7
SI04326686	Hs_NFIL3_8	NFIL3	nuclear factor, interleukin 3 regulated	0.00151717	7
SI04241146	Hs_NMB_7	NMB	neuromedin B	0.00459353	7
SI03031889	Hs_NMI_7	NMI	N-myc (and STAT) interactor	0.003836864	6
SI02662625	Hs_NMI_6	NMI	N-myc (and STAT) interactor	0.009123962	7
SI00068677	Hs_NMT2_4	NMT2	N-myristoyltransferase 2	0.001107475	7
SI04893693	Hs_NRAS_11	NRAS	neuroblastoma RAS viral (v-ras) oncogene homolog	0.001971218	5
SI00065205	Hs_NRTN_2	NRTN	neurturin	2.56E-05	7
SI04331397	Hs_NUP88_8	NUP88	nucleoporin 88kDa	0.007950477	6
SI04180057	Hs_OAZ1_6	OAZ1	ornithine decarboxylase antizyme 1	0.007174441	8
SI04301234	Hs_OAZ1_7	OAZ1	ornithine decarboxylase antizyme 1	0.008580424	8
SI03236793	Hs_OSBPL3_5	OSBPL3	oxysterol binding protein-like 3	0.002177418	7
SI00676872	Hs_PADI2_4	PADI2	peptidyl arginine deiminase, type II	0.015436682	6

SI00077266	Hs_PAPSS1_3	PAPSS1	3'-phosphoadenosine 5'-phosphosulfate synthase 1	0.002207052	6
SI04297314	Hs_PCOLCE2_7	PCOLCE2	procollagen C-endopeptidase enhancer 2	0.001594344	9
SI03097871	Hs_PDIA6_1	PDIA6	protein disulfide isomerase family A, member 6	0.002385759	6
SI00753690	Hs_TXNDC7_2	PDIA6	protein disulfide isomerase family A, member 6	0.015088553	6
SI00288071	Hs_PDXK_5	PDXK	pyridoxal (pyridoxine, vitamin B6) kinase	0.005243422	6
SI04658990	Hs_PDXK_13	PDXK	pyridoxal (pyridoxine, vitamin B6) kinase	0.014333326	5
SI04908953	Hs_PELI1_8	PELI1	pellino homolog 1 (Drosophila)	0.007221379	5
SI00040691	Hs_PFN2_4	PFN2	profilin 2	0.013305142	6
SI04206265	Hs_PGBD5_5	PGBD5	piggyBac transposable element derived 5	0.001160672	5
SI04252283	Hs_PGM1_6	PGM1	phosphoglucomutase 1	0.006065396	8
SI00090391	Hs_PHGDH_2	PHGDH	phosphoglycerate dehydrogenase	0.013370645	3
SI00094990	Hs_PICALM_1	PICALM	phosphatidylinositol binding clathrin assembly protein	1.17E-07	9
SI04210297	Hs_PITPNA_6	PITPNA	phosphatidylinositol transfer protein, alpha	4.40E-08	8
SI03033289	Hs_PLAUR_5	PLAUR	plasminogen activator, urokinase receptor	0.000144726	6
SI04203444	Hs_PLS3_7	PLS3	plastin 3 (T isoform)	2.20E-05	8
SI00092120	Hs_PNRC1_1	PNRC1	proline-rich nuclear receptor coactivator 1	0.001650582	7
SI04364472	Hs_POLR1E_4	POLR1E	polymerase (RNA) I polypeptide E, 53kDa	0.001211935	6
SI04226474	Hs_POLR2F_9	POLR2F	polymerase (RNA) II (DNA directed) polypeptide F	0.001594018	7
SI04367146	Hs_PQLC1_7	PQLC1	PQ loop repeat containing 1	0.000289096	8
SI03058517	Hs_PRKCDBP_8	PRKCDBP	protein kinase C, delta binding protein	0.001238282	7
SI02659860	Hs_PRKCDBP_6	PRKCDBP	protein kinase C, delta binding protein	0.017566453	6
SI03084179	Hs_PRKX_8	PRKX	protein kinase, X-linked	0.000836827	7
SI04244828	Hs_PRNP_10	PRNP	prion protein	0.000186998	8
SI03019324	Hs_PRNP_6	PRNP	prion protein	0.015931471	6
SI02629599	Hs_PSMB2_3	PSMB2	proteasome (prosome, macropain) subunit, beta type, 2	0.011900313	6
SI00374087	Hs_DSCR2_3	PSMG1	proteasome (prosome, macropain) assembly chaperone 1	2.50E-06	8
SI02659111	Hs_PTPLA_7	PTPLA	protein tyrosine phosphatase-like (proline instead of catalyti	0.016030255	6
SI04438168	Hs_PTTG1_10	PTTG1	pituitary tumor-transforming 1	0.00060379	7
SI04148361	Hs_PUS7_1	PUS7	pseudouridylate synthase 7 homolog (S. cerevisiae)	0.002194928	6
SI04218221	Hs_QKI_6	QKI	quaking homolog, KH domain RNA binding (mouse)	0.011178761	7
SI04367342	Hs_QKI_7	QKI	quaking homolog, KH domain RNA binding (mouse)	0.017537111	6
SI02644509	Hs_RAP2A_5	RAP2A	RAP2A, member of RAS oncogene family	0.011878709	7
SI04348757	Hs_RBM15_8	RBM15	RNA binding motif protein 15	8.74E-06	7
SI00704816	Hs_RNPC1_4	RBM38	RNA binding motif protein 38	0.000476638	9
SI03224900	Hs_DSCR1_5	RCAN1	regulator of calcineurin 1	0.010264371	5
SI02629942	Hs_RDX_5	RDX	radixin	0.003640701	5
SI04162858	Hs_REXO2_2	REXO2	REX2, RNA exonuclease 2 homolog (S. cerevisiae)	0.000975792	8
SI03106873	Hs_RNF144_8	RNF144A	ring finger protein 144A	0.000674665	7
SI00706531	Hs_RPL39L_1	RPL39L	ribosomal protein L39-like	0.013626946	5
SI04270399	Hs_RPP25_7	RPP25	ribonuclease P/MRP 25kDa subunit	0.000182725	7
SI04313379	Hs_RRAGD_8	RRAGD	Ras-related GTP binding D	0.010720701	6
SI03112340	Hs_RRAS2_9	RRAS2	related RAS viral (r-ras) oncogene homolog 2	0.009532824	6
SI02639658	Hs_RSU1_5	RSU1	Ras suppressor protein 1	0.00071432	8
SI00710598	Hs_SAP30_2	SAP30	Sin3A-associated protein, 30kDa	0.000343097	6
SI00046319	Hs_SATB1_4	SATB1	SATB homeobox 1	0.000948557	6
SI03125605	Hs_SAV1_5	SAV1	salvador homolog 1 (Drosophila)	0.000955019	7
SI03066833	Hs_SCARB1_9	SCARB1	scavenger receptor class B, member 1	0.005543388	6
SI04171825	Hs_SCHIP1_6	SCHIP1	schwannomin interacting protein 1	0.00606721	6
SI04289684	Hs_SEH1L_10	SEH1L	SEH1-like (S. cerevisiae)	0.012083626	8
SI03042613	Hs_SERPINB5_8	SERPINB5	serpin peptidase inhibitor, clade B (ovalbumin), member 5	0.013682332	6
SI02653637	Hs_SFN_5	SFN	stratifin	0.000775443	5
SI04207063	Hs_SFT2D2_4	SFT2D2	SFT2 domain containing 2	3.32E-05	8
SI03113901	Hs_OPRS1_5	SIGMAR1	sigma non-opioid intracellular receptor 1	2.64E-05	9
SI00148995	Hs_PTPNS1_2	SIRPA	signal-regulatory protein alpha	0.000225751	7

SI03062647	Hs_SIRPA_1	SIRPA	signal-regulatory protein alpha	0.001164226	8
SI00076727	Hs_SIX3_1	SIX3	SIX homeobox 3	0.004808197	5
SI00725529	Hs_SLC7A5_3	SLC7A5	solute carrier family 7 (cationic amino acid transporter, y+ s	0.00376484	7
SI03046995	Hs_SMURF2_6	SMURF2	SMAD specific E3 ubiquitin protein ligase 2	0.000920045	8
SI00134302	Hs_SMURF2_3	SMURF2	SMAD specific E3 ubiquitin protein ligase 2	0.002090292	5
SI00102795	Hs_SOCS5_3	SOCS5	suppressor of cytokine signaling 5	3.11E-12	9
SI00079800	Hs_SOS1_2	SOS1	son of sevenless homolog 1 (Drosophila)	0.009557549	8
SI04212355	Hs_SOSTDC1_8	SOSTDC1	sclerostin domain containing 1	8.94E-07	9
SI00729414	Hs_SOX10_2	SOX10	SRY (sex determining region Y)-box 10	0.006505506	6
SI02758714	Hs_SRPK1_7	SRPK1	SFRS protein kinase 1	0.000805326	8
SI04438931	Hs_STK38_10	STK38	serine/threonine kinase 38	2.86E-05	8
SI02224313	Hs_STK38_6	STK38	serine/threonine kinase 38	0.000494706	8
SI04167814	Hs_STMN1_7	STMN1	stathmin 1/oncoprotein 18	0.007083201	7
SI04195002	Hs_JOSD3_4	TAF1D	TATA box binding protein (TBP)-associated factor, RNA poly	0.002612512	8
SI00012411	Hs_TAP1_1	TAP1	transporter 1, ATP-binding cassette, sub-family B (MDR/TAI	1.64E-05	7
SI00012432	Hs_TAP1_4	TAP1	transporter 1, ATP-binding cassette, sub-family B (MDR/TAI	0.000298716	7
SI00739865	Hs_TBC1D1_3	TBC1D1	TBC1 (tre-2/USP6, BUB2, cdc16) domain family, member 1	0.002542705	7
SI03062073	Hs_TGFBI_6	TGFBI	transforming growth factor, beta-induced, 68kDa	0.002470267	7
SI00050022	Hs_TLR2_2	TLR2	toll-like receptor 2	8.78E-05	8
SI04297804	Hs_TM4SF1_7	TM4SF1	transmembrane 4 L six family member 1	0.000363882	7
SI03225936	Hs_TMEFF1_5	TMEFF1	transmembrane protein with EGF-like and two follistatin-like	0.009027555	6
SI03211894	Hs_TMSL8_2	TMSB15A	thymosin beta 15a	0.014988689	6
SI02637166	Hs_TNFAIP3_5	TNFAIP3	tumor necrosis factor, alpha-induced protein 3	0.000984753	6
SI04191026	Hs_TPM4_6	TPM4	tropomyosin 4	0.000269152	6
SI02665075	Hs_TPX2_5	TPX2	TPX2, microtubule-associated, homolog (Xenopus laevis)	6.96E-05	7
SI04136342	Hs_TSPYL5_6	TSPYL5	TSPY-like 5	0.002223141	7
SI04316648	Hs_TTLL4_8	TTLL4	tubulin tyrosine ligase-like family, member 4	2.60E-07	8
SI04216681	Hs_SAE2_1	UBA2	ubiquitin-like modifier activating enzyme 2	0.000192764	8
SI04157118	Hs_UBAP2_6	UBAP2	ubiquitin associated protein 2	0.001472267	7
SI02224390	Hs_UCK2_6	UCK2	uridine-cytidine kinase 2	0.008827251	6
SI04244163	Hs_UNC84B_9	UNC84B	unc-84 homolog B (C. elegans)	0.008452817	5
SI03177111	Hs_UPP1_5	UPP1	uridine phosphorylase 1	0.000211396	7
SI02664214	Hs_VCL_11	VCL	vinculin	0.002924539	6
SI04143412	Hs_VGLL4_6	VGLL4	vestigial like 4 (Drosophila)	0.011180773	6
SI00051653	Hs_VLDLR_4	VLDLR	very low density lipoprotein receptor	0.00177792	5
SI00051632	Hs_VLDLR_1	VLDLR	very low density lipoprotein receptor	0.00211578	7
SI00051646	Hs_VLDLR_3	VLDLR	very low density lipoprotein receptor	0.015091019	6
SI00060711	Hs_WARS_2	WARS	tryptophanyl-tRNA synthetase	3.97E-06	6
SI00060704	Hs_WARS_1	WARS	tryptophanyl-tRNA synthetase	0.015378625	7
SI00111216	Hs_WWTR1_1	WWTR1	WW domain containing transcription regulator 1	0.006067384	5
SI00111230	Hs_WWTR1_3	WWTR1	WW domain containing transcription regulator 1	0.006904822	7
SI04295858	Hs_YBX1_5	YBX1	Y box binding protein 1	0.011464614	5
SI00052003	Hs_ZIC1_2	ZIC1	Zic family member 1 (odd-paired homolog, Drosophila)	0.009565665	7

Appendix Table A3. siRNAs with preferential growth inhibition in non-TNBC cell lines

Product.Id	Product.Name	NCBI.gene.symbol	Gene.Description	Gene.symbol.times
SI02778657	Hs_FNDC3B_6	FNDC3B	fibronectin type III domain containing 3B	2
SI04279275	Hs_NOL1_7	NOP2	NOP2 nucleolar protein homolog (yeast)	1
SI03204922	Hs_FXYD6_5	FXYD6	FXYD domain containing ion transport regulator 6	1
SI04277553	Hs_FABP5_10	FABP5	fatty acid binding protein 5 (psoriasis-associated)	1
SI00437941	Hs_HIST1H4C_4	HIST1H4C	histone cluster 1, H4c	1
SI03035221	Hs_SLC26A2_5	SLC26A2	solute carrier family 26 (sulfate transporter), member 2	3
SI00288197	Hs_RPS6KA3_6	RPS6KA3	ribosomal protein S6 kinase, 90kDa, polypeptide 3	1
SI00009289	Hs_L1CAM_3	L1CAM	L1 cell adhesion molecule	1
SI02757762	Hs_AKT3_12	AKT3	v-akt murine thymoma viral oncogene homolog 3 (protein kina	1
SI03044846	Hs_SLC26A2_6	SLC26A2	solute carrier family 26 (sulfate transporter), member 2	3
SI04199643	Hs_SLPI_5	SLPI	secretory leukocyte peptidase inhibitor	2
SI04248594	Hs_SF3B3_7	SF3B3	splicing factor 3b, subunit 3, 130kDa	1
SI04311111	Hs_RHEB_10	RHEB	Ras homolog enriched in brain	1
SI00345821	Hs_CHI3L1_1	CHI3L1	chitinase 3-like 1 (cartilage glycoprotein-39)	1
SI03046554	Hs_PNRC1_7	PNRC1	proline-rich nuclear receptor coactivator 1	2
SI00114534	Hs_CYB5R2_3	CYB5R2	cytochrome b5 reductase 2	1
SI04252381	Hs_HLA-A_9	HLA-A	major histocompatibility complex, class I, A	1
SI00064939	Hs_MCM2_4	MCM2	minichromosome maintenance complex component 2	1
SI04269125	Hs_SLPI_7	SLPI	secretory leukocyte peptidase inhibitor	2
SI02629368	Hs_PRKCA_8	PRKCA	protein kinase C, alpha	1
SI00288148	Hs_BUB1_5	BUB1	budding uninhibited by benzimidazoles 1 homolog (yeast)	1
SI00448497	Hs_IQCG_4	IQCG	IQ motif containing G	1
SI00081711	Hs_MSLN_2	MSLN	mesothelin	2
SI04935133	Hs_SGK196_1	SGK196	protein kinase-like protein SgK196	1
SI04271918	Hs_MCM4_9	MCM4	minichromosome maintenance complex component 4	1
SI03045812	Hs_CKS1B_9	CKS1B	CDC28 protein kinase regulatory subunit 1B	1
SI00012418	Hs_TAP1_2	TAP1	transporter 1, ATP-binding cassette, sub-family B (MDR/TAP)	1
SI00719593	Hs_SLAMF8_3	SLAMF8	SLAM family member 8	1
SI04148494	Hs_LY75_8	LY75	lymphocyte antigen 75	1
SI03137190	Hs_C1orf38_5	C1orf38	chromosome 1 open reading frame 38	3
SI00645505	Hs_MIA_3	MIA	melanoma inhibitory activity	1
SI00088172	Hs_HTATIP2_1	HTATIP2	HIV-1 Tat interactive protein 2, 30kDa	1
SI04318209	Hs_FLNA_10	FLNA	filamin A, alpha (actin binding protein 280)	1
SI00028161	Hs_CD38_4	CD38	CD38 molecule	1
SI04144315	Hs_CDC42EP1_5	CDC42EP1	CDC42 effector protein (Rho GTPase binding) 1	1
SI02633267	Hs_EPHB3_5	EPHB3	EPH receptor B3	1
SI00088872	Hs_RAD51AP1_4	RAD51AP1	RAD51 associated protein 1	1
SI04254453	Hs_C11orf75_1	C11orf75	chromosome 11 open reading frame 75	1
SI04236519	Hs_ART3_6	ART3	ADP-ribosyltransferase 3	2
SI00038206	Hs_MX2_1	MX2	myxovirus (influenza virus) resistance 2 (mouse)	1
SI04365424	Hs_SOX10_6	SOX10	SRY (sex determining region Y)-box 10	1
SI04138988	Hs_NAB1_8	NAB1	NGFI-A binding protein 1 (EGR1 binding protein 1)	1
SI04247929	Hs_STEAP3_3	STEAP3	STEAP family member 3	1
SI04336164	Hs_GMPS_13	GMPS	guanine monphosphate synthetase	1
SI02643326	Hs_PBK_7	PBK	PDZ binding kinase	2
SI02653049	Hs_HCAP-G_6	NCAPG	non-SMC condensin I complex, subunit G	1
SI00304290	Hs_ARP3BETA_4	ACTR3B	ARP3 actin-related protein 3 homolog B (yeast)	1
SI03098123	Hs_CD44_10	CD44	CD44 molecule (Indian blood group)	1
SI04325664	Hs_CALML4_7	CALML4	calmodulin-like 4	2

SI04249350	Hs_SERBP1_1	SERBP1	SERPINE1 mRNA binding protein 1	2
SI00299817	Hs_CDKN2A_9	CDKN2A	cyclin-dependent kinase inhibitor 2A (melanoma, p16, inhibits	2
SI00432432	Hs_GTPBP2_1	GTPBP2	GTP binding protein 2	2
SI04344186	Hs_GOLT1B_5	GOLT1B	golgi transport 1 homolog B (S. cerevisiae)	1
SI04234055	Hs_SAE2_2	UBA2	ubiquitin-like modifier activating enzyme 2	1
SI00045290	Hs_RARRES1_1	RARRES1	retinoic acid receptor responder (tazarotene induced) 1	1
SI02638062	Hs_MALT1_5	MALT1	mucosa associated lymphoid tissue lymphoma translocation g	1
SI04306736	Hs_HNRPH3_8	HNRNPH3	heterogeneous nuclear ribonucleoprotein H3 (2H9)	1
SI04156999	Hs_PLA2G4A_7	PLA2G4A	phospholipase A2, group IVA (cytosolic, calcium-dependent)	1
SI04138897	Hs_CEP57_3	CEP57	centrosomal protein 57kDa	1
SI04278799	Hs_RGL1_8	RGL1	ral guanine nucleotide dissociation stimulator-like 1	1
SI02665082	Hs_TPX2_6	TPX2	TPX2, microtubule-associated, homolog (Xenopus laevis)	1
SI04156089	Hs_MEMO1_1	MEMO1	mediator of cell motility 1	2
SI04320834	Hs_KHDRBS3_8	KHDRBS3	KH domain containing, RNA binding, signal transduction asso	1
SI00757799	Hs_UQCRH_1	UQCRH	ubiquinol-cytochrome c reductase hinge protein	2
SI00753634	Hs_TXNDC4_2	ERP44	endoplasmic reticulum protein 44	2
SI00012824	Hs_CD59_4	CD59	CD59 molecule, complement regulatory protein	1
SI04331754	Hs_PODXL_9	PODXL	podocalyxin-like	2
SI04344487	Hs_ZNF259_11	ZNF259	zinc finger protein 259	1
SI04279499	Hs_CDC5L_8	CDC5L	CDC5 cell division cycle 5-like (S. pombe)	1
SI04190928	Hs_S100A10_9	S100A10	S100 calcium binding protein A10	1
SI02659503	Hs_CDKN2A_12	CDKN2A	cyclin-dependent kinase inhibitor 2A (melanoma, p16, inhibits	2
SI04284350	Hs_DSG2_8	DSG2	desmoglein 2	1
SI04176452	Hs_NUP88_6	NUP88	nucleoporin 88kDa	2
SI04267746	Hs_STMN1_8	STMN1	stathmin 1/oncoprotein 18	1
SI04172910	Hs_RIF1_10	RIF1	RAP1 interacting factor homolog (yeast)	1
SI04347910	Hs_NT5DC2_2	NT5DC2	5'-nucleotidase domain containing 2	1
SI03049081	Hs_RASSF4_7	RASSF4	Ras association (RalGDS/AF-6) domain family member 4	2
SI04333042	Hs_FSCN1_7	FSCN1	fascin homolog 1, actin-bundling protein (Strongylocentrotus p	1
SI03180527	Hs_UBE2E3_6	UBE2E3	ubiquitin-conjugating enzyme E2E 3 (UBC4/5 homolog, yeast)	1
SI03068191	Hs_RFC4_8	RFC4	replication factor C (activator 1) 4, 37kDa	1
SI04355407	Hs_NUP88_9	NUP88	nucleoporin 88kDa	2
SI02664130	Hs_MSN_8	MSN	moesin	1
SI00659176	Hs_NK4_4	IL32	interleukin 32	1
SI04175416	Hs_CTPS_6	CTPS	CTP synthase	2
SI04239487	Hs_SLC5A6_7	SLC5A6	solute carrier family 5 (sodium-dependent vitamin transporter)	2
SI00022596	Hs_ANGPT1_2	ANGPT1	angiopoietin 1	2
SI00077273	Hs_PAPSS1_4	PAPSS1	3'-phosphoadenosine 5'-phosphosulfate synthase 1	1
SI02664389	Hs_CAV2_10	CAV2	caveolin 2	1
SI03182375	Hs_UPF3B_6	UPF3B	UPF3 regulator of nonsense transcripts homolog B (yeast)	1
SI00114653	Hs_GPRC5B_4	GPRC5B	G protein-coupled receptor, family C, group 5, member B	1
SI04167429	Hs_C1orf38_8	C1orf38	chromosome 1 open reading frame 38	3
SI00357308	Hs_CXCL10_2	CXCL10	chemokine (C-X-C motif) ligand 10	1
SI00073640	Hs_CEBPB_4	CEBPB	CCAAT/enhancer binding protein (C/EBP), beta	1
SI03117660	Hs_CTSL_7	CTSL1	cathepsin L1	1
SI00129339	Hs_PLSCR1_4	PLSCR1	phospholipid scramblase 1	1
SI04192293	Hs_SLC5A6_6	SLC5A6	solute carrier family 5 (sodium-dependent vitamin transporter)	2
SI04434465	Hs_SERPINH1_10	SERPINH1	serpin peptidase inhibitor, clade H (heat shock protein 47), me	1
SI03051930	Hs_FZD7_6	FZD7	frizzled homolog 7 (Drosophila)	1
SI04168304	Hs_MFHAS1_6	MFHAS1	malignant fibrous histiocytoma amplified sequence 1	1

SI03170727	Hs_TTLL4_6	TTLL4	tubulin tyrosine ligase-like family, member 4	1
SI03177377	Hs_CSTB_6	CSTB	cystatin B (stefin B)	1
SI00648284	Hs_MRPL15_4	MRPL15	mitochondrial ribosomal protein L15	1
SI04135712	Hs_MCM5_5	MCM5	minichromosome maintenance complex component 5	1
SI00381493	Hs_EVA1_1	MPZL2	myelin protein zero-like 2	1
SI04347721	Hs_DSC3_7	DSC3	desmocollin 3	1
SI04283615	Hs_RBM15_6	RBM15	RNA binding motif protein 15	1
SI00771708	Hs_ZNF292_4	ZNF292	zinc finger protein 292	1
SI04166239	Hs_MYBL1_10	MYBL1	v-myb myeloblastosis viral oncogene homolog (avian)-like 1	1
SI02625693	Hs_CCNE1_6	CCNE1	cyclin E1	1
SI04219726	Hs_TEX10_8	TEX10	testis expressed 10	1
SI02622284	Hs_ASK_5	DBF4	DBF4 homolog (S. cerevisiae)	1
SI00092127	Hs_PNRC1_2	PNRC1	proline-rich nuclear receptor coactivator 1	2
SI00698208	Hs_RANBP1_4	RANBP1	RAN binding protein 1	1
SI00076965	Hs_TP53BP2_4	TP53BP2	tumor protein p53 binding protein, 2	1
SI04337795	Hs_FLJ20186_8	DEF8	differentially expressed in FDCP 8 homolog (mouse)	1
SI00734188	Hs_ST5_4	ST5	suppression of tumorigenicity 5	2
SI00287798	Hs_SGK_5	SGK1	serum/glucocorticoid regulated kinase 1	1
SI03176593	Hs_IGF2BP2_1	IGF2BP2	insulin-like growth factor 2 mRNA binding protein 2	1
SI04323543	Hs_TES_8	TES	testis derived transcript (3 LIM domains)	1
SI00081718	Hs_MSLN_3	MSLN	mesothelin	2
SI00732935	Hs_SRD5A1_1	SRD5A1	steroid-5-alpha-reductase, alpha polypeptide 1 (3-oxo-5 alpha	1
SI04134151	Hs_PLAGL1_5	PLAGL1	pleiomorphic adenoma gene-like 1	1
SI04385199	Hs_SMC2_2	SMC2	structural maintenance of chromosomes 2	2
SI00113925	Hs_MTMR2_2	MTMR2	myotubularin related protein 2	1
SI04258002	Hs_BCL11A_7	BCL11A	B-cell CLL/lymphoma 11A (zinc finger protein)	1
SI00605584	Hs_MARCKS_5	MARCKS	myristoylated alanine-rich protein kinase C substrate	1
SI03030713	Hs_CDKN2C_8	CDKN2C	cyclin-dependent kinase inhibitor 2C (p18, inhibits CDK4)	2
SI04161927	Hs_PODXL_6	PODXL	podocalyxin-like	2
SI02777194	Hs_SCARB1_6	SCARB1	scavenger receptor class B, member 1	1
SI00063966	Hs_EZH2_3	EZH2	enhancer of zeste homolog 2 (Drosophila)	1
SI02654064	Hs_KIF20A_7	KIF20A	kinesin family member 20A	1
SI00030429	Hs_E2F3_4	E2F3	E2F transcription factor 3	1
SI04275698	Hs_GTPBP2_7	GTPBP2	GTP binding protein 2	2
SI00753648	Hs_TXNDC4_4	ERP44	endoplasmic reticulum protein 44	2
SI03099754	Hs_AK2_10	AK2	adenylate kinase 2	1
SI02662569	Hs_HMGA1_6	HMGA1	high mobility group AT-hook 1	1
SI00004571	Hs_ITGB2_3	ITGB2	integrin, beta 2 (complement component 3 receptor 3 and 4 su	1
SI04194015	Hs_MEMO1_2	MEMO1	mediator of cell motility 1	2
SI02640673	Hs_TNFRSF21_6	TNFRSF21	tumor necrosis factor receptor superfamily, member 21	1
SI04355281	Hs_PHLDA1_7	PHLDA1	pleckstrin homology-like domain, family A, member 1	1
SI03171014	Hs_PLEKHB1_5	PLEKHB1	pleckstrin homology domain containing, family B (evectins) me	1
SI03106453	Hs_C3_10	C3	complement component 3	2
SI00693224	Hs_ProSAPiP1_4	ProSAPiP1	ProSAPiP1 protein	1
SI03031084	Hs_FANCA_5	FANCA	Fanconi anemia, complementation group A	1
SI02654057	Hs_CCNB2_6	CCNB2	cyclin B2	1
SI04268985	Hs_RHBDL2_6	RHBDL2	rhomboid, veinlet-like 2 (Drosophila)	1
SI00079359	Hs_NFIB_2	NFIB	nuclear factor I/B	1
SI00141806	Hs_RASSF4_3	RASSF4	Ras association (RalGDS/AF-6) domain family member 4	2
SI03102701	Hs_BTN3A2_6	BTN3A2	butyrophilin, subfamily 3, member A2	1

SI00046760	Hs_CX3CL1_2	CX3CL1	chemokine (C-X3-C motif) ligand 1	1
SI04151749	Hs_CENPA_7	CENPA	centromere protein A	1
SI04439708	Hs_GTSE1_9	GTSE1	G-2 and S-phase expressed 1	2
SI04434241	Hs_ASNS_8	ASNS	asparagine synthetase	1
SI00104272	Hs_MAPRE2_4	MAPRE2	microtubule-associated protein, RP/EB family, member 2	1
SI04366369	Hs_LAPTM5_8	LAPTM5	lysosomal multispanning membrane protein 5	2
SI04265527	Hs_CTPS_8	CTPS	CTP synthase	2
SI04366831	Hs_PFDN2_7	PFDN2	prefoldin subunit 2	2
SI04342884	Hs_DDIT4_8	DDIT4	DNA-damage-inducible transcript 4	1
SI04297573	Hs_PELI1_7	PELI1	pellino homolog 1 (Drosophila)	1
SI04214987	Hs_CALML4_6	CALML4	calmodulin-like 4	2
SI04360251	Hs_CDK2AP1_7	CDK2AP1	cyclin-dependent kinase 2 associated protein 1	2
SI03096639	Hs_FNDC3B_7	FNDC3B	fibronectin type III domain containing 3B	2
SI02223977	Hs_PRKD3_5	PRKD3	protein kinase D3	1
SI04274893	Hs_ART3_7	ART3	ADP-ribosyltransferase 3	2
SI00051534	Hs_VEGF_4	VEGFA	vascular endothelial growth factor A	1
SI03118745	Hs_CD97_12	CD97	CD97 molecule	1
SI04138862	Hs_ST5_5	ST5	suppression of tumorigenicity 5	2
SI03111038	Hs_ETV6_5	ETV6	ets variant 6	1
SI04229638	Hs_LAPTM5_7	LAPTM5	lysosomal multispanning membrane protein 5	2
SI04438378	Hs_DLG7_8	DLGAP5	discs, large (Drosophila) homolog-associated protein 5	1
SI03184048	Hs_CDK2AP1_5	CDK2AP1	cyclin-dependent kinase 2 associated protein 1	2
SI04212614	Hs_HLA-E_7	HLA-E	major histocompatibility complex, class I, E	1
SI03076689	Hs_C3_9	C3	complement component 3	2
SI03045910	Hs_PRKCDBP_7	PRKCDBP	protein kinase C, delta binding protein	1
SI02625770	Hs_CDKN2C_7	CDKN2C	cyclin-dependent kinase inhibitor 2C (p18, inhibits CDK4)	2
SI04183326	Hs_SSRP1_5	SSRP1	structure specific recognition protein 1	1
SI02223935	Hs_YES1_6	YES1	v-yes-1 Yamaguchi sarcoma viral oncogene homolog 1	1
SI03084487	Hs_SOD2_7	SOD2	superoxide dismutase 2, mitochondrial	2
SI04327260	Hs_RPIA_9	RPIA	ribose 5-phosphate isomerase A	1
SI03053106	Hs_ADCY7_6	ADCY7	adenylate cyclase 7	1
SI03032512	Hs_RRAS2_7	RRAS2	related RAS viral (r-ras) oncogene homolog 2	1
SI00059458	Hs_CTSS_3	CTSS	cathepsin S	1
SI04153716	Hs_SLC39A14_6	SLC39A14	solute carrier family 39 (zinc transporter), member 14	2
SI04195415	Hs_NUP93_7	NUP93	nucleoporin 93kDa	1
SI02645678	Hs_OGFRL1_7	OGFRL1	opioid growth factor receptor-like 1	1
SI03107783	Hs_SOD2_8	SOD2	superoxide dismutase 2, mitochondrial	2
SI00091630	Hs_UGP2_3	UGP2	UDP-glucose pyrophosphorylase 2	1
SI00002184	Hs_SLC26A2_3	SLC26A2	solute carrier family 26 (sulfate transporter), member 2	3
SI03057208	Hs_CASP1_16	CASP1	caspase 1, apoptosis-related cysteine peptidase (interleukin 1	1
SI04438007	Hs_PSTPIP2_9	PSTPIP2	proline-serine-threonine phosphatase interacting protein 2	1
SI04171335	Hs_TLE4_5	TLE4	transducin-like enhancer of split 4 (E(sp1) homolog, Drosophil	1
SI00100268	Hs_KLK5_3	KLK5	kallikrein-related peptidase 5	1
SI00757813	Hs_UQCRH_3	UQCRH	ubiquinol-cytochrome c reductase hinge protein	2
SI04287458	Hs_LAMP3_7	LAMP3	lysosomal-associated membrane protein 3	1
SI03038672	Hs_PTGS2_9	PTGS2	prostaglandin-endoperoxide synthase 2 (prostaglandin G/H sy	1
SI04358781	Hs_CEP170_6	CEP170	centrosomal protein 170kDa	1
SI00046312	Hs_SATB1_3	SATB1	SATB homeobox 1	1
SI04324817	Hs_OSBPL3_7	OSBPL3	oxysterol binding protein-like 3	1
SI03019919	Hs_LOC146909_5	KIF18B	kinesin family member 18B	1

SI04151231	Hs_LMO4_7	LMO4	LIM domain only 4	1
SI00375956	Hs_ECHDC1_2	ECHDC1	enoyl Coenzyme A hydratase domain containing 1	1
SI03159177	Hs_OAZ1_5	OAZ1	ornithine decarboxylase antizyme 1	1
SI04291476	Hs_PFDN2_6	PFDN2	prefoldin subunit 2	2
SI04291175	Hs_KLF11_8	KLF11	Kruppel-like factor 11	1
SI04213895	Hs_CALD1_8	CALD1	caldesmon 1	1
SI02663017	Hs_CTSB_7	CTSB	cathepsin B	1
SI04144959	Hs_KIAA0746_5	KIAA0746	KIAA0746 protein	1
SI00299460	Hs_BIRC5_6	BIRC5	baculoviral IAP repeat-containing 5	1
SI04183340	Hs_ARHGEF9_6	ARHGEF9	Cdc42 guanine nucleotide exchange factor (GEF) 9	2
SI00146440	Hs_ABCC10_4	ABCC10	ATP-binding cassette, sub-family C (CFTR/MRP), member 10	1
SI04313351	Hs_PRAME_9	PRAME	preferentially expressed antigen in melanoma	1
SI04203969	Hs_SLC39A14_8	SLC39A14	solute carrier family 39 (zinc transporter), member 14	2
SI00035588	Hs_RANBP5_3	IPO5	importin 5	2
SI04279527	Hs_ANKRD27_11	ANKRD27	ankyrin repeat domain 27 (VPS9 domain)	1
SI04357612	Hs_LCP1_7	LCP1	lymphocyte cytosolic protein 1 (L-plastin)	1
SI04138057	Hs_PIR_7	PIR	pirin (iron-binding nuclear protein)	1
SI00288526	Hs_PBK_6	PBK	PDZ binding kinase	2
SI04352978	Hs_C20orf42_8	FERMT1	fermitin family homolog 1 (Drosophila)	1
SI00629104	Hs_MCM7_4	MCM7	minichromosome maintenance complex component 7	1
SI04435312	Hs_HCK_12	HCK	hemopoietic cell kinase	1
SI03080154	Hs_ANGPT1_9	ANGPT1	angiopoietin 1	2
SI04311412	Hs_DDX21_7	DDX21	DEAD (Asp-Glu-Ala-Asp) box polypeptide 21	1
SI02653980	Hs_SMC2L1_7	SMC2	structural maintenance of chromosomes 2	2
SI00706552	Hs_RPL39L_4	RPL39L	ribosomal protein L39-like	1
SI04210689	Hs_ARHGEF9_7	ARHGEF9	Cdc42 guanine nucleotide exchange factor (GEF) 9	2
SI04375868	Hs_PAK1IP1_8	PAK1IP1	PAK1 interacting protein 1	1
SI04252346	Hs_WBP5_7	WBP5	WW domain binding protein 5	1
SI00323477	Hs_C1orf38_1	C1orf38	chromosome 1 open reading frame 38	3
SI04137602	Hs_CGI-96_5	RRP7A	ribosomal RNA processing 7 homolog A (S. cerevisiae)	1
SI03080175	Hs_HRASLS_5	HRASLS	HRAS-like suppressor	1
SI04433954	Hs_ADA_10	ADA	adenosine deaminase	1
SI04352362	Hs_PUS7_3	PUS7	pseudouridylate synthase 7 homolog (S. cerevisiae)	1
SI04256182	Hs_SERBP1_2	SERBP1	SERPINE1 mRNA binding protein 1	2
SI03100237	Hs_CENPN_3	CENPN	centromere protein N	1
SI04181765	Hs_S100B_6	S100B	S100 calcium binding protein B	1
SI03071285	Hs_TIMP2_8	TIMP2	TIMP metallopeptidase inhibitor 2	1
SI04212579	Hs_RRAGD_5	RRAGD	Ras-related GTP binding D	1
SI00067571	Hs_ARHGEF2_4	ARHGEF2	rho/rac guanine nucleotide exchange factor (GEF) 2	1
SI02628080	Hs_IRF1_5	IRF1	interferon regulatory factor 1	1
SI04324824	Hs_NCAPG2_3	NCAPG2	non-SMC condensin II complex, subunit G2	1
SI04265814	Hs_BBOX1_8	BBOX1	butyrobetaine (gamma), 2-oxoglutarate dioxygenase (gamma-	1
SI04352096	Hs_DSCR2_7	PSMG1	proteasome (prosome, macropain) assembly chaperone 1	1
SI04439701	Hs_GTSE1_8	GTSE1	G-2 and S-phase expressed 1	2
SI02629592	Hs_PSMB2_2	PSMB2	proteasome (prosome, macropain) subunit, beta type, 2	1
SI00005880	Hs_NP_4	NP	nucleoside phosphorylase	1
SI00689108	Hs_POLR2F_4	POLR2F	polymerase (RNA) II (DNA directed) polypeptide F	1
SI00025865	Hs_DPYSL2_3	DPYSL2	dihydropyrimidinase-like 2	1
SI00035581	Hs_RANBP5_2	IPO5	importin 5	2
SI02624986	Hs_NCK2_8	NCK2	NCK adaptor protein 2	1

Bibliography

1. Liedtke C, Mazouni C, Hess KR, Andre F, Tordai A, Mejia JA, Symmans WF, Gonzalez-Angulo AM, Hennessy B, Green M, Hortobagyi GN, Pusztai L. Response to neoadjuvant therapy and long-term survival in patients with triple-negative breast cancer. J Clin Oncol 2008;26(8):1275-1281.

2. Gluz O, Liedtke C, Gottschalk N, Pusztai L, Nitz U, Harbeck N. Triple-negative breast cancer: Current status and future directions. Ann Oncol 2009;20(12):1913-1927.

3. Rouzier R, Perou CM, Symmans WF, Ibrahim N, Cristofanilli M, Anderson K, Hess KR, Stec J, Ayers M, Wagner P, Morandi P, Fan C, Rabiul I, Ross JS, Hortobagyi GN, Pusztai L. Breast cancer molecular subtypes respond differently to preoperative chemotherapy. Clin Cancer Res 2005;11:5678-85.

4. Jiang Y, Harlocker SL, Molesh DA, Dillon DC, Stolk JA, Houghton RL, Repasky EA, Badaro R, Reed SG, Xu J. Discovery of differentially expressed genes in human breast cancer using subtracted cDNA libraries and cDNA microarrays. Oncogene 2002;21:2270-82.

5. Pusztai L, Ayers M, Stec J, Clark E, Hess K, Stivers D, Damokosh A, Sneige N, Buchholz TA, Esteva FJ, Arun B, Cristofanilli M, Booser D, Rosales M, Valero V, Adams C, Hortobagyi GN, Symmans WF. Gene expression profiles obtained from fine-needle aspirations of breast cancer reliably identify routine prognostic markers and reveal

large-scale molecular differences between estrogen-negative and estrogen-positive tumors. Clin Cancer Res 2003;9(7):2406-15.

6. Sotiriou C, Neo SY, McShane LM, Korn EL, Long PM, Jazaeri A, Martiat P, Fox SB, Harris AL, Liu ET. Breast cancer classification and prognosis based on gene expression profiles from a population-based study. Proc Natl Acad Sci USA 2003;100:10393-8.

7. Sotiriou C, Pusztai L. Gene-expression signatures in breast cancer. N Engl J Med 2009;360(8):790-800.

8. Perou CM, Sørlie T, Eisen MB, van de Rijn M, Jeffrey SS, Rees CA, Pollack JR, Ross DT, Johnsen H, Akslen LA, Fluge O, Pergamenschikov A, Williams C, Zhu SX, Lønning PE, Børresen-Dale AL, Brown PO, Botstein D. Molecular portraits of human breast tumours. Nature 2000;406:747-752.

9. Sørlie T, Perou CM, Tibshirani R, Aas T, Geisler S, Johnsen H, Hastie T, Eisen MB, van de Rijn M, Jeffrey SS, Thorsen T, Quist H, Matese JC, Brown PO, Botstein D, Lønning PE, Børresen-Dale AL. Gene expression patterns of breast carcinomas distinguish tumor subclasses with clinical implications. Proc Natl Acad Sci USA 2001;98:10869-74.

10. The Cancer Genome Atlas Network. Comprehensive molecular portraits of human breast tumours. Nature 2012;490:61–70.

11. Arnedos M, Scott V, Job B, De La Cruz J, Commo F, Mathieu MC, Wolp-Diniz R, Richon C, Campone M, Bachelot T, Dalenc F, Dessen P, Lacroix L, Lazar V, Soria JC, Delaloge S, Andre F. Array CGH and PIK3CA/AKT1 mutations to drive patients to specific targeted agents: a clinical experience in 108 patients with metastatic breast cancer. Eur J Cancer 2012;48(15):2293-9.

12. Shiang CY, Qi Y, Wang B, Lazar V, Wang J, Fraser Symmans W, Hortobagyi GN, Andre F, Pusztai L. Amplification of fibroblast growth factor receptor-1 in breast cancer and the effects of brivanib alaninate. Breast Cancer Res Treat 2010;123(3):747-55.

13. Stratowa C and Wilgenbus KK. Gene expression profiling in drug discovery and development. Current Opinion in Molecular Therapeutics 1999;1(6):671-679.

14. Dey N, Smith BR, Leyland-Jones B. Targeting basal-like breast cancers. Curr Drug Targets. 2012;13(12):1510-24

15. Ferraro DA, Gaborit N, Maron R, Cohen-Dvashi H, Porat Z, Pareja F, Lavi S, Lindzen M, Ben-Chetrit N, Sela M, Yarden Y. Inhibition of triple-negative breast cancer models by combinations of antibodies to EGFR. Proc Natl Acad Sci U S A. 2013;110(5):1815-20.

16. Emad A. Rakha, Jorge S. Reis-Filho and Ian O. Ellis. Basal-Like Breast Cancer: A Critical Review. JCO 2008;26:2568-2581.

17. Yamamoto Y, Iwase H. Clinicopathological features and treatment strategy for triple-negative breast cancer. Int J Clin Oncol. 2010;15(4):341-51.

18. Crown J, O'Shaughnessy J, Gullo G. Emerging targeted therapies in triple-negative breast cancer. Ann Oncol. 2012;23:Suppl 6:vi56-65.

19. LoRusso PM. Mammalian target of rapamycin as a rational therapeutic target for breast cancer treatment. Oncology. 2013;84(1):43-56.

20. Pivot X, Schneeweiss A, Verma S, Thomssen C, Passos-Coelho JL, Benedetti G, Ciruelos E, von Moos R, Chang HT, Duenne AA, Miles DW. Efficacy and safety of bevacizumab in combination with docetaxel for the first-line treatment of elderly patients with locally recurrent or metastatic breast cancer: results from AVADO. Eur J Cancer. 2011;47(16):2387-95.

21. Rossari JR, Metzger-Filho O, Paesmans M, Saini KS, Gennari A, de Azambuja E, Piccart-Gebhart M. Bevacizumab and Breast Cancer: A Meta-Analysis of First-Line Phase III Studies and a Critical Reappraisal of Available Evidence. J Oncol. 2012;2012:417673.

22. Pal SK, Childs BH, Pegram M. Triple negative breast cancer: unmet medical needs. Breast Cancer Res Treat. 2011;125(3):627-36.

23. Nimpf J, Schneider WJ. From cholesterol transport to signal transduction: low density lipoprotein receptor, very low density lipoprotein receptor, and apolipoprotein E receptor-2. Biochim Biophys Acta 2000;1529:287-298.

24. Yang XV, Banerjee Y, Fernández JA, Deguchi H, Xu X, Mosnier LO, Urbanus RT, de Groot PG, White-Adams TC, McCarty OJ, Griffin JH. Activated protein C ligation of ApoER2 (LRP8) causes Dab1-dependent signaling in U937 cells. Proc Natl Acad Sci USA 2009;106(1):274-279.

25. MAQC Consortium. The MicroArray Quality Control (MAQC) project shows inter- and intraplatform reproducibility of gene expression measurements. Nature Biotech 2006;24(9):1151-1161.

26. Wang Y, Klijn JG, Zhang Y, Sieuwerts AM, Look MP, Yang F, Talantov D, Timmermans M, Meijer-van Gelder ME, Yu J, Jatkoe T, Berns EM, Atkins D, Foekens JA. Gene-expression profiles to predict distant metastasis of lymph-node-negative primary breast cancer. Lancet 2005;365(9460):671-9.

27. Reddy SS, Connor TE, Weeber EJ, Rebeck W. Similarities and differences in structure, expression, and functions of VLDLR and ApoER2. Mol Neurodegener. 2011;6:30.

28. Hack I, Hellwig S, Junghans D, Brunne B, Bock HH, Zhao S, Frotscher M. Divergent roles of ApoER2 and Vldlr in the migration of cortical neurons. Development. 2007;134(21):3883-91.

29. O'Dell RS, Ustine CJ, Cameron DA, Lawless SM, Williams RM, Zipfel WR, Olson EC. Layer 6 cortical neurons require Reelin-Dab1 signaling for cellular orientation, Golgi deployment, and directed neurite growth into the marginal zone. Neural Dev. 2012;7:25.

30. Liu CC, Kanekiyo T, Xu H, Bu G. Apolipoprotein E and Alzheimer disease: risk, mechanisms and therapy. Nat Rev Neurol. 2013;9(2):106-18.

31. Garnis C, Campbell J, Davies JJ, Macaulay C, Lam S, Lam WL. Involvement of multiple developmental genes on chromosome 1p in lung tumorigenesis. Hum Mol Genet. 2005;14(4):475-82.

32. Pencheva N, Tran H, Buss C, Huh D, Drobnjak M, Busam K, Tavazoie SF. Convergent multi-miRNA targeting of ApoE drives LRP1/LRP8-dependent melanoma metastasis and angiogenesis. Cell. 2012;151(5):1068-82.

33. Becker J, Fröhlich J, Perske C, Pavlakovic H, Wilting J. Reelin signalling in neuroblastoma: migratory switch in metastatic stages. Int J Oncol. 2012;41(2):681-9.

34. Webb DJ, Nguyen DH, Sankovic M, Gonias SL. The very low density lipoprotein receptor regulates urokinase receptor catabolism and breast cancer cell motility in vitro. J Biol Chem. 1999;274(11):7412-20.

35. Ma KL, Liu J, Ni J, Zhang Y, Lv LL, Tang RN, Ni HF, Ruan XZ, Liu BC. Inflammatory stress exacerbates the progression of cardiac fibrosis in high-fat-fed apolipoprotein E knockout mice via endothelial-mesenchymal transition. Int J Med Sci. 2013;10(4):420-6.

36. De Feo E, Simone B, Persiani R, Cananzi F, Biondi A, Arzani D, Amore R, D'Ugo D, Ricciardi G, Boccia S. A case-control study on the effect of Apolipoprotein E genotypes on gastric cancer risk and progression. BMC Cancer. 2012;12:494.

37. Mostafa Saadat. Apolipoprotein E (APOE) Polymorphisms and Susceptibility to Breast Cancer: A Meta-Analysis. Cancer Res Treat. 2012;44(2):121–126.

38. Chen YC, Pohl G, Wang TL, Morin PJ, Risberg B, Kristensen GB, Yu A, Davidson B, Shih IeM. Apolipoprotein E is required for cell proliferation and survival in ovarian cancer. Cancer Res. 2005;65(1):331-7.

39. Venanzoni MC, Giunta S, Muraro GB, Storari L, Crescini C, Mazzucchelli R, Montironi R, Seth A. Apolipoprotein E expression in localized prostate cancers. Int J Oncol. 2003;22(4):779-86.

40. Benn M, Tybjærg-Hansen A, Stender S, Frikke-Schmidt R, Nordestgaard BG. Low-density lipoprotein cholesterol and the risk of cancer: a mendelian randomization study. J Natl Cancer Inst. 2011;103(6):508-19.

41. Porrata-Doria T, Matta JL, Acevedo SF. Apolipoprotein E Allelic Frequency Altered in Women with Early-onset Breast Cancer. Breast Cancer (Auckl). 2010;4:43-8.

42. Gong Y, Yan K, Lin F, Anderson K, Sotiriou C, Andre F, Holmes FA, Valero V, Booser D, Pippen JE Jr, Vukelja S, Gomez H, Mejia J, Barajas LJ, Hess KR, Sneige N, Hortobagyi GN, Pusztai L, Symmans WF. Determination of oestrogen-receptor status and ERBB2 status of breast carcinoma: a gene-expression profiling study. Lancet Oncol 2007;8:203-11.

43. Pounds S, Morris SW. Estimating the occurrence of false positive and false negatives in microarray studies by approximating and partitioning the empirical distribution of p-values. Bioinformatics 2003;19:1236-1242.

44. Desmedt C, Piette F, Loi S, Wang Y, Lallemand F, Haibe-Kains B, Viale G, Delorenzi M, Zhang Y, d'Assignies MS, Bergh J, Lidereau R, Ellis P, Harris AL, Klijn JG, Foekens JA, Cardoso F, Piccart MJ, Buyse M, Sotiriou C; TRANSBIG Consortium. Strong time dependence of the 76-gene prognostic signature for node-negative breast cancer patients in the TRANSBIG multicenter independent validation series. Clin Cancer Res 2007;13:3207-14.

45. Schmidt M, Böhm D, von Törne C, Steiner E, Puhl A, Pilch H, Lehr HA, Hengstler JG, Kölbl H, Gehrmann M. The humoral immune system has a key prognostic impact in node-negative breast cancer. Cancer Res 2008;68:5405-13.

46. Neve RM, Chin K, Fridlyand J, Yeh J, Baehner FL, Fevr T, Clark L, Bayani N, Coppe JP, Tong F, Speed T, Spellman PT, DeVries S, Lapuk A, Wang NJ, Kuo WL, Stilwell JL, Pinkel D, Albertson DG, Waldman FM, McCormick F, Dickson RB, Johnson MD, Lippman M, Ethier S, Gazdar A, Gray JW. A collection of breast cancer cell lines for the study of functionally distinct cancer subtypes. Cancer Cell 2006;10:515-27.

47. Liedtke C, Wang J, Tordai A, Symmans WF, Hortobagyi GN, Kiesel L, Hess K, Baggerly KA, Coombes KR, Pusztai L. Clinical evaluation of chemotherapy response predictors developed from breast cancer cell lines. Breast Cancer Res Treat 2010;121(2):301-309.

48. Tibes R, Qiu Y, Lu Y, Hennessy B, Andreeff M, Mills GB, Kornblau SM. Reverse phase protein array: validation of a novel proteomic technology and utility for analysis of primary leukemia specimens and hematopoietic stem cells. Mol Cancer Ther 2006;5(10):2512-21.

49. Dehaven CD, Evans AM, Dai H. Organization of GC/MS and LC/MS metabolomics data into chemical libraries. J Cheminform 2010;2(9):1-12.

50. Evans AM, DeHaven CD, Barrett T, Mitchell M, Milgram E. Integrated, nontargeted ultrahigh performance liquid chromatography/electrospray ionization tandem mass spectrometry platform for the identification and relative quantification of the small-molecule complement of biological systems. Anal Chem 2009;81(16):6656-6667.

51. Axelson M, Larsson O. Low density lipoprotein (LDL) cholesterol is converted to 27-hydroxycholesterol in human fibroblasts. Evidence that 27-hydroxycholesterol can be an important intracellular mediator between LDL and the suppression of cholesterol production. J Biol Chem. 1995;270(25):15102-10.

52. Hilvo M, Denkert C, Lehtinen L, Müller B, Brockmöller S, Seppänen-Laakso T, Budczies J, Bucher E, Yetukuri L, Castillo S, Berg E, Nygren H, Sysi-Aho M, Griffin JL, Fiehn O, Loibl S, Richter-Ehrenstein C, Radke C, Hyötyläinen T, Kallioniemi O, Iljin K, Oresic M. Novel theranostic opportunities offered by characterization of altered membrane lipid metabolism in breast cancer progression. Cancer Res. 2011;71(9):3236-45.

53. Menendez JA, Lupu R. Fatty acid synthase and the lipogenic phenotype in cancer pathogenesis. Nat Rev Cancer 2007;7:763-77.

54. Hirsch HA, Iliopoulos D, Joshi A, Zhang Y, Jaeger SA, Bulyk M, Tsichlis PN, Shirley Liu X, Struhl K. A transcriptional signature and common gene networks link cancer with lipid metabolism and diverse human diseases. Cancer Cell 2010;17:348-61.

55. Chajes V, Lanson M, Fetissof F, Lhuillery C, Bougnoux P. Membrane fatty acids of breast carcinoma: contribution of host fatty acids and tumor properties. Int J Cancer 1995;63:169-75.

56. Hudis CA, Gianni L. Triple-negative breast cancer: an unmet medical need. Oncologist. 2011;16 Suppl 1:1-11.

57. André F, Zielinski CC. Optimal strategies for the treatment of metastatic triple-negative breast cancer with currently approved agents. Ann Oncol. 2012;23 Suppl 6:vi46-51.

58. Rody A, Karn T, Liedtke C, Pusztai L, Ruckhaeberle E, Hanker L, Gaetje R, Solbach C, Ahr A, Metzler D, Schmidt M, Müller V, Holtrich U, Kaufmann M. A clinically relevant gene signature in triple negative and basal-like breast cancer. Breast Cancer Res. 2011;13(5):R97.

59. Warburg O. On the origin of cancer cells. Science. 1956;123(3191):309-14.

60. Fritz V, Fajas L. Metabolism and proliferation share common regulatory pathways in cancer cells. Oncogene. 2010;29(31):4369-77.

61. Porstmann T, Griffiths B, Chung YL, Delpuech O, Griffiths JR, Downward J, Schulze A. PKB/Akt induces transcription of enzymes involved in cholesterol and fatty acid biosynthesis via activation of SREBP. Oncogene. 2005;24(43):6465-81.

62. Porstmann T, Santos CR, Griffiths B, Cully M, Wu M, Leevers S, Griffiths JR, Chung YL, Schulze A. SREBP activity is regulated by mTORC1 and contributes to Akt-dependent cell growth. Cell Metab. 2008;8(3):224-36.

63. DeBerardinis RJ, Lum JJ, Hatzivassiliou G, Thompson CB.The biology of cancer: metabolic reprogramming fuels cell growth and proliferation. Cell Metab. 2008;7(1):11-20.

64. Jiang L, Deberardinis RJ. Cancer metabolism: When more is less. Nature. 2012;489(7417):511-2.

65. Dong C, Yuan T, Wu Y, Wang Y, Fan TW, Miriyala S, Lin Y, Yao J, Shi J, Kang T, Lorkiewicz P, St Clair D, Hung MC, Evers BM, Zhou BP. Loss of FBP1 by Snail-mediated repression provides metabolic advantages in basal-like breast cancer. Cancer Cell. 2013;23(3):316-31.

66. Black AR, Black JD, Azizkhan-Clifford J. Sp1 and krüppel-like factor family of transcription factors in cell growth regulation and cancer. J Cell Physiol. 2001;188(2):143-60.

67. Matoba S, Kang JG, Patino WD, Wragg A, Boehm M, Gavrilova O, Hurley PJ, Bunz F, Hwang PM. p53 regulates mitochondrial respiration. Science. 2006 ;312(5780):1650-3.

68. Junk DJ, Cipriano R, Stampfer M, Jackson MW. Constitutive CCND1/CDK2 activity substitutes for p53 loss, or MYC or oncogenic RAS expression in the transformation of human mammary epithelial cells. PLoS One. 2013;8(2):e53776.

69. Badura M, Braunstein S, Zavadil J, Schneider RJ. DNA damage and eIF4G1 in breast cancer cells reprogram translation for survival and DNA repair mRNAs. Proc Natl Acad Sci U S A. 2012;109(46):18767-72.

70. Nowsheen S, Aziz K, Tran PT, Gorgoulis VG, Yang ES, Georgakilas AG. Epigenetic inactivation of DNA repair in breast cancer. Cancer Lett. 2012 May 23. [Epub ahead of print], http://dx.doi.org/10.1016/j.canlet.2012.05.015

71. Khajah MA, Al Saleh S, Mathew PM, Luqmani YA. Differential effect of growth factors on invasion and proliferation of endocrine resistant breast cancer cells. PLoS One. 2012;7(7):e41847.

72. Umemura S, Yoshida S, Ohta Y, Naito K, Osamura RY, Tokuda Y. Increased phosphorylation of Akt in triple-negative breast cancers. Cancer Sci. 2007;98(12):1889-92.

73. Jerby L, Wolf L, Denkert C, Stein GY, Hilvo M, Oresic M, Geiger T, and Ruppin E. Metabolic Associations of Reduced Proliferation and Oxidative Stress in Advanced Breast Cancer. Cancer Res 2012;72:5712

74. Diers AR, Broniowska KA, Chang CF, Hogg N. Pyruvate fuels mitochondrial respiration and proliferation of breast cancer cells: effect of monocarboxylate transporter inhibition. Biochem J. 2012;444(3):561-71.

75. Kim S, Kim DH, Jung WH, Koo JS. Metabolic phenotypes in triple-negative breast cancer. Tumour Biol. 2013 Feb 27. [Epub ahead of print], http://dx.doi.org/10.1007/s13277-013-0707-1

76. Boyle P. Triple-negative breast cancer: epidemiological considerations and recommendations. Ann Oncol. 2012;23 Suppl 6:vi7-12.

77. Criscitiello C, Azim HA Jr, Schouten PC, Linn SC, Sotiriou C. Understanding the biology of triple-negative breast cancer. Ann Oncol. 2012;23 Suppl 6:vi13-8.

78. Ossovskaya V, Wang Y, Budoff A, Xu Q, Lituev A, Potapova O, Vansant G, Monforte J, Daraselia N. Exploring molecular pathways of triple-negative breast cancer. Genes Cancer. 2011;2(9):870-9.

79. Lee KH, Hsu EC, Guh JH, Yang HC, Wang D, Kulp SK, Shapiro CL, Chen CS. Targeting energy metabolic and oncogenic signaling pathways in triple-negative breast

cancer by a novel adenosine monophosphate-activated protein kinase (AMPK) activator. J Biol Chem. 2011;286(45):39247-58.

80. Prat A, Adamo B, Cheang MC, Anders CK, Carey LA, Perou CM. Molecular characterization of basal-like and non-basal-like triple-negative breast cancer. Oncologist. 2013;18(2):123-33.

81. Dutta B, Pusztai L, Qi Y, André F, Lazar V, Bianchini G, Ueno N, Agarwal R, Wang B, Shiang CY, Hortobagyi GN, Mills GB, Symmans WF, Balázsi G. A network-based, integrative study to identify core biological pathways that drive breast cancer clinical subtypes. Br J Cancer. 2012;106(6):1107-16.

82. Karn T, Pusztai L, Holtrich U, Iwamoto T, Shiang CY, Schmidt M, Müller V, Solbach C, Gaetje R, Hanker L, Ahr A, Liedtke C, Ruckhäberle E, Kaufmann M, Rody A. Homogeneous datasets of triple negative breast cancers enable the identification of novel prognostic and predictive signatures. PLoS One. 2011;6(12):e28403.

83. Landor SK, Mutvei AP, Mamaeva V, Jin S, Busk M, Borra R, Grönroos TJ, Kronqvist P, Lendahl U, Sahlgren CM. Hypo- and hyperactivated Notch signaling induce a glycolytic switch through distinct mechanisms. Proc Natl Acad Sci U S A. 2011;108(46):18814-9.

84. Witkiewicz AK, Whitaker-Menezes D, Dasgupta A, Philp NJ, Lin Z, Gandara R, Sneddon S, Martinez-Outschoorn UE, Sotgia F, Lisanti MP. Using the "reverse Warburg effect" to identify high-risk breast cancer patients: stromal MCT4 predicts poor clinical outcome in triple-negative breast cancers. Cell Cycle. 2012;11(6):1108-17.

85. Possemato R, Marks KM, Shaul YD, Pacold ME, Kim D, Birsoy K, Sethumadhavan S, Woo HK, Jang HG, Jha AK, Chen WW, Barrett FG, Stransky N, Tsun ZY, Cowley GS, Barretina J, Kalaany NY, Hsu PP, Ottina K, Chan AM, Yuan B, Garraway LA, Root DE, Mino-Kenudson M, Brachtel EF, Driggers EM, Sabatini DM. Functional genomics reveal that the serine synthesis pathway is essential in breast cancer. Nature. 2011;476(7360):346-50.

86. Kang HS, Lee SC, Park YS, Jeon YE, Lee JH, Jung SY, Park IH, Jang SH, Park HM, Yoo CW, Park SH, Han SY, Kim KP, Kim YH, Ro J, Kim HK. Protein and lipid MALDI profiles classify breast cancers according to the intrinsic subtype. BMC Cancer. 2011;11:465.

87. Catasus L, Gallardo A, Llorente-Cortes V, Escuin D, Muñoz J, Tibau A, Peiro G, Barnadas A, Lerma E. Low-density lipoprotein receptor-related protein 1 is associated with proliferation and invasiveness in Her-2/neu and triple-negative breast carcinomas. Hum Pathol. 2011;42(11):1581-8.

88. Juul N, Szallasi Z, Eklund AC, Li Q, Burrell RA, Gerlinger M, Valero V, Andreopoulou E, Esteva FJ, Symmans WF, Desmedt C, Haibe-Kains B, Sotiriou C, Pusztai L, Swanton C. Assessment of an RNA interference screen-derived mitotic and ceramide pathway metagene as a predictor of response to neoadjuvant paclitaxel for primary triple-negative breast cancer: a retrospective analysis of five clinical trials. Lancet Oncol. 2010;11(4):358-65.

89. Galluzzi L, Kepp O, Kroemer G. Reverse Warburg: straight to cancer. Cell Cycle. 2012;11(6):1059.

90. Witkiewicz AK, Whitaker-Menezes D, Dasgupta A, Philp NJ, Lin Z, Gandara R, Sneddon S, Martinez-Outschoorn UE, Sotgia F, Lisanti MP. Using the "reverse Warburg effect" to identify high-risk breast cancer patients: stromal MCT4 predicts poor clinical outcome in triple-negative breast cancers. Cell Cycle. 2012;11(6):1108-17.

91. Schafer ZT, Grassian AR, Song L, Jiang Z, Gerhart-Hines Z, Irie HY, Gao S, Puigserver P, Brugge JS. Antioxidant and oncogene rescue of metabolic defects caused by loss of matrix attachment. Nature. 2009;461(7260):109-13.

92. Davis AA, Kaklamani VG. Metabolic syndrome and triple-negative breast cancer: a new paradigm. Int J Breast Cancer. 2012;2012:809291.

93. Hanahan D, Weinberg RA. Hallmarks of cancer: the next generation. Cell. 2011;144(5):646-74.

94. Litzenburger BC, Creighton CJ, Tsimelzon A, Chan BT, Hilsenbeck SG, Wang T, Carboni JM, Gottardis MM, Huang F, Chang JC, Lewis MT, Rimawi MF, Lee AV. High IGF-IR activity in triple-negative breast cancer cell lines and tumorgrafts correlates with sensitivity to anti-IGF-IR therapy. Clin Cancer Res. 2011;17(8):2314-27.

95. Wazir U, Al Sarakbi W, Jiang WG, Mokbel K. Evidence of an autocrine role for leptin and leptin receptor in human breast cancer. Cancer Genomics Proteomics. 2012;9(6):383-7.

96. Benatar T, Yang W, Amemiya Y, Evdokimova V, Kahn H, Holloway C, Seth A. IGFBP7 reduces breast tumor growth by induction of senescence and apoptosis pathways. Breast Cancer Res Treat. 2012;133(2):563-73.

97. Reckless J, Metcalfe JC, Grainger DJ. Tamoxifen Decreases Cholesterol Sevenfold and Abolishes Lipid Lesion Development in Apolipoprotein E Knockout Mice. Circulation. 1997;95:1542-1548.

98. Ferraro DA, Gaborit N, Maron R, Cohen-Dvashi H, Porat Z, Pareja F, Lavi S, Lindzen M, Ben-Chetrit N, Sela M, Yarden Y. Inhibition of triple-negative breast cancer models by combinations of antibodies to EGFR. Proc Natl Acad Sci U S A. 2013;110(5):1815-20.

99. Berrada N, Delaloge S, André F. Treatment of triple-negative metastatic breast cancer: toward individualized targeted treatments or chemosensitization? Ann Oncol. 2010;21 Suppl 7:vii30-5.

100. Anders C, Carey LA. Understanding and treating triple-negative breast cancer. Oncology (Williston Park). 2008;22(11):1233-9.

101. Carey LA, Rugo HS, Marcom PK, Mayer EL, Esteva FJ, Ma CX, Liu MC, Storniolo AM, Rimawi MF, Forero-Torres A, Wolff AC, Hobday TJ, Ivanova A, Chiu WK, Ferraro M, Burrows E, Bernard PS, Hoadley KA, Perou CM, Winer EP. TBCRC 001: randomized phase II study of cetuximab in combination with carboplatin in stage IV triple-negative breast cancer. J Clin Oncol. 2012;30(21):2615-23.

102. Shiu KK, Tan DS, Reis-Filho JS. Development of therapeutic approaches to 'triple negative' phenotype breast cancer. Expert Opin Ther Targets. 2008;12(9):1123-37.

103. Hilvo M, Denkert C, Lehtinen L, Müller B, Brockmöller S, Seppänen-Laakso T, Budczies J, Bucher E, Yetukuri L, Castillo S, Berg E, Nygren H, Sysi-Aho M, Griffin JL,

Fiehn O, Loibl S, Richter-Ehrenstein C, Radke C, Hyötyläinen T, Kallioniemi O, Iljin K, Oresic M. Novel theranostic opportunities offered by characterization of altered membrane lipid metabolism in breast cancer progression. Cancer Res. 2011;71(9):3236-45.

104. McGowan MM, Eisenberg BL, Lewis LD, Froehlich HM, Wells WA, Eastman A, Kuemmerle NB, Rosenkrantz KM, Barth RJ Jr, Schwartz GN, Li Z, Tosteson TD, Beaulieu BB Jr, Kinlaw WB. A proof of principle clinical trial to determine whether conjugated linoleic acid modulates the lipogenic pathway in human breast cancer tissue. Breast Cancer Res Treat. 2013;138(1):175-83.

105. Alikhani N, Ferguson RD, Novosyadlyy R, Gallagher EJ, Scheinman EJ, Yakar S, LeRoith D. Mammary tumor growth and pulmonary metastasis are enhanced in a hyperlipidemic mouse model. Oncogene. 2013;32(8):961-7.

106. Lee J, Lee I, Han B, Park JO, Jang J, Park C, Kang WK. Effect of Simvastatin on Cetuximab Resistance in Human Colorectal Cancer with KRAS Mutations. J Natl Cancer Inst. 2011;103(8):674-688.

107. van der Spek E, Bloem AC, van de Donk NW, Bogers LH, van der Griend R, Kramer MH, de Weerdt O, Wittebol S, Lokhorst HM. Dose-finding study of high-dose simvastatin combined with standard chemotherapy in patients with relapsed or refractory myeloma or lymphoma. Haematologica. 2006;91(4):542-5.

Vita

Christine Shiang was born in Taipei, Taiwan to Thomas Shiang and Nina Kuo Shiang. At the age of 5, the family immigrated to the United States with 4 family members; mom, dad, and 2 daughters. Two more daughters were born in Boston and the family, now with 6 members, made their way to Houston, Texas. The four daughters were raised in Sugar Land and completed their educations in Texas.

During her graduate training, Christine was awarded a Department of Defense Breast Cancer Research Program Predoctoral Fellowship, was elected President of the Graduate Student Association, and earned several other scholarships in support of her work.